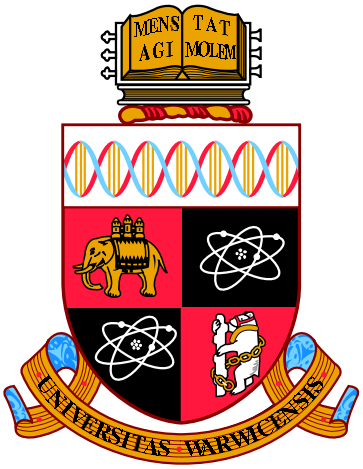

On the Fokker-Planck Approximation to the Boltzmann Collision Operator

by

Benjamin S. Collyer

Thesis

Submitted to the University of Warwick

for the degree of

Doctor of Philosophy

Complexity Science DTC

May 2015

THE UNIVERSITY OF
WARWICK

Contents

Acknowledgments

This thesis would not have been possible without the guidance, patience and kindness from my supervisors, Colm Connaughton and Duncan Lockerby. I would also like to extend my gratitude to the students and members of staff, past and present, of the Complexity Science DTC, for providing a stimulating environment to work in and for making my time here an enjoyable one. In particular, I would like to thank Mike Irvine, Daniel Sprague, Pete and Jen Lawson-Dawson, Marcus Ong, Adam Miller, Samik Datta, Dario Papapapavassiliou, Davide Michieletto, Tom Machon, Jenny Webb, Sophie Rees, Mike Maitland, Chris Oates, Jamie Harris, Matthew Graham, Sergio and Quentin, Pantelis Hadjipantelis, and Anthony Woolcock, the various combinations of whom helped each day seem a little brighter.

To my parents and family, whom I was unable to visit enough, thank you for your understanding and patience. A special thanks goes to Filippo Casati and Ellen Webborn, for being there when I lost my way, and for your unwavering support, help and friendship when times were tough. Finally, I thank coffee, whose continued existence fuels my thoughts and ideas, and in those quiet moments we get alone never fails to raise a smile.

Declarations

This thesis is submitted to the University of Warwick in support of my application for the degree of Doctor of Philosophy. It has been composed by myself and has not been submitted in any previous application for any degree. The common random numbers variance reduction method presented in Chapter 4 has been published independently by Gorji et al. [2015]; this was discovered after having developed the method for myself.

Abstract

The Boltzmann equation (BE) is a mesoscopic model that provides a description of how gases undergoing a binary collision process evolve in time, however there is no general analytical approach for finding its solutions and direct numerical treatment using quadrature methods is prohibitively expensive due to the dimensions of the problem. For this reason, models that are able to capture the behaviour of solutions to the BE, but which are simpler to treat numerically and analytically are highly desirable. The Fokker-Planck collision operator is one such collision model, which is suited well to numerical solutions using stochastic particle methods, and is the subject of this thesis.

The stochastic numerical solutions of the Fokker-Planck model suffer heavily from noise when the speed of the flow is low. We develop two methods that are able to reduced the variance of the estimators of the particle method. The first is a common random number method, which produces a correlated equilibrium solution where thermodynamic fields are known. The second is a importance sampling method, where weights are attached to the particles. This means that particles close to equilibrium do not contribute to the noise of the estimators. We also develop a randomised quasi-Monte Carlo scheme for solving the diffusion equation, which has a faster rate of convergence than simple Monte Carlo methods.

The relative simplicity of the functional form of the Fokker-Planck collision operator makes it possible to find analytic solutions in simple cases. We consider a spatially homogeneous, isotropic gas with elastic collisions in the presence of forcing and dissipation and derive self-consistent non-equilibrium steady-state solutions. Previous numerical evidence exists that suggest such forcing and dissipation mechanisms, widely separated, give rise to steady-states of the BE that are close to Maxwellian, with a direct energy cascade and an inverse particle cascade. Using our analytic solutions, we are able to investigate the dependence of such solutions on the forcing and dissipation scales, and find that in the inertial range, the interaction is non-local. We then show that the "extreme driving" mechanism, responsible for a family of non-universal power-law solutions for inelastic granular gases, where the flux of energy is towards lower scales, is also able to produce inverse energy cascades for the elastic system.

1

Introduction

"Oh! the little more, and how much it is!
And the little less, and what worlds away!"

– Robert Browning, *By the Fireside*

The atomistic description of nature has a long history that dates back to Leucippus, Democritus, and Epicurus - natural philosophers born in ancient Greece who struggled against the prevailing Aristotelian view of the world. Despite attention from medieval Arabian scholars, and works from the Renaissance period penned by such influential thinkers as Galileo and Francis Bacon, atoms remained controversial and largely hypothetical objects up until the beginning of the 19th century, when scientists such as John Dalton with his "law of multiple proportions", and Robert Brown's dust grains moving erratically on the surface of water, now given the epithet of "Brownian Motion", began mounting experimental evidence for the atom. And so it is perhaps surprising, that without any direct evidence of atoms that Swiss polymath Daniel Bernouilli in 1738 was able to lay the foundations for the kinetic theory of gases when he explained the phenomenon of gas pressure using the idea of tiny high speed particles, whizzing around and colliding according to the known laws of mechanics.

This would provide the foundations for James Clerk Maxwell and later Ludwig Boltzmann to develop the theory into the kinetic theory of gases into the form as it is largely recognised today. The central pillar of which, is Boltzmann's eponymous equation, which provides a link between the dynamic and the thermodynamic description of gases made of particles that undergo binary collisions.

Today, the kinetic theory of gases still provides a wide and rich area for academic research, for practical and theoretical purposes alike. Engineers are concerned with developing tools that let them predict the behaviour of low density, rarefied gases, which is becoming increasingly important as technologies for both building things that are extremely small and also building things that travel at great velocity through the upper atmosphere are increasingly developed. Having models with the ability to make calculations and quickly and reliably as possible is of the essence. Naturally, part of the challenge can be met by the ever increasing processing power, coming in the form of multicore CPU and GPU supercomputers. It is possible in the future that computers will one day have the memory and processing power to evolve Newton's laws acting on suitably large number of particles with quantum computing. However, this technological revolution is still some distance away, and in the mean time being able to tackle these problems by generating understanding that allows us to make simplifications while keeping the essence of the problems we are trying to solve, is certainly a worthwhile approach.

For theoretical physicists, the equations of kinetic theory are a route into non-equilibrium statistical mechanics. In contrast to equilibrium statistical mechanics, where all thermodynamic properties can be derived from a partition function founded on the principal of equipartition of energy, there is no general theory that systematically allows one to count and to weight states of a system that is not in equilibrium. Kinetic models based on microscopic rules, allow an investigation into such systems where traditional macroscopic models are unable to predict the wide and diverse behaviour seen in such systems.

In this thesis I contribute to progress in both spheres, by using a model which approximates the behaviour of the Boltzmann equation. The model is in the form of a Fokker-Planck equation, which approximates the collision process of a gas by a non-linear advection and diffusion process in the velocity space of a distribution of a single particle. I will begin in Chapter 2 by describing an overview of kinetic theory as it is applied to rarefied gases, providing historical context for the Fokker-Planck model and it's origins in Chapter 3. I will demonstrate it's applicability as a model for rarefied gases, by demonstrating that it obeys the conservation laws and providing an H-Theorem for the model. Finally in Chapter 3 I describe some of the recent advances allowing for efficient stochastic particle-based solutions.

In Chapters 4 and 5 I focus on low-speed applications, where stochastic particle based simulations suffer greatly from noise. I will propose novel techniques, including a common random numbers scheme, an importance sampling algorithm and a quasi-Monte Carlo method, that can be applied to the particle-based stochastic solutions in such situations, to help alleviate the effects of noise on computation times.

Later in Chapters 6 and 7, I use the Fokker-Planck model to address the problem of finding and characterising non-equilibrium steady states. I find analytic solutions in the presence of a specific form of forcing and dissipation, allowing the locality of the solutions to be checked. I also derive a Fokker-Planck model equation describing a gas where the particles collide in-elasticially, where fluxes of energy travel in the opposite direction to when the collisions are elastic. Solutions to this equation lend support to the existence of solutions in the presence of an "extreme driving" forcing mechanism.

2

Background

"He who has begun, has half done."

– Horace, *Epistles I*

2.1 Rarefied gases

A gas, which in this thesis we choose to refer to as a fluid made up of a large number of interacting particles, where the interaction between particles occurs on very short length scales, is classified as being *rarefied* when the ratio of the particles' *mean free path*, the average distance a molecule will travel between collisions (or interaction), denoted λ, to a characteristic length scale of the fluid, L, is not negligible. This ratio is named after Danish physicist Martin Knudsen ($1871-1949$), and is denoted

$$\mathrm{Kn} = \frac{\lambda}{L}\,. \tag{2.1}$$

The length scale, L, is generally dependent on the geometry of the gas flow in question. For example, it could be the diameter of tube or the thickness of a boundary layer. It was Knudsen who was first to notice that it is this dimensionless quantity, and not solely the mean free path, that is relevant for characterising a rarefied gas [Rathakrishnan, 2013]. The Knudsen number can be related to two other important quantities of fluid dynamics, namely the *Mach number*, Ma (defined as the ratio of the characteristic speed of the flow to the characteristic speed of an individual particle) and the *Reynolds number* (defined as the ratio of the inertial

forces to the viscous forces within the fluid), Re by

$$\mathrm{Kn} = \sqrt{\frac{\gamma\pi}{2}}\,\frac{\mathrm{Ma}}{\mathrm{Re}} \tag{2.2}$$

where γ is the ratio of specific heats (the ratio of the heat capacity at a constant pressure to the heat capacity at a constant volume), and Kn and Re are defined using the same characteristic length scale. Just as it is possible to characterise flows by the Mach number and Reynolds number, we can also use the Knudsen number to characterise the flow into different flow regimes. This characterisation of degree of rarefaction by the Knudsen number can be summarised as follows. When $\mathrm{Kn} < 0.001$ the classical hydrodynamic equations, Navier-Stokes-Fourier equations or Euler, and conventional no-slip at gas-solid interfaces are relevant. Here, the fluid can be described accurately in terms of closed expressions involving the macroscopic variables- velocity, pressure, temperature and density.

The range of Knudsen numbers $0.001 < \mathrm{Kn} < 0.1$ is known as the *slip regime*. This is the range of Knudsen numbers that rarefaction effects, that is effects not predictable using classical fluid mechanics, start to occur. In this range, most of the non-equilibrium effects in the boundary layer start to appear gradually and are in general dominated by the phenomenon of 'slip', which can be summarised as the appearance of non-zero velocities and temperature jumps at solid boundary interfaces. Because the rarefaction effects are dominated by the slip behaviour, the Navier-Stokes-Fourier (NSF) equations supplemented with the correct slip boundary condition are able to model the flow with a good degree of accuracy [Schaaf and Chambré, 1961]. Lockerby et al. [2004] provides a current account of appropriate boundary conditions to supplement the Navier-Stokes-Fourier or Euler equations, as a function of Knudsen number.

A rarefied gas that has a Knudsen number in the range $0.1 < \mathrm{Kn} < 10$, is considered to be in *transition regime*, named because it describes the scales between where the gas can be modelled using traditional computational fluid dynamics and the collisionless regime. Here the Knudsen boundary layer, where the transfer of mass, momentum and heat are not well described by the classical hydrodynamic equations, is large enough for the classical hydrodynamical equations to not provide physically accurate solutions. In the range $10 < \mathrm{Kn}$, the collisions within the gas are so rare that the gas can be considered to be collisionless. Experimental evidence for this characterisation has been conducted by Tison [1993], and more recently

Marino [2009], where the authors consider rarefaction effects of gas moving through micro-tubes.

The inability of the classical hydrodynamics equations, such as the Navier-Stokes-Fourier equations, to model a gas in the transition regime is often claimed to be a result of the breakdown of the continuum assumption. This is the assumption that the gas can be well described as a continuous material, the break down of which requires a description based upon a more detailed account of the underlying particle collision process. This is a widespread misunderstanding that has propagated through the fluid dynamics community (for example, see[White et al., 2013]), indeed assuming that the dynamics of the macroscopic quantities of the material in consideration can be approximated by equations involving spatial and temporal derivatives does not lead to the NSF equations on its own. Typically even when a gas is considered rarefied, the flow in consideration will still be comprised of numbers greater than 10^{20} particles per unit volume, and so in principal there is no reason why equations that govern the transport of smoothly varying hydrodynamic quantities are less appropriate. A more appropriate explanation of the observation that the NSF equations fail in the transition regime, is that the linear constitutive equations relating viscosity, shear stress and strain rate, are not justified when the local thermodynamic state is not near equilibrium [Gad-el Hak, 2003].

This characterisation of rarefaction in terms of the Knudsen number informs us that a gas will become rarefied when either the mean free path of the flow, λ is increased, or the characteristic length scale of the flow L is decreased. And so it follows that the study of rarefied gas dynamics has found its predominant application in two main areas: hypersonics and micro/nano scale flows. The use of the Boltzmann equation in such applications would surely please Boltzmann were he around today to witness them. He 1905 he stated:

> "*That is why I do not regard technological achievements as unimportant by-products of natural science but as logical proofs. Had we not attained these practical achievements, we should not know how to infer. Only those inferences are correct that lead to practical success"* Ludwig Boltzmann, 1905

Whilst I depart from his views on an epistemological level, one cannot deny the successes that his eponymous equation, which I will go on to describe, have achieved.

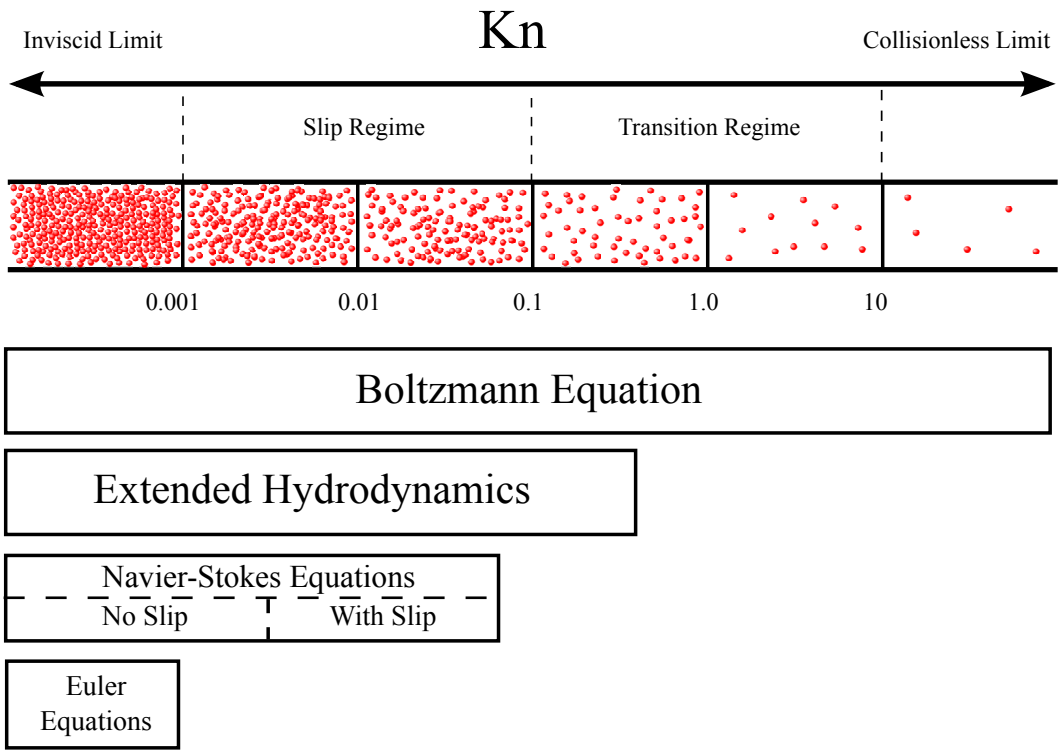

Figure 2.1: Characterisation of flows by Knudsen number, and where different models are applicable. The Boltzmann equation in theory is able to model the entire range. The Euler equations are relevant for very low Knudsen numbers, where viscosity is negligible. The Navier-Stokes-Fourier equations, which are able to describe viscous flows, are able to model gas flows are up to $Kn = 0.001$, or if slip boundary conditions are included, up to $Kn = 0.1$.

High speed external flows associated with aviation in the upper-atmosphere are relevant for interplanetary rocket flight or for orbiting satellites, and so it is perhaps unsurprising that interest in simulating rarefied gas flows took off in the 1950s. The flow in such situations is rarefied because the altitude required to fly at hypersonic speeds means the surrounding gas will be of low density. With the increasing interest in aircraft with the ability to fly at hypersonic speeds through the upper-levels of the atmosphere, the need to be able to predict aspects of the flow field also grew. Because accurate numerical solutions were very difficult to obtain, the literature had a large focus on experiment [Bird, 1976]. As the field gradually matured, theoretical considerations increased and now a vast field of literature exists [Cercignani et al., 1994].

In the last 20 years engineering advances in the field of micro-electrical mechanical systems, or MEMS, has driven the effort for modelling gases when the characteristic length of an internal geometry (and characteristic velocity) are very small. Such devices include pressure gauges [Górecka-Drzazga, 2009], vacuum generators for extracting chemical or biological samples [Miao et al., 2006], actuators for active control of aerodynamic flows [Huang et al., 2004], heat exchangers [Gad-el Hak, 2010], mass flow and temperature sensors [Wang et al., 2009]. Calculations of rarefied flows within such small devices pose different challenges to those encountered by hypersonic rarefied flows, and this will be main topic addressed within Chapter 3. The remaining sections of this chapter will be devoted to describing the fundamentals of gas kinetic theory, leading towards the development of the Fokker-Planck model which is the focus of this thesis.

2.2 The statistical mechanics of the Boltzmann equation

The fundamental paradigm of *kinetic theory* (and indeed statistical mechanics as a whole) is to renounce the study of a physical system in terms of a detailed description of the many components that form it. A full description of the system would involve following the trajectories, specifically the position and momentum, of roughly 10^{23} particles. Instead, it is far more sensible to speak about the system *statistically*, and introduce probability density $P(\mathbf{x}, \mathbf{v}, t)$ for a single particle, which quantifies the chance of finding a particle within $d\mathbf{x}$ of a given position $\mathbf{x}$ and within $d\mathbf{v}$ of a given velocity $\mathbf{v}$ at a time t. It was James Clerk Maxwell who was first to realise this, and in 1859 produced an argument to derive an expression for P when

the distribution is known to be in thermal equilibrium (and hence stationary), which assumes only that the distribution is isotropic and that velocities of a particle in orthogonal directions are uncorrelated. From his equilibrium distribution he went on to calculate viscosities and thermal conductivities, and found that transport coefficients were dependent only on the temperature, and not on the density, which at the time was a surprise to many [Maxwell, 1860]. Maxwell, himself went on then to perform experiments which confirmed his results.

However, with his 'Kinetic Theory of Gases', it was Ludwig Boltzmann who was first to successfully attempt to explain the properties of dilute gases with knowledge of the elementary collision process between pairs of molecules [Boltzmann, 1872]. This represented a milestone in theoretical physics, connecting the field of dynamics to the field of thermodynamics. The underlying assumption of his famous equation, allowing the closure of the hierarchical equations (both the BBGKY and Boltzmann hierarchy derived from Newton's Laws), is that the joint probability density function of two particles that are *about to collide* can be factorised as the production of two one-particle particle density distributions

$$P_2(\mathbf{x}_1, \mathbf{x}_2, \mathbf{v}_1, \mathbf{v}_2) = P(\mathbf{x}_1, \mathbf{v}_1)P(\mathbf{x}_2, \mathbf{v}_2). \tag{2.3}$$

Another way of stating this is that the pre-collision positions and velocities of any two particles are uncorrelated. This assumption became known as *molecular chaos*, and clearly an inappropriate assumption in general (in fact if it was true in general, collisions would have absolutely no effect on the time evolution of P since probabilities would necessarily remain constant over trajectories). Clearly, the positions and velocities of molecules that have only just collided must be correlated, and so molecular chaos is not an assumption that can be justified from the dynamics alone. Therefore, the property of molecular chaos must be there for the initial distribution of the gas and must be preserved by the dynamics in order for the Boltzmann equation to be a valid description. The mathematical justification of this is still an open topic of research, however.

For systems with small numbers of particles this assumption clearly breaks down because collisions between particles will intuitively act to create correlations, but

in the Boltzmann-Grad limit[1] the probability of two preselected particles colliding diminishes, allowing the assumption to be made. This is ultimately responsible for the time asymmetry that allowed Boltzmann to discover his famous H-Theorem of 1872, which appeared to predict an increase in entropy from apparently reversible microscopic dynamics. This observation has become known as Loschmidt's paradox.

At this stage instead of talking about the one particle probability distribution $P(\mathbf{x}, \mathbf{v}, t)$, it becomes useful to multiply P by a constant factor to produce a one particle mass distribution function $f(\mathbf{x}, \mathbf{v}, t)$ where $f(\mathbf{x}, \mathbf{v}, t)d\mathbf{x}d\mathbf{v}$ represents the expected number of particles at time t whose position is located within a ball of radius dx centred on $\mathbf{x}$ in space, and whose velocity lies within a ball of radius dv centred on $\mathbf{v}$. Boltzmann's famous equation for a dilute gas with hard sphere interactions is

$$\frac{\partial f}{\partial t} + \mathbf{v} \cdot \nabla_{\mathbf{x}} f = Q(f, f) \tag{2.4}$$

$Q(f, f)$ is the Boltzmann collision operator (where Q is written in a bi-linear form, which we define more generally in section 2.4), and is given by

$$Q(f, f) = \int_{\mathbb{R}^3} \int_{S^+} \left(f' f'_* - f f_* \right) g\sigma(g, \Omega)\, d\mathbf{v}_*\, d\Omega, \tag{2.5}$$

where $\mathbf{g} = \mathbf{v} - \mathbf{v}_*$ is the relative velocity of colliding molecules, S^+ is the unit hemisphere, σ is the collision cross section (the area around the particle in which the centre of another particle must be within, in order for a collision to occur), and

$$\begin{aligned} f' &= f(\mathbf{x}, \mathbf{v}', t), \\ f'_* &= f(\mathbf{x}, \mathbf{v}'_*, t), \\ f &= f(\mathbf{x}, \mathbf{v}, t), \\ f_* &= f(\mathbf{x}, \mathbf{v}_*, t), \end{aligned} \tag{2.6}$$

where

[1] The Boltzmann-Grad limit is the limiting regime of the BBGKY hierarchy, where as the number of molecules $N \to \infty$, the range of interaction r satisfies $Nr^2 \to k \in (0, \infty)$. This limit is of physical relevance; for example let us consider argon, which has a Van der Waals interaction radius of the order $10^{-10}m$. For an Avagadros number $N = 10^{26}$ of particles per cubic metre, we have $N/r^2 = 10^6 m^{-2}$.

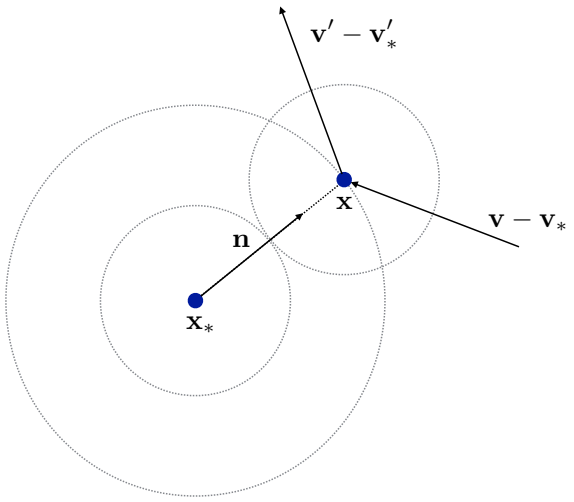

Figure 2.2: The normal vector $\mathbf{n}$ bisects the pre and post relative collision velocities.

$$\mathbf{v}' = \mathbf{v} - \mathbf{n}\,(\mathbf{n}\cdot\mathbf{g}) \qquad \mathbf{v}'_* = \mathbf{v}_* + \mathbf{n}\,(\mathbf{n}\cdot\mathbf{g})\,. \tag{2.7}$$

are the post collision velocities. For simplicity we will restrict our consideration to the hard-sphere interaction model, which has a collisional cross-section given by $\sigma = d^2/4$, where d is the molecular diameter. This interaction model gives a reasonably accurate description of rarefied gas flows, and in general is considered to be a good compromise between simplicity and accuracy (Hadjiconstantinou [2006]).

Derivations of the Boltzmann Equation, both heuristic and rigorous can be found in many statistical mechanics text books, and I refer the reader to Cercignani et al. [1994] for an in-depth discussion. Other general assumptions made in the derivation are that collisions in the gas are binary, the distribution function f does not change significantly during a collision and over length scales of intermolecular forces, f is constant.

2.2.1 Alternative forms of the Boltzmann equation

There are alternative ways of writing the Boltzmann equation, which we will use in subsequent chapters. One common way to write the collision operator is as an integral over an independent incoming velocity and independent post collision

velocities, with conservation of momentum and energy enforced using Dirac delta functions. This form is given by:

$$\partial_t f_1 = \int\int\int W_{12}^{34}\,(f_3 f_4 - f_1 f_2)\; d\mathbf{v}_2\, d\mathbf{v}_3\, d\mathbf{v}_4, \tag{2.8}$$

where,

$$W_{12}^{34} = \Gamma_{12}^{34}\delta(\mathbf{v}_1 + \mathbf{v}_2 - \mathbf{v}_3 - \mathbf{v}_4)\delta(v_1^2 + v_2^2 - v_3^2 - v_4^2) \tag{2.9}$$

is a collision rate function, and the velocities have been relabelled $\mathbf{v}_1 = \mathbf{v}$, $\mathbf{v}_2 = \mathbf{v}_*$, $\mathbf{v}_3 = \mathbf{v}'$, $\mathbf{v}_3 = \mathbf{v}'_*$, and $f_i = f(\mathbf{x}, \mathbf{v}_i)$. Under the linear change of variables

$$\begin{aligned} \mathbf{p} &= \mathbf{v}_1 + \mathbf{v}_2 - \mathbf{v}_3 - \mathbf{v}_4 \\ \mathbf{g} &= \mathbf{v}_2 - \mathbf{v}_1 \\ \mathbf{g}' &= \mathbf{v}_4 - \mathbf{v}_3, \end{aligned} \tag{2.10}$$

whose Jacobian has a determinant of a $1/2$, equation (2.8) becomes

$$\begin{aligned} \partial_t f_1 = \frac{1}{2}\int\int\int \Gamma(\mathbf{p}, \mathbf{g}, \mathbf{g}')\,(f_3 f_4 - f_1 f_2) \\ \times\delta(\mathbf{p})\delta\left(\left(g^2 - g'^2 + 2\mathbf{p}\cdot(\mathbf{g} + 2\mathbf{v}_1) - p^2\right)/2\right)\; d\mathbf{p}\, d\mathbf{g}\, d\mathbf{g}'. \end{aligned} \tag{2.11}$$

By using properties of the delta function, and by observing the integrand is only non-zero when $g = g'$, we can write the integration over $\mathbf{g}'$ as an integration over vectors on the unit sphere multiplied by the magnitude of $\mathbf{g}$, and equation (2.11) becomes

$$\partial_t f_1 = \frac{1}{2}\int\int \Gamma(\mathbf{g}, \Omega) g\,(f_3 f_4 - f_1 f_2)\; d\mathbf{g}\, d\Omega, \tag{2.12}$$

which we may compare with the form of the Boltzmann equation given in equation (2.5) to see that $\Gamma(g, \Omega) = 2\sigma(g, \Omega)$. Here we note it is customary to drop the subscripts from f_1 and $\mathbf{v}_1$, and refer to them simply as f and $\mathbf{v}$.

Another form of the Boltzmann equation which we will use later in this thesis, is the Boltzmann equation written in weak form. With some manipulations that rely on the the transformations (2.7) being their own inverses, it is possible to show [Cercignani et al., 1994] that for an arbitrary (well behaved) test function $\phi(\mathbf{v})$,

$$\int Q(f,f)\phi(\mathbf{v})\,d\mathbf{v} = \frac{1}{2}\int_{\mathbb{R}^3}\int_{\mathbb{R}^3}\int_{S^+} ff_*\left(\phi' + \phi'_* - \phi - \phi_*\right) g\sigma(g,\Omega)\,d\mathbf{v}_*\,d\Omega\,d\mathbf{v}. \quad (2.13)$$

If we let the test function $\phi(\mathbf{v}) = \delta(\mathbf{v}-\mathbf{c})$ then we find (with spatial homogeneity) that

$$\begin{aligned}\partial_t f(\mathbf{c},t) &= \int \delta(\mathbf{v}-\mathbf{c})\partial_t f(\mathbf{v},t)\,d\mathbf{v} \\ &= \int Q(f,f)\delta(\mathbf{v}-\mathbf{c})\,d\mathbf{v} \\ &= \frac{1}{2}\int_{\mathbb{R}^3}\int_{\mathbb{R}^3}\int_{S^+} ff_*\left(\delta' + \delta'_* - \delta - \delta_*\right) g\sigma(g,\Omega)\,d\Omega\,d\mathbf{v}_*\,d\mathbf{v}. \end{aligned} \quad (2.14)$$

This is a form of collision operator we will revisit when viewing granular gases.

2.3 Moments of the distribution function

Complete knowledge of the mass distribution function often provides a description that is more detailed than necessary or useful, and in general our interest is limited to certain moments of the distribution. Because f is the mass distribution function, it is possible to find the total mass by integrating over the whole phase space

$$M = \int_{\mathbb{R}^3}\int_{\mathbb{R}^3} f(\mathbf{x},\mathbf{v},t)\,d\mathbf{x}d\mathbf{v}. \quad (2.15)$$

The mass density is given by

$$\rho(x,t) = \int_{\mathbb{R}^3} f(\mathbf{x},\mathbf{v},t)\,d\mathbf{v}, \quad (2.16)$$

and the mean or bulk momentum is given by

$$\rho \mathbf{u}(\mathbf{x}, t) = \int_{\mathbb{R}^3} \mathbf{v} f(\mathbf{x}, \mathbf{v}, t)\, d\mathbf{v}'. \tag{2.17}$$

The internal energy of the gas may be defined as

$$\rho e(\mathbf{x}, t) = \frac{1}{2} \int_{\mathbb{R}^3} |\mathbf{c}|^2 f(\mathbf{x}, \mathbf{v}, t)\, d\mathbf{v}' \tag{2.18}$$

where $\mathbf{c} = \mathbf{v} - \mathbf{u}$ is the molecular velocity relative to the local mean velocity.Pressure is related to the internal energy of the gas by the ideal gas law $p = \rho RT$, where R is the ideal gas constant, and the relationship $e = 3/2RT$ for monatomic gases. Other moments of physical relevance include the pressure tensor p_{ij} and heat flux q_i, which are given by

$$p_{ij} = \int c_i c_j f\, d\mathbf{v}, \qquad q_i = \int c_i |\mathbf{c}|^2\, d\mathbf{v}. \tag{2.19}$$

2.4 Properties of the Boltzmann Equation

2.4.1 Collisional Invariants

Let us consider well-behaved test functions $\psi : \mathbb{R}^3 \to \mathbb{R}$. We wish to determine what functions ψ are available so that the quantity

$$\int \psi(\mathbf{v}) Q(f, f)\, d\mathbf{v} = 0. \tag{2.20}$$

To achieve this, we use a generalised bi-linear collision operator

$$Q(f, h) = \frac{1}{2} \int_{\mathbb{R}^3} \int_{S^+} \left(f' h'_* + f'_* h' - f h_* - f_* h \right) g\sigma(g, \Omega)\, d\mathbf{v}_*\, d\Omega, \tag{2.21}$$

where we notice that when we chose $h = f$ we recover the collision operator (2.5) that we defined originally. We now study the object.

$$\int \psi(\mathbf{v})Q(f,h)\,d\mathbf{v} = \frac{1}{2}\int_{\mathbb{R}^3}\int_{\mathbb{R}^3}\int_{S^+} \left(f'h'_* + f'_*h' - fh_* - f_*h\right)\psi(\mathbf{v})g\sigma(g,\Omega)\,d\mathbf{v}_*\,d\mathbf{v}\,d\Omega. \tag{2.22}$$

Interchanging starred and unstarred variables lets us rewrite this as

$$\int \psi(\mathbf{v})Q(f,h)\,d\mathbf{v} = \frac{1}{2}\int_{\mathbb{R}^3}\int_{\mathbb{R}^3}\int_{S^+} \left(f'h'_* + f'_*h' - fh_* - f_*h\right)\psi(\mathbf{v}_*)g\sigma(g,\Omega)\,d\mathbf{v}_*\,d\mathbf{v}\,d\Omega. \tag{2.23}$$

Now, because the transformation given by the collision rules (2.7) is its own inverse, exchanging the primed (post-collision) and unprimed (pre-collision) variables does not change the integral, so

$$\int \psi(\mathbf{v})Q(f,h)\,d\mathbf{v} = \frac{1}{2}\int_{\mathbb{R}^3}\int_{\mathbb{R}^3}\int_{S^+} \left(fh_* + f_*h - f'h'_* - f'_*h'\right)\psi(\mathbf{v}')g\sigma(g,\Omega)\,d\mathbf{v}'_*\,d\mathbf{v}'\,d\Omega. \tag{2.24}$$

The absolute value of the determinant of the Jacobian of the transformation (2.7) is unity, so we are free to replace $d\mathbf{v}'_*\,d\mathbf{v}'$ by $d\mathbf{v}_*\,d\mathbf{v}$, hence

$$\int \psi(\mathbf{v})Q(f,h)\,d\mathbf{v} = \frac{1}{2}\int_{\mathbb{R}^3}\int_{\mathbb{R}^3}\int_{S^+} \left(fh_* + f_*h - f'h'_* - f'_*h'\right)\psi(\mathbf{v}')g\sigma(g,\Omega)\,d\mathbf{v}_*\,d\mathbf{v}\,d\Omega. \tag{2.25}$$

Finally, we may swap the starred and unstarred variables in (2.25) to obtain

$$\int \psi(\mathbf{v})Q(f,h)\,d\mathbf{v} = \frac{1}{2}\int_{\mathbb{R}^3}\int_{\mathbb{R}^3}\int_{S^+} \left(fh_* + f_*h - f'h'_* - f'_*h'\right)\psi(\mathbf{v}'_*)g\sigma(g,\Omega)\,d\mathbf{v}_*\,d\mathbf{v}\,d\Omega. \tag{2.26}$$

Combining (2.22), (2.23), (2.25) and (2.27), and setting $h = f$, we see that

$$\int \psi(\mathbf{v})Q(f,f)\,d\mathbf{v} = \frac{1}{4}\int_{\mathbb{R}^3}\int_{\mathbb{R}^3}\int_{S^+} \left(f'f'_* - f_*f\right)\left(\psi(\mathbf{v}_*) + \psi(\mathbf{v}_*) - \psi(\mathbf{v}') - \psi(\mathbf{v}'_*)\right) g\sigma(g,\Omega)\,d\mathbf{v}_*\,d\mathbf{v}\,d\Omega. \tag{2.27}$$

Consequently, it is clear that the collision operator vanishes when

$$\psi(\mathbf{v}'_*) + \psi(\mathbf{v}') = \psi(\mathbf{v}_*) + \psi(\mathbf{v}) \tag{2.28}$$

for all $\mathbf{v}$, $\mathbf{v}_*$, $\mathbf{v}'$, $\mathbf{v}'_*$ satisfying Equation (2.7). This can only be satisfied if $\psi(\mathbf{v}) = a + \mathbf{b}\cdot\mathbf{v} + c\,|\mathbf{v}|^2$, for arbitrary constants $a, c \in \mathbb{R}$, $\mathbf{b} \in \mathbb{R}^3$, the proof of which may be found in [Cercignani et al., 1994]. Therefore, elements of the linearly independent set $\psi = \left\{1, \mathbf{v}, |\mathbf{v}|^2\right\}$ are known as the *collisional invariants*.

2.4.2 Conservation

An elementary property that is required of a collision operator, which models elastic hard sphere interactions, is for it to respect the conservation of mass, momentum and energy. If we take the derivative of the density, ρ, with respect to time it can be seen that

$$\begin{aligned}\frac{\partial\rho}{\partial t} + \frac{\partial}{\partial x_i}(u_i\rho) &= \int \frac{\partial}{\partial t} f(\mathbf{x},\mathbf{v},t)\,d\mathbf{v} + \frac{\partial}{\partial x_i}(u_i\rho)\\ &= \int -v_i\frac{\partial}{\partial x_i} f(\mathbf{x},\mathbf{v},t) + Q(f,f)\,d\mathbf{v} + \frac{\partial}{\partial x_i}(u_i\rho)\\ &= -\frac{\partial}{\partial x_i}\int v_i f(\mathbf{x},\mathbf{v},t)\,d\mathbf{v} + \frac{\partial}{\partial x_i}(u_i\rho) = 0.\end{aligned}$$

where we have used the fact that 1 is a collisional invariant and have assumed that f decays quickly at infinity. Similarly one can show that taking time derivatives of the momentum and energy

$$\partial_t(\rho u_j) + \frac{\partial}{\partial x_i}(\rho u_i u_j + p_{ij}) = 0, \tag{2.29}$$

$$\partial_t\left(\frac{1}{2}\rho\,|u|^2 + \rho e\right) + \frac{\partial}{\partial x_i}\left(\rho v_i\left(\frac{1}{2}\,|u|^2 + e\right) + v_j p_{ij} + q_i\right) = 0, \tag{2.30}$$

which we supply a full derivation of in the Appendices. Because the time derivatives of these quantities can be written as a divergence, the Divergence Theorem enforces that when these quantities are integrated over the spatial domain, they are conserved when there are no fluxes at the boundaries.

2.4.3 Equilibrium and the H-Theorem

Classical statistical mechanics dictates that if the system is closed, and the distribution is stationary, i.e. there are no net fluxes in the system then the particle distribution function should be described by the Maxwell-Boltzmann distribution

$$f_{MB} = \frac{\rho}{(2\pi RT)^{3/2}} \exp\left(\frac{-(\mathbf{v}-\mathbf{u})^2}{2RT}\right) \tag{2.31}$$

named after both James Clerk Maxwell and Ludwig Boltzmann. If $\mathbf{u} = \mathbf{u}(x,t)$, $\rho = \rho(x,t)$ or $T = T(x,t)$ then $f_{MB}(\mathbf{x},\mathbf{v},t)$ is said to be a *local Maxwellian*. It can be shown that

$$Q(f,f) = 0 \iff f = f_{MB} \tag{2.32}$$

and so the only stationary distribution is the equilibrium Maxwell-Boltzmann distribution. Boltzmann's famous H-Theorem is established when considering the quantity $f \log f$. Combined with Equation (2.5) we see that

$$\partial_t \mathcal{H} + \nabla_x \cdot \mathbf{J}_{\mathcal{H}} = S \tag{2.33}$$

where

$$\mathcal{H} = \int f \log f \, dv \tag{2.34}$$

$$\mathbf{J}_{\mathcal{H}} = \int \mathbf{v} f \log f \, dv \tag{2.35}$$

$$S = \int \log f Q(f,f) \, dv. \tag{2.36}$$

It can be shown that $S \leq 0$, and using the result at the end of §1.3.1 we see that $S = 0 \iff f = f_{MB}$. If we assume spatial homogeneity of f, then we see $\mathcal{H}$ is a

functional that decays in time and is strictly bounded below by f_{MB}. This is what has become known as Boltzmann's H Theorem. It would be tempting to conclude from this that as $t \to \infty$ $f_0 \to f_{MB}$, but strictly mathematically this is not the case as it presupposes the global existence of solutions for a range of initial data. This is dealt with by Arkeryd [1972]. When considering the spatially heterogeneous case, this adds an extra layer of complexity, and considerations such as the boundary conditions need to be considered. A detailed discussion of the subject can be found in the lecture notes authored by Cercignani and Sattinger [1998].

The significance of the H theorem is that seemingly from a collision process which is fundamentally time reversible, there is a function of the state space $\mathcal{H}$ that decreases in time. That is, a direction of time emerges. There is an analogy to be drawn between $\mathcal{H}$ and the Shannon entropy of thermodynamics, so one might be tempted to claim that the 2nd law of thermodynamics has been proved from the dynamics of the particles. However, this is not the case as a direction of time has been introduced implicitly by assuming the molecular chaos assumption Equation (2.3).

2.5 Existence of solutions

Before describing methods for numerically finding solutions to the integro/differential equations (2.4)-(2.5), it is important to briefly mention what is known mathematically about the solutions. At the time of writing, there is no global existence (or uniqueness) proof, of solutions to the classical Boltzmann equation [Alexandre et al., 2011]. However, rigorous mathematical treatment of the Boltzmann equation goes back to David Hilbert, and so I will briefly mention some of the more significant results. Carleman [1933] first proved existence and uniqueness of solutions in the spatially homogeneous setting with radial initial data. Later, Ukai et al. [1974] proved existence of global solutions to the spatially dependent problem for initial data close to equilibrium. DiPerna and Lions [1989] established global weak solutions for initial data without size restrictions, by considering collision kernels with an angular cut-off. This was the first global existence result for the Boltzmann equation which contributed to Pierre-Louis Lions being awarded a Fields Medal in 1994. The latest significant development was a proof showing global existence and uniqueness for collision kernels that model long range interactions, without any angular cut-offs ([Gressman and Strain, 2011]).

However despite being in consideration for over a century, existence and uniqueness in general remains an open problem in the field of the analysis of PDEs, and seems to be as challenging as establishing existence and uniqueness of global solutions to the Navier-Stokes equations. Nevertheless, just as for the Navier-Stokes equations it appears that if there are initial conditions for which global solutions do not exist, these are likely to be a set of zero measure or at least so small as to not be of practical concern.

2.5.1 Direct numerical solutions

The Boltzmann equation is a fundamentally harder equation to solve numerically than the Navier-Stokes-Fourier equations, not only because the solution is defined over a six (plus one) dimensional state space, but because the collision operator is an integration over 5 dimensions. To illustrate this, suppose you wished to find the unsteady solution to the Boltzmann equation with a conventional computational fluid dynamics method, such as a finite difference or finite element method, and were to discretise each dimension into 100 points. This would require a grid of10^{14} points. To update the distribution at each point, the collision integral is required to be evaluated, so a sum must be taken over each of the 10^{14} points, where each term is itself a sum over all the collision parameters, with no apriori guarantee that the resulting distribution conserves the collisional invariants. The only such methods that rely on CFD approaches are based upon the Nordsieck, Hicks and Yen 1969, 1970 type method, which employs finite differences for the transport terms on the left hand side of the equation, and employs Monte-Carlo sampling to evaluate the collision integral. This method was successfully applied to one-dimensional steady flow problems (Hicks et al 1972) and was developed further by Aristov and Tcheremissine who applied the method to two-dimensional steady problems.

A different type of deterministic solver was created by Goldstein et al. [1989] who developed a method that is now known as the *discrete velocity method* (DVM). The method works by discretising the velocity space, allowing the Boltzmann equation to be written as a set of non-linear hyperbolic differential equations. This effectively allows the construction of discrete collision mechanics at the nodes of the discretisation. The method was then developed by, however in all cases, the computational cost is effectively of order MN^6 where N is the number of discrete velocities in each velocity direction, and M is the number of discretisations used to perform the angular integration, and typically $M \sim N^{1/3}$. It should be noted that the choice of discrete velocities which allow the DVM to be conservative means that the order

of accuracy is lower than that obtained by using a standard quadrature [Filbet and Russo, 2004]. The computational expense required for a fully 3D solution is still prohibitive, however recently Mouhot et al. [2013] have created a method based on the DVM procedure that has a computational complexity of order $\hat{N}^3 N^3 \log N$ where numerical evidence suggests that $\hat{N}$ can be taken very small in comparison to N, which greatly reduces the computational costs. In theory this method is very well suited to low speed near continuum flows as it allows the discretisation to be coarser without sacrificing accuracy, although in the transition and continuum regimes their solutions are yet to be well validated [Venugopal and Girimaji, 2015].

2.6 Continuum methods

2.6.1 The Chapman-Enskog expansion and Burnett equations

In this section I will briefly discuss the Chapman-Enskog expansion of the collision operator, which will demonstrate how it is possible to derive macroscopic transport equations from the Boltzmann equation. As we saw in §2.4.2, it is possible to derive macroscopic conservation laws from the Boltzmann equation. By themselves, these conservation laws do not represent macroscopic transport equations as alone they are not a closed set of equations; p_{ij} and q need to be described in terms of the other macroscopic quantities. The Chapman-Enskog expansion allows one to close the conservation equations by expanding the distribution function in increasing powers of the Knudsen number. Let $\epsilon = \mathrm{Kn}$, then the Chapman-Enskog expansion is obtained by writing

$$f = f^{(0)} + \epsilon f^{(1)} + \epsilon^2 f^{(2)} + \dots \tag{2.37}$$

Omitting many of the details, which one may find in [Struchtrup], because the zeroth term has no Kn dependence f_0 is forced to be a local Maxwellian with the same mass, momentum and temperature as f. Every non-invariant moment of the distribution function can be found in terms of contributions from the moments of the expanded functions of f, i.e.

$$p_{ij} = p_{ij}^{(0)} + \epsilon p_{ij}^{(1)} + \epsilon^2 p_{ij}^{(2)} + \dots \tag{2.38}$$

$$q_i = q_i^{(0)} + \epsilon q_i^{(1)} + \epsilon^2 q_i^{(2)} + \dots \tag{2.39}$$

If the series is truncated at zeroth order, $f = f_{MB}$, $p_{ij} = p = 2/3\rho e$ $q_i = 0$, then the closed set of macroscopic transport equations that is attained are the well known compressible Euler Equations

$$\partial_t \rho + \nabla \cdot \rho v = 0 \tag{2.40}$$

$$\partial_t u + (u \cdot \nabla)\, u + \frac{1}{\rho}\nabla p = 0 \tag{2.41}$$

$$\partial_t T + (u \cdot \nabla)\, T + \frac{2}{3} T\, \nabla \cdot v = 0 \tag{2.42}$$

If instead, the series is truncated at first order, we see that the stress (the deviatoric part of the pressure tensor p_{ij}) and the heat flux are given by

$$\sigma_{ij} = -2\mu \frac{\partial u_i}{\partial x_j} \quad \text{and} \quad q_i = -\kappa \frac{\partial T}{\partial x_i} \tag{2.43}$$

which are the Navier-Stokes law and Fourier Law respectively, with viscosity and heat conductivity

$$\mu = \mu_0 \left(\frac{T_0}{T}\right)^{\omega} \qquad \kappa = \frac{15}{4}\mu \tag{2.44}$$

(where μ_0 is the viscosity at a reference temperature T_0, and $\omega = (\gamma+3)/(2\gamma-2)$) which leads to the experimentally verified Prandtl number $Pr = 2/3$.

It is clear that for large enough Knudsen numbers a level of decryption beyond the NSF equations is required. This is what the Burnett (expansion to second order in Kn) and the super Burnett equations (expansion to 3rd order Kn) attempt to obtain. However, the closure of the Chapman-Enskog expansion at these orders of Knudsen number have been shown by Bobylev [1982] to be unstable, so that small oscillations will blow up in time. Because of this, they have limited practical use.

2.6.2 Moment Methods

Despite the success of the Chapman-Enskog expansion in deriving the Navier-Stokes and Fourier Laws, higher order expansions such as the Burnett and super Burnett equations, are demonstrably unstable, and as such have limited practical use. An alternative class of methods known, as *moment methods* attempt to

derive macroscopic transport equations from sets of predetermined moments of the distribution function. The most famous of these uses the set of 13 moments $\{\rho, \mathbf{u}, e, \sigma_{ij}, \mathbf{q}\}$, was first preposed by Grad [1949] . The basic idea is to write the distribution function as a series of Hermite polynomials where the coefficients depend only on the set of moments. By doing this, the conservation laws can be closed in such a way that makes the resulting set of macroscopic equations unconditionally stable. However, problems arise for larger Mach numbers where solutions to the equations develop unphysical discontinuous shock profiles. Attempts have been made to regularise the equations, resulting in a new set of equations the R13 equations, where shock profiles are continuous at all Mach numbers, however this leads to difficulties that arise when choosing boundary conditions. This procedure has also been applied to a larger set of moment, giving the R26 equations [Gu et al., 2014], which are accurate up to the same order as the Burnett equations.

2.6.3 Direct Simulation Monte-Carlo

As it stands today, the *Direct Simulation Monte Carlo* (DSMC) method provides the benchmark for calculations of rarefied flows. It was initially developed by G.A. Bird during the 1960s and 1970s ([Bird, 1976], [Bird, 1978], [Bird, 1994]), and was primarily used for aerospace and hypersonic applications. It has also found success in modelling detonations (Sharma et al. [2002]). What makes it especially attractive is not only its theoretical underpinning (Wagner [1992]), and its excellent agreement with experiment (Oran et al. [1998]), but also the intuitive and relatively simple way that it can be understood.

It is a stochastic process that is derived directly from the collision rules, and as such the method has a computational complexity of order N, where N is the number of stochastic particles used. Each simulated particle represents a certain number of particles n of the real gas that is to be modelled, and has a position $\mathbf{x_i}$ and velocity $\mathbf{v_i}$. The position and velocity of each particle are updated during the simulation so that at any point $t \in [0, T]$ they are distributed according to $\hat{f}$ in the phase space $(\mathbf{x}, \mathbf{v})$, where $\hat{f}$ is an approximate solution to the Boltzmann equation.

The spatial domain is partitioned into computational cells from which averages are obtained to create estimates for ρ, $\mathbf{u}$ and T at the centre point of each cell. That is, for cell k

$$\rho_k = m \sum_{i=1}^{N} \delta_k(x_i) \tag{2.45}$$

$$\mathbf{u}_k = \frac{1}{\rho_k} \sum_{i=1}^{N} \mathbf{v}_i \delta_k(x_i) \tag{2.46}$$

$$T_k = \frac{1}{3k_B\rho_k} \sum_{i=1}^{N} (\mathbf{u}_i - \mathbf{v}_i)^2 \delta_k(x_i), \tag{2.47}$$

where the membership delta function δ_k returns 1 when particle i is in cell k, and 0 otherwise.Time is discretised and the evolution of $(\mathbf{x}_i, \mathbf{v}_i)$ for each particle is split into two parts

$$\frac{\partial f}{\partial t} = \frac{\partial f}{\partial t}|_{\text{move}} + \frac{\partial f}{\partial t}|_{\text{coll}}, \tag{2.48}$$

where

$$\frac{\partial f}{\partial t}|_{\text{move}} = -v \cdot \Delta_x f \tag{2.49}$$

describes the effect of free motion of the particles, which is computationally accounted for by the advection of each particle so that $\mathbf{x}^i = \mathbf{x}^i + \Delta t \mathbf{v}^i$. In order to take the $\frac{\partial f}{\partial t}|_{\text{coll}}$ term into account the following collision procedure is conducted. Considering a computational cell containing a certain number of representative particles, the probability of collision for a given pair is given by

$$P = F_N \sigma_T c \Delta t / V_c, \tag{2.50}$$

where F_N is the particle weight, σ is the collisional cross-section, c is the relative speed of the sample pair, and V_c is the cell volume. If there are N particles in a particular cell, then this would result in $\sim N^2$ possible collision pairs from which to sample. In order to alleviate this problem, Bird's No Time Counter method allows this to be done in order N time. The maximum collision probability is estimated as

$$P_{\max} = F_N \left(\sigma c\right)_{\max} \Delta t / V_c, \tag{2.51}$$

where $(\sigma c)_{\max}$ is a parameter of the calculation, chosen ahead of time. Then the total number of pairs to check is

$$\frac{1}{2} N \bar{N} F_N (\sigma c)_{\max} \Delta t / V_c, \tag{2.52}$$

and the probability of collisions is

$$P = \frac{\sigma c}{(\sigma c)_{\max}}, \tag{2.53}$$

so for a given pair, a uniformly distributed random number between 0 and 1 is chosen and should that random number be less than P, the particles are assigned new velocities according to the collision model. This procedure was shown by Wagner to generate solutions that approach the solutions to the full non-linear Boltzmann Equation in the limit of diminishing cell size, time step, and infinite number of particles. This operator splitting has been shown to be second order accurate in time, and also second order accurate in space.

The DSMC algorithm has proved very effective and has been extended to include chemical reactions, mixtures of gases and polyatomic effects. However it suffers from two main problems. The first is that as $\mathrm{Kn} \to 0$, the number of required collisions grows like Kn^{-1}. This stiffness is problematic when, for example, coupling DSMC to a Navier-Stokes solver for the purpose of multi-scale problems (Radtke et al. [2012]). Another problem is the large relative statistical noise present in solutions to low-speed flows, which we will discuss further in Chaper 4.

2.7 Approximations

2.7.1 Linearised Boltzmann

If one assumes that the distribution function f is very close to a Maxwellian distribution f_{MB} then it is possible to obtain the linearised Boltzmann equation. This assumption is clearly only valid then for low Mach number flows. If the distribution function is written as

$$f = f_{MB} + f_{MB}^{1/2} h, \tag{2.54}$$

where h is an unknown function, then the linearised Boltzmann collision operator is given by

$$Lh = 2f_{MB}^{-1/2} Q(f_{MB}^{1/2} h, f_{MB}). \tag{2.55}$$

This form of the linearisation means that in simple cases variational principals can be used to find approximate solutions.

2.7.2 BGK Collision Operator

The challenges involved in directly generating numerical solutions to the full-non linear Boltzmann-Equation have made it desirable to find equations that are able to reproduce the rich and diverse behaviour captured by the Boltzmann equation, but do not suffer from the same high computational costs. The most famous of these is the BGK collision operator named after Bhatnagar et al. [1954], and is given by

$$\partial_t f + \mathbf{v} \cdot \nabla_{\mathbf{x}} f = \frac{1}{\tau_{BGK}} \left(f_{MB}(v; c, T) - f(x, v, t) \right), \tag{2.56}$$

where the local Maxwellian f_{MB} has the same density, bulk velocity and temperature as $f(x, v, t)$, and τ_{BGK} is the relaxation time. It would be fair to mention that Welander [1954] independently preposed the same model at roughly the same time. The effect the BGK collision operator (on the right hand side of Equation (2.56)) has on f is to exponentially relax it towards the local Maxwellian distribution, and hence in the phonon, electron and radiative transport literature it is known as the relaxation time approximation model [Chen, 2005].

It has many of the desired properties of a collision operator. Firstly, the time derivative of f is zero if and only if $f = f_{MB}$, it conserves mass, momentum and energy, and has an H-Theorem. On first inspection it appears that the BGK collision operator is linear in f, however because f_{MB} depends on the moments on f it retains the property of non-linearity. The BGK collision operator is predominantly used to make the calculation of the collision operator easier in deterministic solutions for the evolved PDE. It is also used to provide closures to Chapman-Enskog expansion, where calculations of the full non-linear Boltzmann equation have to be performed numerically.

However, the Prandtl number (the non-dimensional ratio of mass to heat diffusivity) is $Pr = \mu/\kappa c_p = 1$ for the BGK operator, whereas for the Boltzmann equation $Pr = 2/3$ (which agrees well with experiment) . This means that the relaxation time τ can be adjusted in order to gain the correct viscosity μ or the correct thermal conductivity κ, but both correct values cannot be satisfied simultaneously. Usually the relaxation time τ is set to give the correct viscosity and so this model is predominantly used for isothermal flows.

Modifications to BGK operator can be applied in order to alleviate this problem. These modifications generally involve either modifying the collision frequency so that $\tau = \tau(\mathbf{v})$ which changes the local density, bulk velocity and temperature of the local Maxwellian, or by making direct alterations to the local Maxwellian (called ES, or ellipsoidal statistical models). A problem with this type of modification is that in general it is difficult to produce H-Theorems for the resulting models.

2.8 Summary

This chapter has provided a brief history and overview of rarefied gases and classical kinetic theory, as well the numerical methods employed to find approximate solutions. Inevitably for such a large subject area, certain areas have remained untouched in this background chapter. For a more in depth discussion of some of the topics discussed in this section, and on those not touched upon, for example the treatment of poly-atomic gases and mixtures, and alternative collision models, the reader is directed to the text books [Bird, 1994; Cercignani et al., 1994]. In the next chapter, the Fokker-Planck gas kinetic collision operator will be introduced.

3

The Fokker-Planck gas kinetic equation

"Truth... is much too complicated to allow anything but approximations."
– John von Neumann

3.1 The Fokker-Planck collision operator

An alternative approximation collision operator to the Boltzmann collision operator, is the Fokker-Planck collision operator, which is the focus of this thesis, and was first considered (to my current knowledge) as an appropriate collision operator for a rarefied gas by Lebowitz et al. [1960]. Originally it was proposed to model the motion of a Brownian particle in a fluid [Chandrasekhar, 1943], but later it was shown to be more widely applicable to liquids and plasmas [Cowling and Chapman, 1960]. I include two derivations of the Fokker-Planck collision operator, the first derivation uses a linear form of the Boltzmann Equation in the context of a Raleigh gas [Chang et al., 1970], the second method considers change of distribution caused by the mechanics of a Brownian particle interacting with a gas in a heat bath [Green, 1951], in Appendix A and Appendix B respectively. In both cases, the fundamental assumption that allows for the collision operator to be constructed is that collisions deflect the colliding particles by small amounts, which can be considered to be a grazing collision limit. The term Fokker-Planck is synonymous with the Kolmogorov forward equation, and can be placed in the class of advection-diffusion operators. As such the operator can be understood as a diffusion process in velocity space, with advection (sometimes referred to as drift).

The Fokker-Planck collision operator is given by

$$\frac{\partial f}{\partial t} + \mathbf{v} \cdot \nabla_{\mathbf{x}} f = \Phi(f), \tag{3.1}$$

where

$$\Phi(f) = \nabla_{\mathbf{v}} \cdot \mathbf{J}(f) \tag{3.2}$$

and

$$\mathbf{J}(f) = \frac{1}{\tau_{FP}} \Big[\mathbf{c} f + \frac{kT}{m} \nabla_{\mathbf{v}} f \Big], \tag{3.3}$$

and, τ_{FP} is the relaxation time and $\mathbf{c}$ is the relative molecular speed. The collision operator is formed from two parts. The first that appears is the drift term, which on it's own has the effect of advecting the density of the distribution towards its mean. This dissipates energy, and can be thought of as a source of friction. The second term, the diffusive term which is temperature dependent, creates enough energy to balance exactly the energy dissipated by the drift term, as we shall see in the next section.

A fully 3-dimensional direct numerical solution based on quadrature methods is still prohibitively expensive, again, due to the dimensionality of the problem. As such, this model received minimal attention in the literature, one notable exception is Cercignani et al. [1994]. However, recently this model has been receiving more attention due to a new numerical scheme devised by Jenny et al. [2010b]. Before outlining this scheme, we will first discuss some of the model's properties.

3.2 Properties of the Fokker-Planck collision operator

Recent contributions regarding the Fokker-Planck gas kinetic collision operator largely consists of work by Jenny's group at EHT Zurich. This literature included numerical schemes and extension to correct the Prandtl number [Jenny et al., 2010b,a], extensions to diatomic molecules [Gorji and Jenny, 2013] and mixtures [Gorji and Jenny, 2012], and a hybrid scheme where a Fokker-Planck solution is coupled to DSMC [Gorji and Jenny, 2015]. In the latter paper they make reference to Bogo-

molov and Dorodnitsyn [2011] where the Fokker-Planck model is obtained in the low Kn limit of the Boltzmann equation written as a Skorohod-type SDE. This approach relies on the assumption that a certain class of non-linear Markovian jump processes can propagate molecular chaos, which is still an open problem [Mischler and Mouhot, 2013]. In any case, the properties of the collision operator appear as statements without proof in the later literature, with references to the older literature. However a review of the older literature shows demonstrations of such properties missing, assuming that properties like conservation and the H-Theorem follow directly through their derivations. This is not immediately clear, and so therefore in this section I will show that the Fokker-Planck collision operator has the desired properties required of such an operator directly.

3.2.1 Conservation

Conservation follows from the invariance of the collision operator with respect to the set of quantities $\psi = \left\{1, \mathbf{v}, |\mathbf{v}|^2\right\}$. It is immediate that

$$\int \Phi(f)\, d\mathbf{v} = \int \nabla \cdot \mathbf{J}\, d\mathbf{v} = 0, \tag{3.4}$$

by using Gauss's Theorem and the fact that f and its derivatives must decay fast enough for the density ρ to be finite, and so Φ conserves mass. Similarly, conservation of momentum also follows from Gauss's Theorem:

$$\begin{aligned}
\int v_i \Phi(f)\, d\mathbf{v} &= -\int J \cdot \nabla v_i\, d\mathbf{v} && (3.5)\\
&= -\int (v_i - u_i) f + \frac{kT}{m} \nabla \cdot (\mathbf{e}_i f)\, d\mathbf{v} && (3.6)\\
&= \frac{kT}{m} \int \nabla \cdot (\mathbf{e}_i f)\, d\mathbf{v} && (3.7)\\
&= 0, && (3.8)
\end{aligned}$$

where $\mathbf{e}_i$ is a unit vector in the i^{th} direction, and so momentum is also conserved. Finally, conservation of energy is a result of the balance between the energy generated from the relaxation towards the mean velocity, and energy dissipated by the diffusion operator:

$$\int |v|^2 \Phi(f)\, d\mathbf{v} = -\int J \cdot \nabla |\mathbf{v}|^2 \, d\mathbf{v} \tag{3.9}$$

$$= -2\int (|\mathbf{v}|^2 - |\mathbf{u}|^2) f + \frac{kT}{m}\mathbf{v} \cdot \nabla f \, d\mathbf{v} \tag{3.10}$$

$$= -6\frac{kT}{m} - 2\frac{kT}{m}\left(-\int f \nabla \cdot \mathbf{v}\, d\mathbf{v}\right) \tag{3.11}$$

$$= -6\frac{kT}{m} + 6\frac{kT}{m} = 0, \tag{3.12}$$

which gives the desired result.

3.2.2 Equilibrium and an H-Theorem

It is trivial to check that in a closed system, the collision operator vanishes if and only if the distribution function is Maxwellian. An H-Theorem, however, is missing from the literature. For simplicity, and without any loss of generality assume that the mean velocity $\mathbf{u} = 0$, the density $\rho = 1$, the relaxation time $\tau = 1$. Also, for simplicity we assume that the distribution is spatially homogeneous. We consider the time derivative of the entropy-like macroscopic variable S,

$$\begin{aligned}
\frac{dS}{dt} &= \frac{d}{dt}\int f \log f \, d\mathbf{v} \\
&= \int \partial_t f (\log f + 1)\, d\mathbf{v} \\
&= \int (\log f + 1) \nabla \cdot \mathbf{J} \, d\mathbf{v} \\
&= -\int \mathbf{J} \cdot \nabla (\log f + 1)\, d\mathbf{v} \\
&= -\int \mathbf{J} \cdot \frac{\nabla f}{f}\, d\mathbf{v} \\
&= -\int (\mathbf{v} f + RT \nabla f) \cdot \frac{\nabla f}{f}\, d\mathbf{v} \\
&= -\int \mathbf{v} \cdot \nabla f + RT \frac{|\nabla f|^2}{f}\, d\mathbf{v} \\
&= \int f \nabla \mathbf{v}\, d\mathbf{v} - RT \int \frac{|\nabla f|^2}{f}\, d\mathbf{v} \\
&= 3 - RT \int \frac{|\nabla f|^2}{f}\, d\mathbf{v}.
\end{aligned}$$

At this point it becomes useful to write $f = f_{MB} f_d$, where f_{MB} is a Maxwellian with the same temperature as f, and f_d measures the deviation from Maxwellian. Then

$$\begin{aligned} RT \int \frac{|\nabla f|^2}{f} \, d\mathbf{v} &= RT \int \frac{1}{f_{MB} f_d} \left| f_d \nabla f_{MB} + f_{MB} \nabla f_d \right|^2 \, d\mathbf{v} \\ &= RT \int \frac{1}{f_{MB} f_d} \left(f_d^2 \left| \nabla f_{MB} \right|^2 + f_{MB}^2 \left| \nabla f_d \right|^2 + 2 f_{MB} f_d \nabla f_d \cdot \nabla f_{MB} \right) \, d\mathbf{v} \\ &= RT \int \frac{f_d}{f_{MB}} \left| \nabla f_{MB} \right|^2 + \frac{f_{MB}}{f_d} \left| \nabla f_d \right|^2 + 2 \nabla f_d \cdot \nabla f_{MB} \, d\mathbf{v} \\ &= RT \int \frac{f}{(RT)^2} \left| \mathbf{v} \right|^2 + \frac{f_{MB}}{f_d} \left| \nabla f_d \right|^2 + 2 \nabla f_d \cdot \nabla f_{MB} \, d\mathbf{v} \\ &= 3 + RT \int \frac{f_{MB}}{f_d} \left| \nabla f_d \right|^2 + 2 \nabla f_d \cdot \nabla f_{MB} \, d\mathbf{v} \end{aligned} \tag{3.13}$$

By using Gauss's Theorem, it is possible to show $\int \nabla f_d \cdot \nabla f_{MB} \, d\mathbf{v} = 0$ and so

$$RT \int \frac{|\nabla f|^2}{f} \, d\mathbf{v} = 3 + RT \int \frac{f_{MB}}{f_d} \left| \nabla f_d \right|^2 \, d\mathbf{v} \geq 3 \tag{3.14}$$

with equality occurring if and only if $f_d = 1$. Putting this together with 3.13 results in the H-Theorem.

3.2.3 Prandtl number correction

Just like the BGK collision operator, a flaw of then Fokker-Planck collision operator is that it produces the incorrect Prandtl number. This is unsurprising, given the Fokker-Planck operator only utilises the first two moments of the distribution. The simplest way of correcting this is the *cubic drift model* introduced by Gorji et al. [2011]. The drift term in the original Fokker-Planck model is given by, $A = \mathbf{c} f / \tau$, and the diffusion coefficient is $D = \sqrt{RT/\tau}$. Instead, if one allows A to depend on higher order moments then

$$A = K\mathbf{c} + \gamma \left(|\mathbf{c}|^2 - 3RT \right) + \Lambda(\mathbf{c} \, |\mathbf{c}|^2 - 2\mathbf{q}/\rho), \tag{3.15}$$

where

$$\Lambda = \frac{-1}{\tau(3RT)^4\rho^3}\,|\det(\pi_{ij})| \tag{3.16}$$

and $K \in \mathbb{R}^{3\times3}$ and $\gamma \in \mathbb{R}^3$ have to be found by determining the solution to the linear equations,

$$K_{il}p_{jl} + k_{jl}p_{il} + 2\gamma_i q_j + 2\gamma_j q_i + 2\rho\Lambda\mathbb{E}[v_i v_j v_k v_k] = 0. \tag{3.17}$$

This model requires more effort computationally, and so far does not have an H Theorem, but has shown to be very accurate at resolving heat fluxes in cavity flows [Gorji et al., 2011].

3.3 SDE formulation

Recent attention to the Fokker-Planck collision operator has started to grow after the [Jenny et al., 2010b] paper was published. The novelty was that they presented an algorithm for solving the equations using particle dynamics, which has the important property that the scheme is conservative on average. This is a property that general solution schemes were lacking, which leads to an accumulation in error over time.

It is a corollary of the Feyman-Kac formula that enables us to link the Fokker-Planck equation to an equivalent stochastic differential equation.

Theorem 3.3.1 *Suppose that a, b are bounded smooth functions (a, b: $\mathbb{R}^n \to \mathbb{R}^n$). Let $X \in \mathbb{R}^n$ be the solution of the stochastic differential equation $dX(t) = a(t, X(t))dt + b(t, X(t))dW(t)$ and let*

$$f(x,t) = \mathbb{E}[\rho(X(t))|X(t_0) = x_0] = \int_{\mathbb{R}} \rho(x)P(x,t;x_0,t_0)\,dy. \tag{3.18}$$

Then the function f solves the Fokker-Planck equation

$$\partial_t f + \sum_{i=1}^{n} \frac{\partial}{\partial x_i}(a_i f) - \frac{1}{2}\sum_{i,j=1}^{n} \frac{\partial^2}{\partial x_i x_j}((bb^T)_{ij} f) = 0, \tag{3.19}$$

$$f(y,t;x,t) = \delta(x-y), \tag{3.20}$$

where δ is the Dirac-delta measure centred on zero.

Alternatively, one can show the same result using Ito's Lemma. If $\mathbf{x}$, $\mathbf{a}$ and $\mathbf{b}$ are defined as follows,

$$\mathbf{x} = \begin{pmatrix} x_1 \\ x_2 \\ x_3 \\ v_1 \\ v_2 \\ v_3 \end{pmatrix}, \quad \mathbf{a} = \begin{pmatrix} v_1 \\ v_2 \\ v_3 \\ c_1/\tau \\ c_2/\tau \\ c_3/\tau \end{pmatrix}, \quad \mathbf{b} = \begin{pmatrix} 0 & 0 & 0 & 0 & 0 & 0 \\ 0 & 0 & 0 & 0 & 0 & 0 \\ 0 & 0 & 0 & 0 & 0 & 0 \\ 0 & 0 & 0 & \sqrt{2RT/\tau} & 0 & 0 \\ 0 & 0 & 0 & 0 & \sqrt{2RT/\tau} & 0 \\ 0 & 0 & 0 & 0 & 0 & \sqrt{2RT/\tau} \end{pmatrix} \tag{3.21}$$

then (3.20) is just the Fokker-Planck kinetic equation, and so if $X = (\mathbf{X}(t), \mathbf{V}(t))$ are random variables distributed according to f then they solve the following coupled stochastic differential equation

$$d\,\mathbf{X}(t) = \mathbf{V}(t)dt \tag{3.22}$$

$$d\,\mathbf{V}(t) = \frac{1}{\tau}(\mathbf{u}(t,\mathbf{X}) - \mathbf{V}(t))dt + \sqrt{2RT(t,\mathbf{X})/\tau}\, d\,\mathbf{W}(t) \tag{3.23}$$

where stochastic derivatives are interpreted in the Ito sense, and $\mathbf{W}(t)$ is a 3 dimensional Weiner process. We can now define mean velocity and temperature by the expectations

$$\mathbf{u}(t,\mathbf{x}) = \mathbb{E}_f[\mathbf{V}(t)|\mathbf{X}(t) = \mathbf{x}] \tag{3.24}$$

$$3RT(t,\mathbf{x}) = \mathbb{E}_f[(\mathbf{u}(t,\mathbf{x}) - \mathbf{V}(t))^T (\mathbf{u}(t,\mathbf{x}) - \mathbf{V}(t)) |\mathbf{X}(t) = \mathbf{x}] \tag{3.25}$$

The advantage of having the equation in it's SDE form is that it lends itself well to numerical solution by stochastic particle methods. A stochastic particle method for this problem means finding a way to evolve a collection of stochastic particles in time $\left\{(\mathbf{X}^i, \mathbf{V}^i)\right\}_{i=1,N}$ so that in the limit of vanishing discretisation, the SDE 3.23 is recovered. Any such method will require the estimation of $\mathbf{u}$ and T, which lends itself to the grid based estimation as described in the DSMC section.

3.4 Jenny's solution scheme

Before describing the Jenny solution scheme [Jenny et al., 2010a], it is worth mentioning other discretisations of the SDEs (3.22) (3.23) and why they are inappropri-

ate. Suppose we take the Euler-Maruyama discretisation of (3.22) (3.23), leading to the set of equations

$$\mathbf{X}^i_{t+1} = \mathbf{X}^i_t + \Delta t \mathbf{V}^i_t \tag{3.26}$$

$$\mathbf{V}^i_{t+1} = \mathbf{V}^i_t - \frac{\Delta t}{\tau}\mathbf{V}^i_t + \sqrt{2RT/\tau}\Delta\mathbf{W}^i_t \tag{3.27}$$

where $\Delta\mathbf{W}^i_t$ are independent identically distributed gaussian random variables, with mean $\mathbf{0}$ and variance Δt. Let us suppose further than f is homogeneous in space, then the expected temperature

$$\mathbb{E}[3R\hat{T}_{t+1}] = \mathbb{E}[\mathbf{V}^i_{t+1}\cdot\mathbf{V}^i_{t+1}] \tag{3.28}$$

$$= (1-\Delta t/\tau)\mathbb{E}[\mathbf{V}^i_t\cdot\mathbf{V}^i_t] + 2R\hat{T}_t\mathbb{E}[\Delta\mathbf{W}^i_t\cdot\Delta\mathbf{W}^i_t]/\tau \tag{3.29}$$

$$= (1-\Delta t/\tau)\mathbb{E}[3R\hat{T}_t] + \mathbb{E}[2R\hat{T}_t]\Delta t/\tau \tag{3.30}$$

$$\neq \mathbb{E}[3R\hat{T}_t]' \tag{3.31}$$

and so the Euler-Marayuma scheme on average will not conserve the internal energy of the simulated particles. This is a pit-fall of other standard higher order SDE discretisation schemes. In contrast, the Jenny scheme is designed so that energy is conserved on average. The scheme presented in [Jenny et al., 2010a] can be summarised as follows:

$$X_i(t+\Delta t) = X_i(t) + U_i(t)\Delta t + (V_i(t)-U_i(t))\tau(1-e^{-\Delta t/\tau}) + \sqrt{B}\xi_{i,1} \tag{3.32}$$

$$V_i(t+\Delta t) = V_i(t) - (1-e^{\Delta t/\tau})(V_i(t)-U_i(t)) + \sqrt{\frac{C^2}{B}\xi_{1,i}} + \sqrt{A-\frac{C^2}{B}}\xi_{2,i},$$

where

$$A = RT(1-e^{-2\Delta t/\tau}) \tag{3.33}$$

$$B = RT\tau^2\left(\frac{2\Delta t}{\tau} - (1-e^{-\Delta t/\tau})(3-e^{-\Delta t/\tau})\right) \tag{3.34}$$

$$C = RT\tau(1-e^{\Delta t/\tau})^2 \tag{3.35}$$

Numerical studies have shown good agreement between this discretisation scheme and DSMC in examples including cavity flows and channel flows [Jenny et al., 2010b;

Gorji et al., 2011].

3.5 Discussion

In this chapter we have introduced the Fokker-Planck gas collision operator, and given a brief account of its origins. We have shown that it obeys the conservation laws and an H-Theorem, which are minimum requirements for a collision operator modelling collisions in a rarefied gas. We have described the numerical solution scheme proposed by [Jenny et al., 2010b; Gorji et al., 2011], who have shown that the model is able to efficiently produce accurate numerical results. This is because, unlike in DSMC, the collisions are not modelled explicitly. This is advantageous, especially for low Kns, because the time discretisation scheme does not require a higher resolution to account for the relative increase of number of collisions. Like DSMC, however, the numerical solution of the Fokker-Planck model is stochastic. This creates problems in low Mach number regimes, where the noise in numerical estimates drowns out the signal. In the next chapter, I will describe this problem further and propose methods which help to reduce the problem of noise.

4

Variance reduction schemes for low speed flows

"...there's plenty of room at the bottom."

– Richard Feynman, *1959*

4.1 Motivating examples

As briefly discussed in the background chapter, recent advances in engineering are allowing the construction of machines and component parts whose size can be of the order of nanometers [Karniadakis et al., 2006]. This new paradigm of technology was predicted by Richard Feynman in his 1959 lecture "There's Plenty of Room at the Bottom", where he prophesied new applications in engineering and physics at lengths beyond the micro-scale. Today, such novel fabrication methods include bulk silicon micro machining [Hoffmann and Voges, 2002], surface silicon micromachining [Lyshevski, 2013], electro discharge machining (EDM) [Dahmardeh et al., 2011] and LIGA (Lithographie Galvanoformung Abformung) [Lin et al., 2002]. Further to these examples, exciting fabrication techniques where sub-micron scale objects which are able to self-assemble are now possible (Whitesides and Grzybowski [2002], Rycenga et al. [2011], Grzelczak et al. [2010]).

One particular example of the need to model gases at the nano-scales is within hard disk drives (HDDs), where in order to compete with the performance of solid state drives (SDDs) the distances between magnetic disk and the head used to write and read from the disk has reduced to 5nm. It's crucial to the design of these heads to be able to predict the force exerted on them from the pressure distribution of

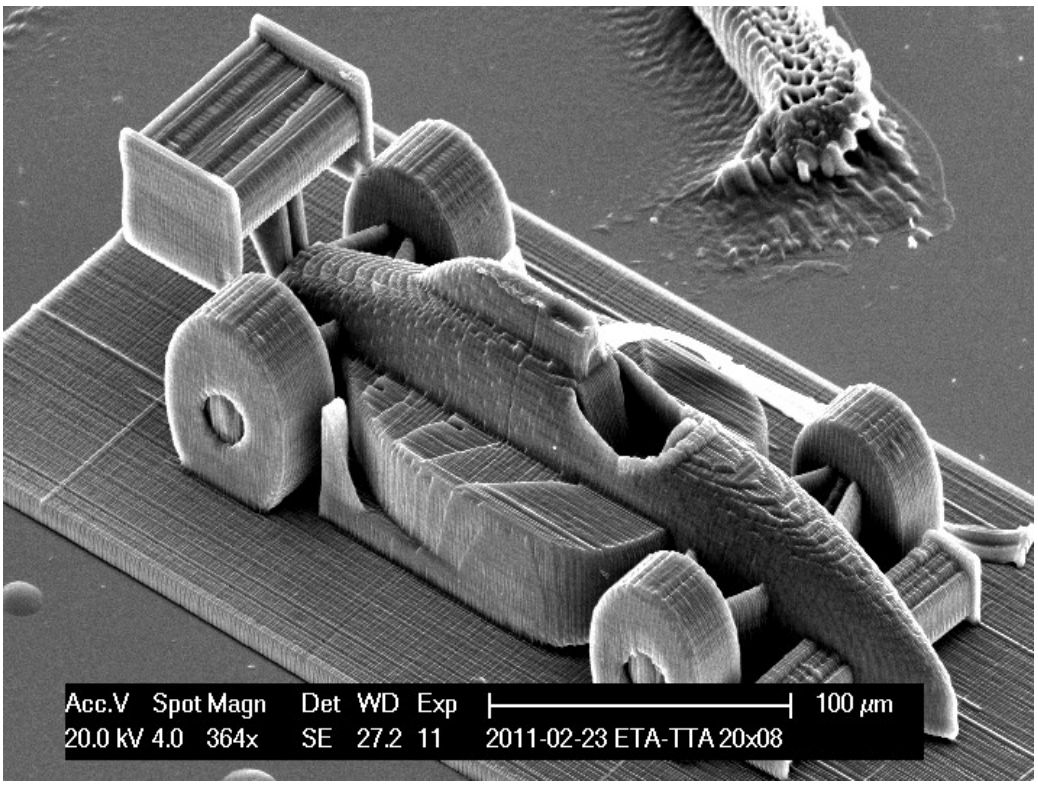

Figure 4.1: The emerging sport of micro-car racing. This model of a racing car was produced by the "two-photon lithography" technique (source: TU Vienna).

the gas [Zhou et al., 2008]. Other examples include actuators [Epstein et al., 1997], micro turbines [Waitz et al., 1998], gas chromatographs [Tian et al., 2005] and micro air vehicles (MAVs). [Fan et al., 2001].

4.2 Variance reduction for DSMC

The basic DSMC algorithm, due to it's stochastic nature, suffers from an unfavourable computational complexity for a given level of statistical error as the Mach number of the flow goes to zero [Hadjiconstantinou et al., 2003]. Recalling the definition of the Mach number from Chapter 2, $\mathrm{Ma} = c/c_0$, where c is a characteristic velocity of the flow and c_0 is the speed of sound, defined as

$$c_0 = \sqrt{\frac{\gamma k T_0}{m}}, \tag{4.1}$$

with $\gamma = c_P/c_v$ the ratio of specific heats, and that if we are close to equilibrium then the sampling error is approximately

$$\sigma_u^2 \approx \frac{kT_0}{mN}, \tag{4.2}$$

where N is the number of samples, results in the noise-to-signal ratio

$$\sigma_u/c \sim \frac{1}{\sqrt{N}\mathrm{Ma}}. \tag{4.3}$$

The absolute statistical error scales as the inverse square root of the number of independent samples, and so for a given level of uncertainty the number of samples required scales as Ma^2 as $\mathrm{Ma} \to 0$. This scaling is clearly prohibitive when considering flows when making calculations for flow fields where $\mathrm{Ma} \ll 1$.

Because of this scaling, numerical schemes that are able to reduce to variance when the Mach number is small have become highly desirable. Currently, there are two modifications developed for DSMC that have the ability to do this. The first, known as *low variance direct simulation Monte-Carlo*, or LVDSMC, works by numerically solving for the part of the distribution f_d which is a deviation from the local Maxwellian, that is

$$f_d = f - f_{MB}. \tag{4.4}$$

This type of strategy for reducing the variance was first considered by Cheremisin [2000] to be applied to the discrete velocity method for use in the limit of small Knudsen numbers where the basic DSMC algorithm becomes stiff, where the deviation from equilibrium is known to be small. However, only modest computational gains were achieved. Only later was it seen by Baker and Hadjiconstantinou [2005] that this method applies when not only for small Knudsen numbers, but also for small Mach numbers.

By considering deviations of the form of Equation (4.4) Homolle and Hadjiconstantinou [2007] were able to simulate only the deviational part of the distribution by taking advantage of a particular form of the hard-sphere linearised collision integral, linearised around a spatially varying equilibrium. Radtke and Hadjiconstantinou [2009] went on to develop the method to be used with the linearised BGK colli-

sion operator, which was followed by an algorithm for simulating the full non-linear BGK collision operator, with f_d the deviation from a global maxwellian distribution [Hadjiconstantinou et al., 2010]. More recently, Radtke et al. [2011] developed the algorithm to cope with the variable hard sphere (VHS) collision operator, linearised around a local Maxwellian. Radtke et al. [2011] went on to extend the method to also sample from the non-linear part of the distribution, but found that for moderate deviations from equilibrium, the number of particles generated by the method blows up and so the method is unstable.

In contrast, the second variance reduction scheme developed for DSMC by Al-Mohssen and Hadjiconstantinou [2010], known as VRDSMC (variance reduced DSMC), achieves a reduction in the variance of statistical samples without major changes to the original DSMC algorithm. It does this by applying an importance sampling technique, which utilises importance weights that biases the Monte-Carlo estimators to sample from an equilibrium distribution, where in theory the hydrodynamic fields are known analytically. This allows the construction of a new estimator that exploits the fact that one knows the errors associated with sampling from equilibrium, and if the original distribution is close to equilibrium, this equilibrium error will constitute the majority of the overall error.The non-trivial part of the algorithm is the evolution of the importance weights in time with the distribution f, which is achieved by considering the DSMC collision rules.

In this remaining sections of this chapter I will first outline the principle that many variance reduction schemes for simulated stochastic processes utilise, before proposing two methods that can be specifically applied to the Fokker-Planck dynamics given in the previous chapter.

4.3 General variance reduction

As found by Jenny and co-authors, the numerical solution to the Fokker-Planck equation outperforms the DSMC algorithm in terms of computational efficiency Jenny et al. [2010b]. Both schemes have a computational complexity of order N, where N is the total number of particles in the computational calculation, however the Fokker-Planck solution algorithm requires fewer operations per particle per time-step. However, because the Fokker-Planck algorithm also produces estimates that are themselves random variables, it suffers from the same unfavourable scaling of noise-to-signal ratio with Mach number as the DSMC method.

In this section we outline the general principal that both our proposed variance reductions scheme utilise. Both methods work by exploiting information about errors in estimates of known quantities. The general principal is as follows. Suppose we have a random variable X, and we wish to estimate $\mathbb{E}[X]$. Let our unbiased estimate of $\mathbb{E}[X]$ be donated by $\hat{X}$, for example the sample mean. Let Y be a different random variable with known expectation $\mathbb{E}[Y]$ with an estimator denoted by $\hat{Y}$. Then we can use the identity:

$$\mathbb{E}[X] = \mathbb{E}[X + cY] - c\mathbb{E}[Y], \tag{4.5}$$

to create a new unbiased estimator for $\mathbb{E}[X]$,

$$X_{VR} = \hat{X} + c\hat{Y} - c\mathbb{E}[Y]. \tag{4.6}$$

The variance of this estimator is

$$\mathrm{Var}[\hat{X}_{VR}] = \mathrm{Var}[\hat{X}] + c^2\mathrm{Var}[\hat{Y}] + 2c\,\mathrm{Cov}[\hat{X}, \hat{Y}], \tag{4.7}$$

and if we minimise this over possible choices of c, then minimiser $c^*$is given by

$$c^* = -\frac{\mathrm{Cov}[\hat{X}, \hat{Y}]}{\mathrm{Var}[\hat{Y}]}, \tag{4.8}$$

hence the variance for this choice of c is

$$\mathrm{Var}[\hat{X}_{VR}] = \mathrm{Var}[\hat{X}] - \frac{\mathrm{Cov}[\hat{X}, \hat{Y}]^2}{\mathrm{Var}[\hat{Y}]}. \tag{4.9}$$

The only condition required for the variance of the estimator to be less than the variance of the original estimator is for $\mathrm{Cov}[\hat{X}, \hat{Y}] > 0$, and so $\hat{X}$ and $\hat{Y}$ being dependent is a necessary condition. This is all supposing that we already know c^*, which presupposes that we already know $\mathrm{Cov}[\hat{X}, \hat{Y}]$. In reality, this is something that is not known a priori and will either have to be estimated throughout the simulation, or perhaps more practically, a rule of thumb established. Using (4.9) relies on constructing a stochastic process Y_t that stays correlated with the stochastic process X_t that we are interested in, for a large enough amount of time to take

estimates within. In the next section we propose schemes that reduce the variance of the sample mean estimators (which we refer to as the standard Monte Carlo estimators) in the Fokker-Planck simulations of rarefied gas.

4.4 Common random numbers

The first method I propose is as follows[1]. The simplest way to exploit the variance reduction given by equation (4.9) is to produce a solution to a problem where the answer is already known, in parallel to the solution we wish to reduce the variance of. If the same set of random numbers are used to produce both solutions then the solutions will be correlated, and hence we may use equation (4.9) to reduce the variance. The simplest way to produce a solution that will be correlated, and one which we know the solution of is to keep the geometry of the original problem and use the random numbers used in the simulation of the random process we are interested to simulate one where the distribution is known to be a global Maxwellian. This type of variance reduction scheme are commonly referred to as *common random numbers* schemes (CRN) [Bratley et al., 1983]. Areas where common random schemes have been employed to reduce the variance of stochastic calculations include financial mathematics [Broadie and Glasserman, 1996], simulating epidemiological models [Stout and Goldie, 2008] and optimisation [Kleinman et al., 1999].

4.4.1 Decay to equilibrium

We will demonstrate the effectiveness of this method first with a homogeneous relaxation to equilibrium, that is for a distribution where $f(t, \mathbf{x}, \mathbf{v}) = f(t, \mathbf{v})$ has no spatial component. We start from an initial distribution of particles that has normally distributed velocities, with zero mean and a standard deviation of c_0, in the 2nd and 3rd dimension, and a density in the 1st dimension made from the sum of two gaussians with means $\pm c_0$.

$$f_0(\mathbf{v}) = (1/2)\left(f_{MB}(v_1, c_0, c_0) + f_{MB}(v_1, -c_0, c_0)\right) f_{MB}(v_2, 0, c_0) f_{MB}(v_3, 0, c_0), \tag{4.10}$$

which we know to relax towards the Maxwellian distribution $f_{MB}(\mathbf{v}, \mathbf{0}, \sqrt{(4/3)c_0^2})$.

[1] During the write-up of this thesis, the author became aware that this method has been published independently [Gorji et al., 2015].

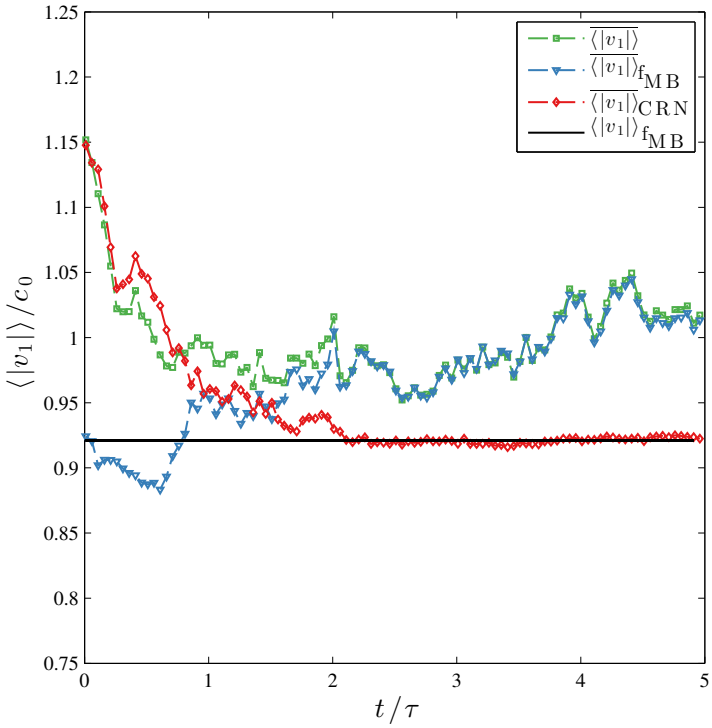

Figure 4.2: Spatially homogeneous decay to equilibrium. Green squares show standard Monte Carlo estimate, blue triangles show equilibrium solution with common random numbers, red diamonds show variance reduced estimate, black line shows theoretical value at equilibrium.

Figure (4.2) shows the results of the homogeneous relaxation towards equilibrium, with 500 particles and 500 time-steps. The results show that the CRN estimator is able to greatly reduce the variance from the standard Monte Carlo estimate. The particles in the non-equilibrium initial condition are initialised with the same random numbers as those with the equilibrium initial condition. Because they have different initial distributions, it takes a number of time-steps for the solutions to correlate fully, and so the variance reduction is stronger as time increases. In subsequent examples of the method, it is possible to initialise the particles with the same initial conditions.

4.4.2 Channel flows

In the decay to equilibrium, we considered a spatially homogeneous problem, and so keeping the position of individual particle trajectories correlated is entirely trivial. In spatially inhomogeneous problems the task is harder, as the dynamics of each particle is dependent on its position, and so it is possible that particles in both

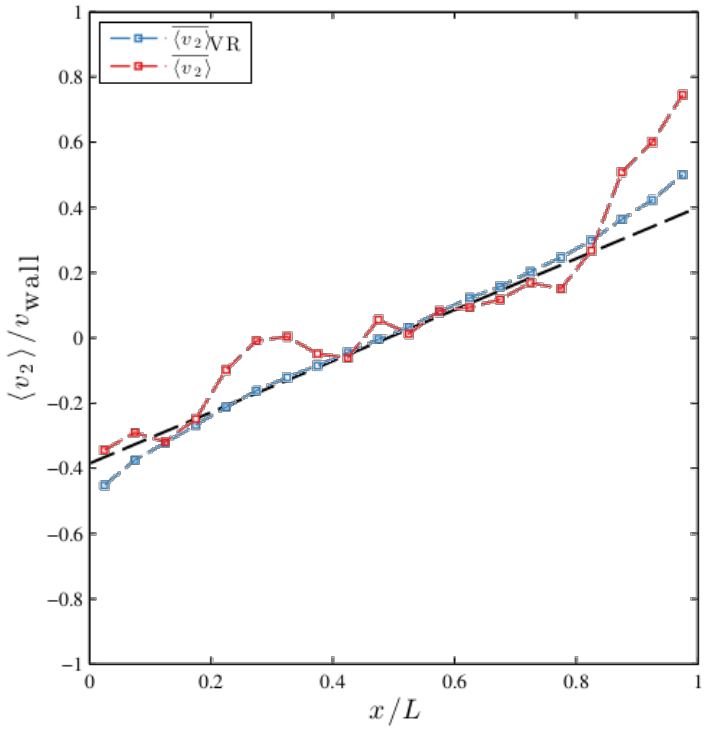

Figure 4.3: Steady state Couette flow. Red is standard Monte Carlo estimate of velocity profile across channel, blue is CRN variance reduced estimator, black dashed is Navier-Stokes profile with Maxwell boundary conditions. Kn = 1.0, $v_{\mathrm{wall}} = 0.01 c_0$.

solutions that start correlated, de-correlate over time. Uniform channel flows are flows where the fluid is bounded by gas-surface interfaces in at least one dimension, and the flow fields vary in the dimension parallel to the walls, varying with respect to the dimension perpendicular to the wall. This means that if the particles in the equilibrium and non-equilibrium solutions have the same initial conditions, then their subsequent velocities and positions in the dimension perpendicular to the walls will be identical, but we expect the velocities in the dimension parallel to the wall to differ.

Figures (4.3-4.4) show variance reduced estimators of the velocity field across thee channel of steady state planar Couette flows, for Kn = 1.0 and Kn = 0.1 respectively. For each solution 25 particles per cell were used, averages obtained from 1000 time steps. The blacked dashed lines in the figures are Navier-Stokes solutions supplemented with the standard phenomenological Maxwell boundary conditions, which provides the slip velocity at the boundary, and are given by

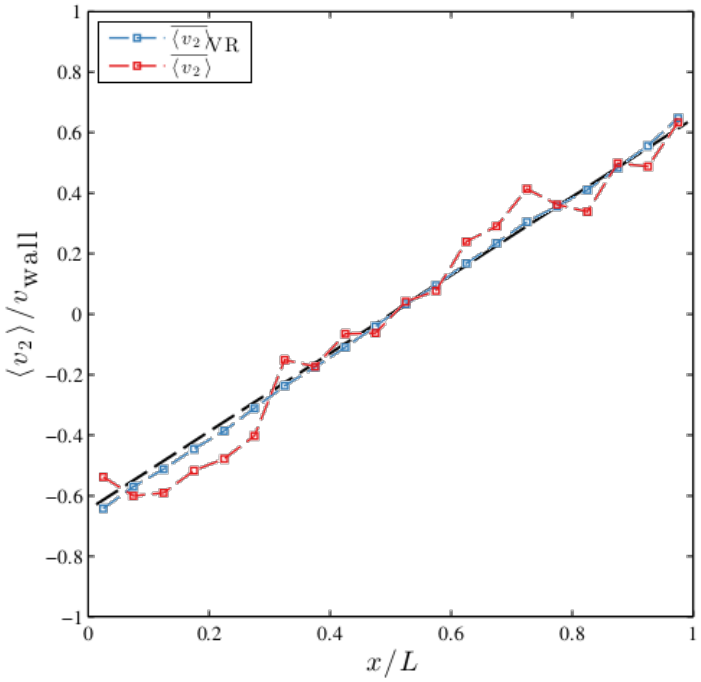

Figure 4.4: Steady state Couette flow. Red is standard Monte Carlo estimate of velocity profile across channel, blue is CRN variance reduced estimator, black dashed is Navier-Stokes profile with Maxwell boundary conditions. Kn $= 0.1$, $v_{\mathrm{wall}} = 0.01 c_0$.

$$v_s = \frac{2 - \sigma_a}{\sigma_a} \sqrt{\frac{\pi}{2}} \lambda \frac{du}{dn}, \tag{4.11}$$

where λi s the mean free path, and n is the normal direction to the wall. σ_a is the accommodation coefficient (named as it describes the propensity of the gas to accommodate to the state of the wall) with $\sigma_a = 0$ designating purely specular reflections and $\sigma_a = 1$ designating purely diffusive gas-surface interactions.

In section 4.5.4 we will quantitively look at the variance reduction in comparison to the basic Monte-Carlo sampling and the method to be introduced in the next section. It should be stressed that this type of variance reduction scheme can only work if the positions of particles within the non-equilibrium and equilibrium calculations remain correlated over a large enough period of time to gain meaningful samples. This is quite a strict condition to fulfil and requires symmetry within the geometry that can be exploited, and in general this method will not be applicable to geometries more complex than channel flows. In the next section, we propose a scheme where

this is possible for arbitrary geometries.

4.5 Importance weights

The method we will now propose to reduce the variance of estimators used for collections of particles evolving according to equation (3.33) uses the same type of importance sampling as the VRDSMC method [Al-Mohssen and Hadjiconstantinou, 2010], but the implementation differs because of the different particle dynamics. The method works in the following way: suppose we are interested in evaluating the expectation of $g(\mathbf{V})$ where $\mathbf{V}$ is distributed according to the distribution function f. Then given N independent samples $\{\mathbf{V}_1 \dots \mathbf{V}_N\}$ distributed according f the following definition gives rise to the estimate:

$$\mathbb{E}_f[g(\mathbf{V})] = \int g(\mathbf{v}) f(\mathbf{v})\, d\mathbf{v} \tag{4.12}$$

$$\approx \frac{1}{N} \sum_{i=1}^{N} g(\mathbf{V}_i). \tag{4.13}$$

We now define a function

$$W(\mathbf{v}) = \frac{f_{\text{ref}}(\mathbf{v})}{f(\mathbf{v})}, \tag{4.14}$$

which is a measure of how likely you are to see this particle with this velocity, relative to how likely you are to observe this particle if it was distributed to a reference density f_{ref}. This definition is well defined as long as the distribution f is absolutely continuous with respect to f_{ref}, meaning that $f_{\text{ref}}(S) = 0$ whenever $f(S) = 0$ for any subset S of the state-space. This definition can be viewed as a Radon Nikodym derivative. It can then be observed that the expectation of $g(\mathbf{v})$ with respect to the reference distribution can be estimated using the original samples:

$$\mathbb{E}_{f_{\text{ref}}}[g(\mathbf{v})] = \int f_{\text{ref}}(\mathbf{v}) g(\mathbf{v})\, d\mathbf{v} \tag{4.15}$$

$$= \int f(\mathbf{v}) \frac{f_{ref}(\mathbf{v})}{f(\mathbf{v})} g(\mathbf{v})\, d\mathbf{v} \tag{4.16}$$

$$= \int f(\mathbf{v}) W(\mathbf{v}) g(\mathbf{v})\, dv \tag{4.17}$$

$$\approx \frac{1}{N} \sum_{i=1}^{N} W(\mathbf{V}_i) g(\mathbf{V}_i). \tag{4.18}$$

This is significant as it allows one to sample from the reference distribution f_{ref}, using the original set of samples from the distribution f. If the reference distribution is Maxwellian, $f_{\text{ref}} = f_{\text{MB}}$ then using equation (4.9) one then has the ability to reduce variance in the same way, with $c = 1$. This is made clear by constructing the estimator

$$\widehat{g(\mathbf{V})} = \frac{1}{N} \sum_{i=1}^{N} g(\mathbf{V}_i) - \frac{1}{N} \sum_{i=1}^{N} W(\mathbf{V}_i) g(\mathbf{V}_i) + \mathbb{E}_{f_{\text{MB}}}[g(\mathbf{V})] \tag{4.19}$$

$$= \frac{1}{N} \sum_{i=1}^{N} g(\mathbf{V}_i)(1 - W(\mathbf{V}_i)) + \mathbb{E}_{f_{\text{MB}}}[g(\mathbf{V})]. \tag{4.20}$$

When the weight function $W \approx 1$, which occurs when f is close to the Maxwellian f_{MB}, the estimator is mostly formed from the contribution by the pre-determined equilibrium expectation, which has zero variance. This is good for low speed flows, as when the Mach number is small, we expect only small deviations from equilibrium. In order to implement this method, one needs a method of evolving the weights and velocities $\{\mathbf{v}_i, W_i\}$ in time, where $W_i = W(\mathbf{v}_i)$. For VRDSMC this is possible because it can be shown directly from the Boltzmann equation, that if two particles are chosen to collide with weights W_i and W_j then the post collision weights must be equal to $\frac{1}{2}(W_i + W_j)$. Because the Fokker-Planck dynamics have no explicit collisions, a different way to update the weights in needed.

Weights can be initialised exactly, because the initial velocities of the particles are distributed according to a prescribed initial distribution f_0. As time is evolved during the calculation, the distribution of velocities will change and hence so must the weights attached to each particle. VRDSMC is able to do this by creating collision rules that ensure that post collision velocities are still able to sample from

the same reference distribution. However, these rules are not relevent for the Fokker-Planck particle dynamics as collisions are not modelled explicitly.

4.5.1 Weight update rule

Instead, let us suppose that a given particle updates its from velocity from $\mathbf{V}_t \to \mathbf{V}_{t+1}$, where $\mathbf{V}_t$ is distributed according to f_t and $\mathbf{V}_{t+1}$ is distributed according to f_{t+1}, and that we have $W_t = f_{eq}(\mathbf{V}_t)/f_t(\mathbf{V}_t)$. We can use the *law of total probability*

$$f_{t+1}(\mathbf{v}) = \int f_{t+1}(\mathbf{v}|\mathbf{V}_t = \mathbf{v}')f_t(\mathbf{v}')\,d\mathbf{v}', \tag{4.21}$$

to write

$$W_{t+1}(\mathbf{V}_{t+1}) = \frac{f_{eq}(\mathbf{V}_{t+1})}{f_{t+1}(\mathbf{V}_{t+1})} = \frac{\int f_{eq}(\mathbf{V_{t+1}}|\mathbf{V}_t = \mathbf{v}')f_{eq}(\mathbf{v}')\,d\mathbf{v}'}{\int f_{t+1}(\mathbf{V_{t+1}}|\mathbf{V}_t = \mathbf{v}')f_t(\mathbf{v}')\,d\mathbf{v}'}\,. \tag{4.22}$$

It then remains to approximate this as the distributions f_{t+1} and f_t are in principal unknown. In principal, there are many ways to achieve this. A simple candidate is:

$$W_{t+1} \approx \widehat{W}_{t+1} := \frac{f_{eq}(\mathbf{V_{t+1}}|\mathbf{V}_t)f_{eq}(\mathbf{V}_t)}{f_{t+1}(\mathbf{V_{t+1}}|\mathbf{V}_t)f_t(\mathbf{V}_t)} \tag{4.23}$$

$$= \frac{f_{eq}(\mathbf{V_{t+1}}|\mathbf{V}_t)}{f_{t+1}(\mathbf{V_{t+1}}|\mathbf{V}_t)}W_t(\mathbf{V}_t). \tag{4.24}$$

This has approximation immediately has some desirable properties. Firstly, the error of the approximation decays with Δt. Also, it is possible to calculate this explicitly from the update rule $\mathbf{V}_t \to \mathbf{V}_{t+1}$ given by equation (3.33). This conditional distribution will be a gaussian centred on $\mathbf{V}_t$ plus the deterministic drift, with a temperature dependent variance. Further to this, it has the correct conditional expectation $\mathbb{E}(\widehat{W}_{t+1}|W_t) = W_t$ when the distribution is stationary. However, on its own it is not a suitable choice as if such a rule is repeated the variance of this approximation diverges, which is a common problem for this type of particle weight importance sampling method [Swiler and West, 2010]. This is a problem, because to reduce the variance of our estimators in a meaningful way, we require the weights to be close to unity. To avoid this problem we use the same kernel density estimator approach as used in [Al-Mohssen and Hadjiconstantinou, 2010]. Kernel density estimation (KDE) is a method that allows one to obtain an estimate $\hat{f}$ of

a density function f from samples distributed according to that density function in the following way:

$$\widehat{f}(\mathbf{v}) = \frac{1}{N}\sum_{i=1}^{N} K_r(\mathbf{v} - \mathbf{V}^{(i)}), \tag{4.25}$$

where K_r is a kernel function that integrates over the state-space to 1, and r is a smoothing parameter that controls the width of the kernal function. We use the same kernels as Al-Mohssen and Hadjiconstantinou [2010]:

$$K_r(\mathbf{v}) = \begin{cases} (4/3\pi r^3)^{-1} & \text{if } \|\mathbf{v}\| < r \\ 0 & \text{otherwise} \end{cases}, \tag{4.26}$$

which returns a 1 divided by the volume of a sphere of radius r if $\mathbf{v}^i$ lies within the sphere of radius r centred on $\mathbf{v}$, and otherwise returns a zero. If we combine this with (4.24), we arrive at

$$W_{t+1}(\mathbf{V}^i) \approx \frac{\sum_{j=1}^{N} K_r(\mathbf{V_i} - \mathbf{V}^j)\widehat{W}_{t+1}(\mathbf{V}^j)}{\sum_{j=1}^{N} K_r(\mathbf{V_i} - \mathbf{V}^j)} \tag{4.27}$$

$$= \frac{1}{|S_r(\mathbf{V}^i)|}\sum_{\mathbf{V}^j \in S_r(\mathbf{V}^i)} \widehat{W}_{t+1}(\mathbf{V}^j), \tag{4.28}$$

where $S_r(\mathbf{V}^i) = \{\mathbf{V}^j : \left|\mathbf{V}^j - \mathbf{V}^i\right| < r\}$ is the set of samples whose members lie within the sphere of radius of r centred on $\mathbf{V}^i$. This KDE step has the effect of smoothing out the variation introduced by using a conditional probabilities to estimate a marginal probability, and making the scheme more stable. Increasing the smoothing parameter r results in an estimator with a smaller variance, however it also increases the bias of the estimation, so ideally r should be chosen to be as small as possible whilst maintaining an acceptable level of variation.

4.5.2 Boundary conditions

We use the same boundary condition methodology as described in Al-Mohssen and Hadjiconstantinou [2010] , that is for diffusely reflecting fully accommodating walls, with temperature T_{wall} and tangential velocity u_{wall}. Supposing that the Maxwellian distribution at the boundary is given by $f_{wall}(\mathbf{v}) = \rho_{wall}P_{MB}(\mathbf{v})$, where P_{MB} is a

Gaussian probability density, and the boundary is the plane $x = 0$, then the no flux boundary condition is

$$\rho_{wall} \int\limits_{v_x<0} v_x P_{MB}(\mathbf{v})\, d\mathbf{v} + \int\limits_{v_x>0} v_x f(\mathbf{v})\, d\mathbf{v} = 0, \tag{4.29}$$

and similarly for the equilibrium solution

$$\rho_{wall,eq} \int\limits_{v_x<0} v_x P_{MB,eq}(\mathbf{v})\, d\mathbf{v} + \int\limits_{v_x>0} v_x W(\mathbf{v}) f(\mathbf{v})\, d\mathbf{v} = 0. \tag{4.30}$$

The second term of both (4.29)-(4.30) is just the flux of particles, and can be estimated by counting the number of computational particles N_{in} that cross through a wall of area Δs in a time period Δt by $N_{in}/\Delta s \Delta t$. At equilibrium this is estimated by $\sum_i^{N_{in}} W_i \Delta s \Delta t$. The first terms of both (4.29)-(4.30) can be calculated using analytical properties of the normal distribution,

$$\int\limits_{v_x<0} v_x P_{MB}(\mathbf{v})\, d\mathbf{v} = \frac{1}{\sqrt{2\pi}} \sqrt{\frac{kT}{m}}. \tag{4.31}$$

Hence if after colliding with a wall, a particle changes velocity from $\mathbf{V}$ to $\mathbf{V}'$, its weight changes according to

$$W' = W(\mathbf{V}') = \frac{f_{eq}(\mathbf{V}')}{f(\mathbf{V}')} \tag{4.32}$$

$$= \frac{\rho_{wall,eq} P_{MB,eq}(\mathbf{V}')}{\rho_{wall} P_{MB}(\mathbf{V}')} \tag{4.33}$$

$$= \sqrt{\frac{T_{wall}}{T_{wall,eq}}} \frac{\sum_i^{N_{in}} W_i}{N_{in}} \frac{P_{MB,eq}(\mathbf{V}')}{P_{MB}(\mathbf{V}')}. \tag{4.34}$$

The validity of using diffusive boundary conditions is subject to discussion, which I will avoid in this thesis, as it is a whole active area of research in itself. In the remaining sections we will demonstrate the effectiveness of the method.The importance sampling scheme outlined above will be referred to as *variance reduced Fokker-Planck* (VRFP).

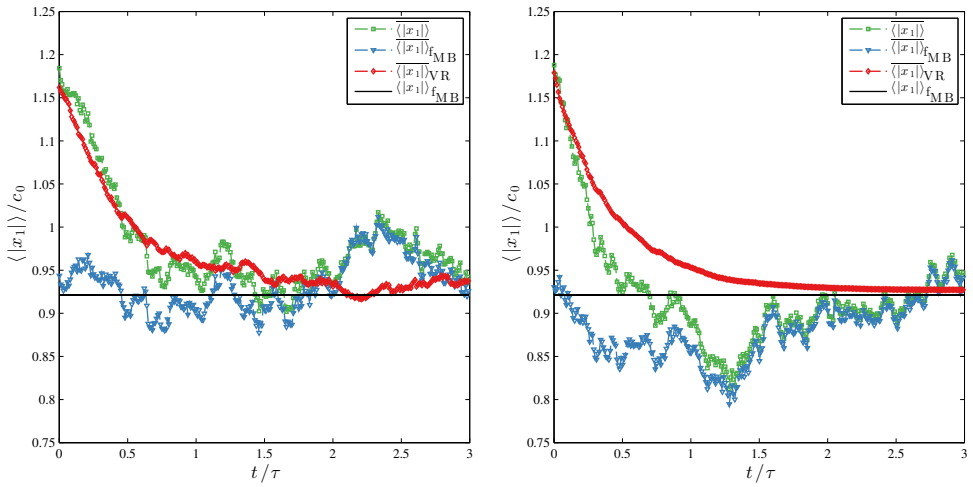

(a) Without stabilisation

(b) With stabilisation

Figure 4.5: Homogeneous relaxation towards equilibrium, (a) without KDE, (b) with KDE, smoothing parameter $r = 0.05c_0$

4.5.3 Homogeneous relaxation to equilibrium

We will demonstrate the effectiveness of this method first with a homogeneous relaxation to equilibrium: that is, when $f(t, \mathbf{x}, \mathbf{v}) = f(t, \mathbf{v})$ has no spatial component. We start from an initial distribution of particles

$$f_0(\mathbf{v}) = (1/2)(f_{MB}(v_1, c_0, c_0) + f_{MB}(v_1, -c_0, c_0))f_{MB}(v_2, 0, c_0)f_{MB}(v_3, 0, c_0), \tag{4.35}$$

which will relax towards the Maxwellian distribution $f_{MB}(\mathbf{v}, \mathbf{0}, \sqrt{(4/3)c_0^2})$. In figures (4.5a)-(4.5b) we show how the variance reduced estimator performs against the standard sample mean estimator, when estimating $\langle |x_1| \rangle$, with and without the KDE stabilisation procedure. In both cases, the variance of the new estimator is smaller than the standard estimator, but the estimator with stabilisation from the KDE reduces the variance even further.

4.5.4 Couette flow

To test the particle weight variance reduction, we have applied to scheme to sample from a steady-state planar Couette flow, and compared the results to results obtained using a common random number scheme. A Couette flow is a flow where the fluid is bounded by two parallel walls moving in opposite directions within their

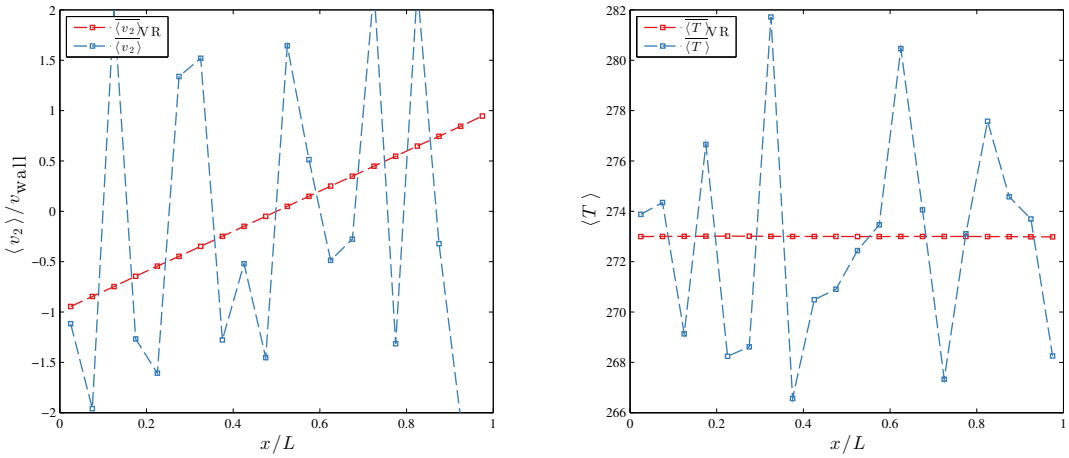

Figure 4.6: Couette flow with wall velocity $v_{\text{wall}} = 0.01c_0$, Kn $= 0.05$, 20 cells and 100 particles per cell.

planes, with velocity $\pm U_{\text{wall}}$. For Knudsen numbers Kn $= 0.05, 0.5, 1.0$ respectively, Figures (4.6), (4.7), (4.8) show the VRFP and standard Monte Carlo estimators of the steady-state flow velocity field parallel to the wall, $v_2(x_1)$, (left) as well as the temperature profile across the channel $T(x_1)$, for a Couette flow with wall velocity $v_{\text{wall}} = 0.01c_0$, where c_0 is the thermal velocity, and Kn $= 0.5$, 20 cells and 100 particles per cell. All the results show a significant improvement in performance over the unweighted standard Monte Carlo estimator.

To quantitively compare the performance of the CRN scheme and the importance sampling estimation against the basic Monte Carlo, we have found solutions to steady-state Couette flows and recorded the average noise-to-signal ratio across the channel, for a fixed number of particles and time steps. This was performed over a range of Mach numbers. Figure (4.9) shows the results. As expected, the basic Monte Carlo estimator has a noise-to-signal ratio that grows as Ma^{-1} as $\text{Ma} \to 0$. The common random numbers scheme maintains the same scaling as the basic Monte Carlo estimator, but has a reduced variance in comparison over all Mach numbers. The reduction in variance appears to be fixed over the range of Mach numbers analysed, with $\sigma_{\text{MC}}/\sigma_{\text{CRN}} \approx 10$, which corresponds to using 100 times as many particles. In contrast, the importance sampling scheme appears to achieve a constant noise-to-signal ratio as the Mach number goes to zero. This results in an unbounded speed-up over the standard Monte-Carlo estimator as the signal size decreases to zero. Because of the independence of the signal strength on the noise-to-signal ratio, there is a signal strength where for larger signal strengths, the CRN scheme

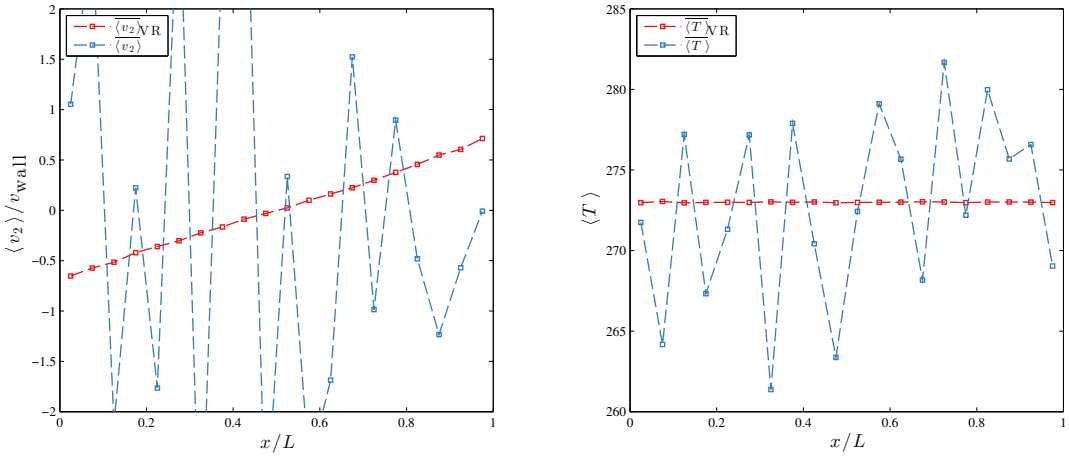

Figure 4.7: Couette flow with wall velocity $v_{\text{wall}} = 0.01c_0$, Kn = 0.5, 20 cells and 100 particles per cell.

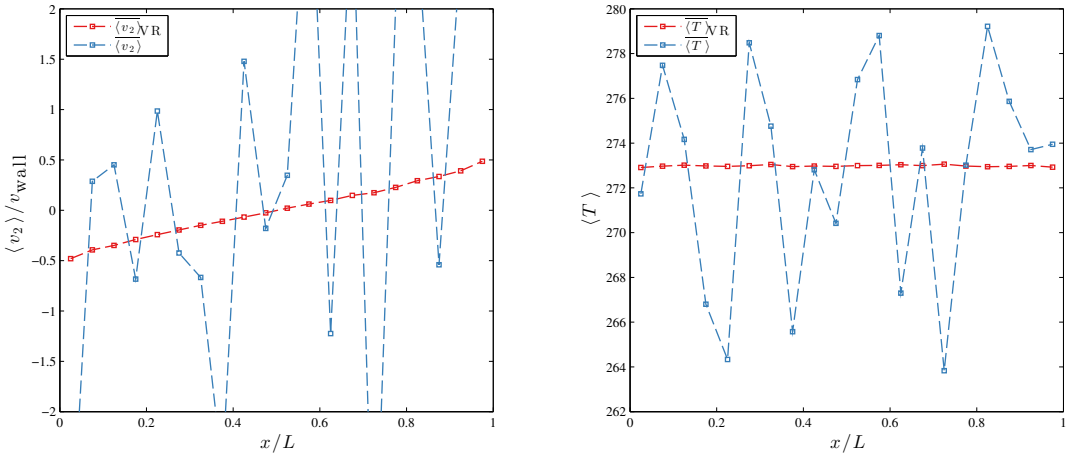

Figure 4.8: Couette flow with wall velocity $v_{\text{wall}} = 0.01c_0$, Kn = 1.0, 20 cells and 100 particles per cell.

outperforms the particle weight scheme, and for the steady-state Couette flow we estimate this to be at a Mach number close to 0.1.

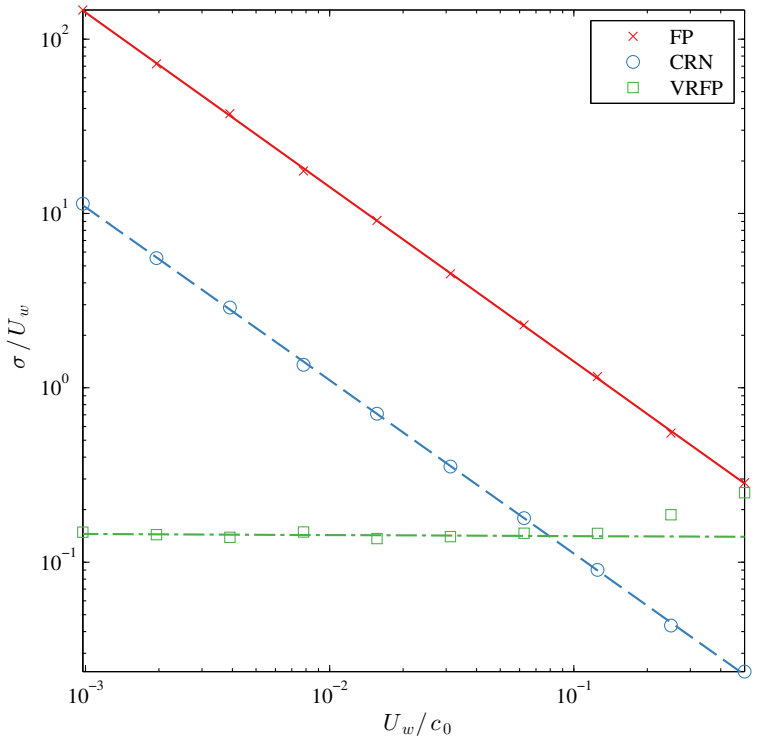

Figure 4.9: Comparison of noise-to-signal ratio vs signal size, between standard Monte Carlo, common random numbers, and importance sampling methods.

4.5.5 Lid-driven cavity flow

To further demonstrate the effectiveness of the method, we apply it to a lid-driven cavity flow, where the fluid is bounded in two dimensions by a square box in the (x_1, x_2) plane, with translational statistical symmetry in the x_3 axis. Three of the bounding walls are stationary, and one of the bounding walls moves within its plane at constant velocity U_{wall}, giving rise to a circulatory flow within the cavity. The common random numbers scheme loses much of its effectiveness in such situations, as the geometry of the problem results in the positions of corresponding particles in each simulation losing correlation.

Figures (4.10a)-(4.10b) show the velocity and non-dimensional temperature field $(T/T_0 - 1)$ of the steady-state flow, with a lid velocity of $U_{\text{wall}} = 0.001c_0$ for the standard Monte Carlo and variance reduced sampling schemes. The results have

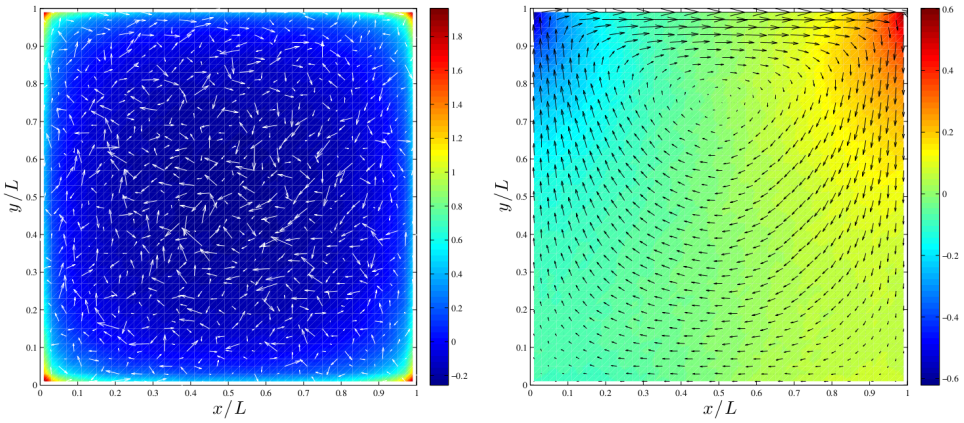

(a) Standard Monte Carlo estimate (b) Variance reduced estimate

Figure 4.10: Couette flow at Kn = 1.0, $U_{\text{wall}} = 0.001c_0$, with and without importance sampling variance reduction.

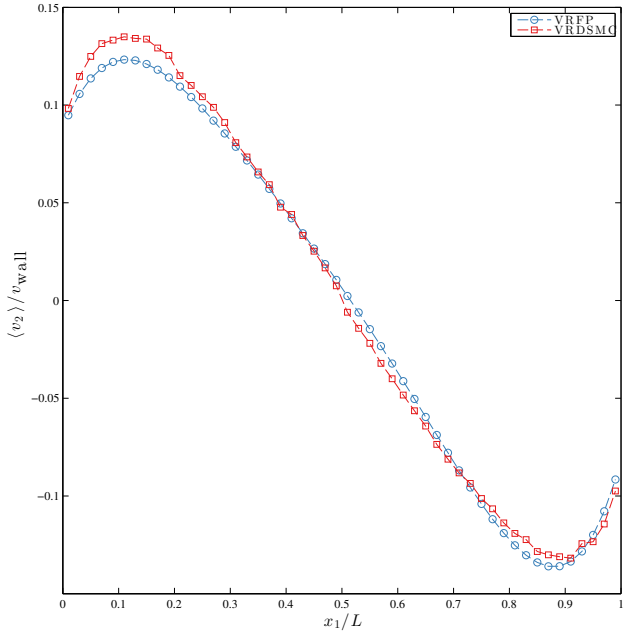

Figure 4.11: Comparison of results of cross-section of velocity fields between variance reduced Fokker-Planck and LVDSMC methods. Cross section taken at $y = 0.5$

been averaged over 5000 time-steps, and 10 independent ensembles on a 50×50 grid, with an average of 30 particles per cell. The standard Monte Carlo scheme is not able to pick up the signal, whereas we see clearly that the importance sampling scheme is. In Figure (4.11) we compare results from the variance reduced Fokker-Planck estimator to that from a LVDSMC simulation over a cross-section of the flow field, taken at $y = 0.5$, and find that the result are in good agreement. At this point we note that the LVDSMC algorithm used in Figure (4.11) solves the linearised hard-sphere collision operator.

In Figures 4.12a -4.12d we show results from lid-driven cavity flows with lid speeds $0.1c_0$, $0.01c_0$, $0.001c_0$ and $0.0001c_0$. As was the case with the Couette flow, we find the level of noise in each calculation is independent of the lid-speed.

4.6 Discussion

In this chapter we have proposed two variance reduction techniques that can be applied to the Fokker-Planck solution operator. The first, a common random number scheme, is is effective when there is a symmetry in the spatial geometry of problem, which can be exploited to keep positions in an equilibrium and non-equilibrium solution correlated. We find that it is able to reduce the standard deviation of samples by a factor of 10. Because the signal-to-noise ratio scales with the inverse square of the number of samples, this would require on the order of 100 times the number of independent ensembles (or 100 times more particles in the simulation under the assumption that the distribution is close to equilibrium) to achieve the same variance reduction without the common random numbers scheme.

The second scheme, is a scheme based on the VRDSMC method, which is able to reduced the variance of estimates regardless of the geometry using importance weights. The source of the statistical error for this method is in the approximation the weight function which allows one to sample from an equilibrium solution. We find that the errors accrued in approximating the weight function are independent of the Mach number of the flow as the Mach number decreases. As the Mach number increases past Mach numbers of $O(1)$, the method is no longer able to accurately determine the weight function. However, as the Mach number of the flow decreases to zero, the performance of the algorithm does not degrade.

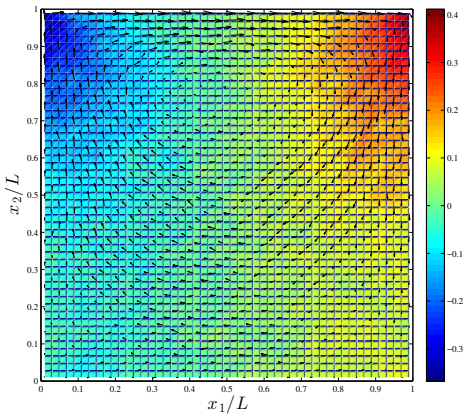

(a) $U_{\text{wall}} = 0.1c_0$

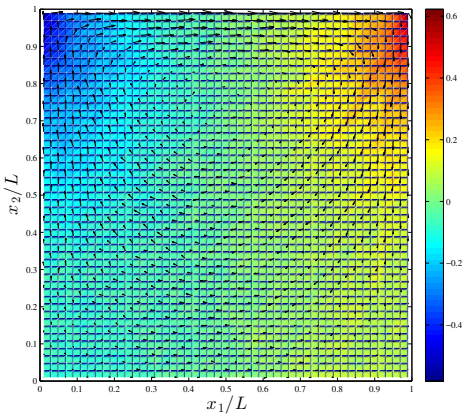

(b) $U_{\text{wall}} = 0.01c_0$

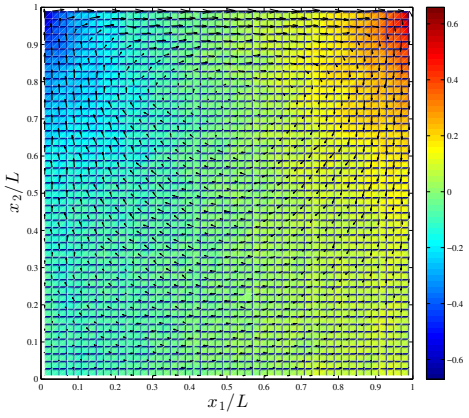

(c) $U_{\text{wall}} = 0.001c_0$

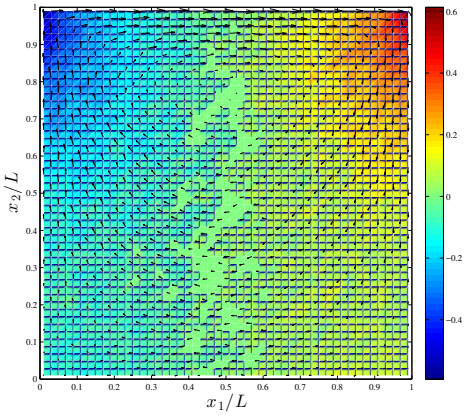

(d) $U_{\text{wall}} = 0.0001c_0$

Figure 4.12: Lid-driven cavity flows with different wall-speeds. 50×50 grid, 25 particles per cell on average, 5000 time steps to reach steady-state, thermodynamic fields averaged from 5000 further time steps. The level of noise is independent to the wall-speed.

5

Quasi-Monte Carlo particle dynamics

"Everything we care about lies somewhere in the middle, where pattern and randomness interlace."

– James Gleick, *The Information: A History, a Theory, a Flood*

The numerical time integration of the SDEs (3.22) (3.23) given by equations (3.33) is performed in a method that can also be generally termed a Monte Carlo approach. By this, what we mean is that in the implementation of the scheme, we repeatedly draw psuedo-random numbers in order to approximate the diffusion process. In this chapter we devise a novel method for numerically integrating a diffusion process using a quasi-Monte Carlo integration scheme with randomisation. This method was developed with the view to applying it to spatially inhomogeneous rarefied gas flows, but we find that the spatial inhomogeneity creates challenges that 23 were not able to overcome.

5.1 The general Monte Carlo approach

A Monte Carlo method is a general term referring to a method for approximating the integral of a function $f : R \to \mathbb{R}$, $R \subset \mathbb{R}^n$, over a subdomain $B \subset R$. Without loss of generality, we take $B = [0,1]^n$, the n-dimensional unit hypercube. Consider the integral

$$I(f) := \int_{[0,1]^n} f(\mathbf{u})\, d\mathbf{u}. \tag{5.1}$$

In order to approximate the integral, the Monte Carlo method takes the sample mean of f evaluated at independent uniformly distributed samples in B,

$$\hat{I}(f) := \frac{1}{N} \sum_{i=1}^{N} f(\zeta_i). \tag{5.2}$$

The expectation of this random variable is

$$\mathbb{E}[\hat{I}(f)] = \mathbb{E}\left[\frac{1}{N} \sum_{i=1}^{N} f(\zeta_i)\right] \tag{5.3}$$

$$= \frac{1}{N} \sum_{i=1}^{N} \mathbb{E}[f(\zeta_i)] \tag{5.4}$$

$$= \mathbb{E}[f(\zeta)] \tag{5.5}$$

$$= I(f) \tag{5.6}$$

and so $\hat{I}$ is an unbiased estimator of I. Given that we have an unbiased estimator, the natural question to ask is does this estimator converge. Convergence for this estimator is established from the strong law of large numbers:

Theorem 5.1.1 Strong Law of Large Numbers (SSLN) *Let X_1, X_2, ... be an infinite sequence of independent identically distributed random numbers, with $\mathbb{E}[X_i] = \mu < \infty$. If $S_n = \sum_{i=1}^{n} X_i$ then*

$$\frac{S_n}{n} \xrightarrow{a.s.} \mu \quad as \quad n \to \infty$$

Once we know the estimator converges, it is then natural to ask is how fast do we expect it to converge? The speed of convergence is provided to us by the Central Limit Theorem:

Theorem 5.1.2 Central Limit Theorem *Let X_1, X_2, ... be an infinite sequence of independent identically distributed random numbers, with $\mathbb{E}[X_i] = \mu < \infty$, and finite variance. If $S_n = \sum_{i=1}^{n} X_i$ then*

$$\frac{S_n}{n} \sim \mu + n^{-1/2}\mathcal{N}(0, \sigma)$$

These are well known standard results, found in all basic statistical reference books. In particular the Central Limit Theorem (CLT) tells us that the speed of convergence

of the Monte Carlo estimator is of order $\mathcal{O}(n^{-1/2})$, which is independent of the number of dimensions. Stated more simply, if we wish to decrease our expected error by a factor of a half then we require four times as many sample points.

In one dimension, this speed of convergence is inferior to standard quadrature methods that use equidistantly spaced points for the set of samples $\{\zeta_i\}$, which typically give an error $O(n^{-k})$ for $k \geq 1$, where n is the number of quadrature points and k, usually called the "order", is dependent on the method. For example, in one dimension, the trapezoidal rule has error of $O(n^{-2})$. To keep the error constant as the dimensions of the integration is increased the distance between quadrature points needs to stay fixed, and the number points required to span a unit hypercube with equal spacing scales as n^d. This results in a error in higher dimensions of $O(n^{-k/d})$. This unfavourable scaling with dimension is what has come to be known as the *curse of dimensionality*, coined by Bellman et al. [1961]. So, because the error of Monte Carlo integration is independent of the the number of dimensions, d, in higher dimensions the Monte Carlo becomes more efficient than methods relying on a grid based quadrature.

5.2 Introduction to Quasi-Monte Carlo

As we have seen in the previous section, for high dimensional problems Monte Carlo methods are able to outperform integration methods that rely on the use of grid based quadrature. Quasi-Monte Carlo (QMC) methods are able to achieve a still better rate of convergence, and hence computational efficiency. By effectively relaxing the constraint that the sample points are chosen independently from one another, but keeping the property that they in some sense uniformly sample the desired space, we will see in the following sections how this may be possible. This approach of using quasi-random numbers for a diffusion problem was first proposed by Lécot and El Khettabi [1999], who proposed an algorithm and proved convergence for the method. This was later taken up by Venkiteswaran and Junk [2005a], who adapted the algorithm to solve the diffusion equation. In this section we describe the general method, and propose a modification to the scheme proposed by [Venkiteswaran and Junk, 2005a].

5.2.1 Low discrepancy sequences

Instead of relying on independently identically distributed uniform random numbers (or rather psuedo-random numbers which are computationally generated), the quasi-

Monte Carlo method relies on deterministic sequences of random numbers that are able to cover the unit cube in a way that is more homogenous. Such sequences of numbers are referred to as *low discrepancy* sequences. The quantification of the uniformity or homogeneity is given to us by the *discrepancy*, where we will use the Niederreiter [1992] notation. Given a point set $P = \{\xi_1, \xi_2 \dots \xi_N\}$ in $[0,1]^d$, the *extreme discrepancy* is defined as:

$$D_N(P) = \sup_{B \in \mathcal{B}} \left| \frac{A(B,P)}{N} - \lambda_d(B) \right|, \tag{5.7}$$

where $\mathcal{B}$ is the family of sets of the form $B = \prod_{i=1}^{d} [a_i, b_i)$, for arbitrary $\mathbf{a}, \mathbf{b} \in [0,1)^d$, $a_i \leq b_i$, λ_d is the d-dimensional Lebesgue measure and $A(B,P)$ is the number of points from P that lie in B. In a general sense, the extreme discrepancy is a worst case measure of how badly the point set approximates the Lebesgue measure, in that it measures the error in representing volumes of subsets by fractions of points in the subsets. Another useful quantity is the *star discrepancy*, which is defined as the supremum over the family of sets $\mathcal{S}$ of the the form $\prod_{i=1}^{d}[0, a_i)$

$$D_N^*(P) = \sup_{B \in \mathcal{S}} \left| \frac{A(B,P)}{N} - \lambda_d(B) \right|, \tag{5.8}$$

which is related to the extreme discrepancy by the following proposition:

Proposition 5.2.1 *For any point set* $\mathcal{P} = \{\xi_1, \xi_2 \dots \xi_N\}$ *in* $[0,1)^d$

$$D_N^*(\mathcal{P}) \leq D_N(\mathcal{P}) \leq 2^d D_N^*(\mathcal{P}) \,.$$

The proof of which is relatively simple and may be found here [Dick and Pillichshammer, 2010], which provides an excellent review of discrepancy theory and quasi-Monte Carlo integration. The star discrepancy is a useful quantity as it bounds the error of the QMC estimator:

Theorem 5.2.2 (The Koksma-Hlawka Inequality) *Let f have bounded variation $V(f)$ on I^d. Then for any point set $\mathcal{P} = \{\xi_1, \xi_2..\xi_N\}$*

$$\left|\hat{I}(f) - I(f)\right| \leq V(f)D_N^*(P).$$

$V(f)$ is the *total variation* of f, and is given by

$$V(f) = \int_{\mathbb{R}^d} |\nabla f| \, d\mathbf{v}, \tag{5.9}$$

which, importantly, has no dependence on N. The left hand side of the Koksma-Hlawka inequality is the absolute error, and just like root mean square error of a Monte Carlo method, is a quantity we would like to decay quickly with N. The bound given in the inequality is tight in the sense that for a given point set, and $\epsilon > 0$ there exists a function f of bounded variation, with error that lies within ϵ of this bound. In this sense, the Koksma-Hlawka inequality provides the worse case error. For example, when $\xi_i \sim U[0,1)^d$ Chung [1949] was able to show from the *law of iterated logarithms* that

$$\lim_{N\to\infty} \sup \frac{\sqrt{2N}D_N^*}{\sqrt{\log(\log(N))}} = 1\,, \tag{5.10}$$

and so uniformly random samples have a discrepancy of order $\mathcal{O}((\log(\log(N))/N)^{-1/2})$, which is true for any d. This bound is not as informative as the result provided by the Central Limit Theorem (given that the CLT gives an equality for the root mean square error). We will go on to see in the next section there are deterministic sequences of numbers that achieve a better scaling with N than (5.10). The reason that it is possible to get better results than independently chosen random samples is that points chosen in this way tend to clump together, as we can see in Figure 5.1.

5.2.2 Examples of low discrepancy sequences

In this subsection I will briefly describe some of the deterministic sequences that are able to achieve a better scaling with the number of points in the sequence, N, than (5.10), but I will refer the reader again to [Dick and Pillichshammer, 2010] for precise definitions of the constructions of the sequence, as they are in general technical. First of all, it might be salient to reiterate that given we are interested in

uniformly distributed points in $[0,1)^d$, why not just use the set of $N = m^d$ regular lattice points Γ_m defined by

$$\Gamma_m := \frac{1}{m}\mathbb{Z}^d (\mathrm{mod}\, 1). \tag{5.11}$$

It can be shown that the star discrepancy of this point set is given by

$$D_N^*(\Gamma_m) := 1 - \left(1 - \frac{1}{m}\right)^d, \tag{5.12}$$

which satisfies the inequality

$$\frac{1}{N^{1/d}} \leq D_N^*(\Gamma_m) \leq \frac{d}{N^{1/d}}, \tag{5.13}$$

which for $d = 1$ can be shown to optimal [Dick and Pillichshammer, 2010], but for $d \geq 2$ is a suboptimal point set. Instead, let us consider one of the simplest low discrepancy sequences in one dimension, the *Van der Corput* sequence, which can be generalised to higher dimensions. The nth term of the sequence in base b is defined as

$$\Phi_b(n) = \sum_{i=0}^{R(n)} \frac{a_i}{b^{i+1}}, \tag{5.14}$$

where a_i are the coefficients of the powers of b in the expansion of n in base b, that is

$$n = \sum_{i=1}^{\infty} a_i b^i, \tag{5.15}$$

and $R(n)$ is the largest index for which $a_{R(n)}$ is not equal to zero. So for example, the first few terms in the sequence in base 2 is $\left\{\frac{1}{2}, \frac{1}{4}, \frac{3}{4}, \frac{1}{8}, \frac{5}{8}, \frac{3}{8}, \frac{1}{16}, \frac{9}{16}, \ldots\right\}$. This sequence can be shown to have a discrepancy of $O((\log N)/N)$, which is inferior to the 1-d regular lattice, but can be generalised into higher dimensions to achieve a better scaling than lattice points.

The Van der Corput sequence generalises in d dimensions to the *Halton sequence*. If $p_1, \ldots, p_d$ are the first d prime numbers, then the terms in the Halton sequence are given by

$$\xi_i = (\Phi_{p_1}(i), \Phi_{p_2}(i), \ldots, \Phi_{p_d}(i)), \tag{5.16}$$

which results in a discrepancy bounded by

$$D_N^* \leq C_d \frac{(\log N)^d}{N} + \mathcal{O}\left(\frac{(\log N)^{d-1}}{N}\right), \tag{5.17}$$

where the constant C_d scales super-exponentially with dimension [Morokoff and Caflisch, 1994]. See Figure (5.2) for the first 1000 terms of the Halton sequence. Another commonly used set of quasi-random numbers is the *Sobol sequence*.The Sobol sequence is generated using the binary expansion of an integer n,

$$n = n_1 2^0 + n_2 2^1 + n_3 2^2 + \ldots \tag{5.18}$$

This is used to generate the nth element of the jth dimension of the sequence

$$\xi_j^{(n)} = n_1 \nu_j^{(1)} \oplus n_2 \nu_j^{(2)} \oplus \ldots n_m \nu_j^{(m)}, \tag{5.19}$$

where $\oplus$ is the bitwise exclusive or (XOR) addition and $\nu_j^{(i)}$ are generated from the q-term recurrence relation

$$\nu_j^{(i)} = a_1 \nu_j^{(i-1)} a_2 \oplus \nu_j^{(i-2)} \oplus \ldots \oplus a_q \nu_j^{(i-q+1)} \oplus \nu_j^{(i-q)} \oplus \nu_j^{(i-q)} / 2^q. \tag{5.20}$$

The discrepancy of the Sobol sequence is also given by the inequality (5.17), with the coefficient in front of the leading term also scaling super-exponentially with dimension, but still significantly smaller than the Halton sequence [Morokoff and Caflisch, 1994]. See Figure (5.3) for the first 1000 terms of the Sobol sequence.

5.2.3 (t, m, s)-nets and (t, s)-sequences

There are certain types of low-discrepancy sequences that fulfil a stronger property of uniformity, which are called (t, m, s)-nets. A set of b^m points $\mathcal{P}$ is a (t, m, s)-net in base b if every interval of the form

$$\prod_{i=1}^{d} \left[A_i / b^{d_i}, (A_i + 1)/b^{d_i} \right), \tag{5.21}$$

where $A_i < b^{d_i}$ for each $1 \leq i \leq s$ and with $d_1 + d_2 + \ldots + d_s = m - t$, that is, intervals with volume b^{t-m}, contain exactly b^t points of $\mathcal{P}$. The parameter $t \in \mathbb{N}$ is called the *quality parameter*, and the smaller t is, the more uniform the set of points is. Further, a (t, s)-sequence is defined where for all integers $n \geq 0$ and $m > t$, all points $\xi_i \in \mathcal{P}$ satisfying $nb^m \leq i \leq (n + 1)b^m$ form a (t, m, s)-net. The Sobol sequence is an example of a (t, s) sequence, with t growing super-linearly with s.

One sequence that satisfies the conditions required to be a $(0, s)$-sequence is the Faure sequence, which is constructed from a permutation of the Halton sequence that uses the same base for each dimension [Niederreiter, 1988]. The base of the sequence is chosen to be the smallest prime greater or equal to the dimension of the sequence, which restricts the number of particles used in the simulations to powers of this base. The discrepancy of the sequence is again bounded by (5.17), but unlike the Sobol and Halton sequences, the Faure has the advantage of having a coefficient C_d that goes to zero with dimension. In the next section we will describe why having the (o, s)-nets property will be useful for the method.

5.3 QMC applied to the diffusion equation

We consider the diffusion equation with constant diffusion coefficient, also known as the heat equation, for $f : \mathbb{R}^d \times [0, T] \ \rightarrow \mathbb{R}$:

$$\partial_t f = \Delta f \qquad t > 0 \tag{5.22}$$

$$f(\mathbf{v}, 0) = f_0(\mathbf{v}). \tag{5.23}$$

This initial data problem has a well known fundamental solution, or Green's function, given by:

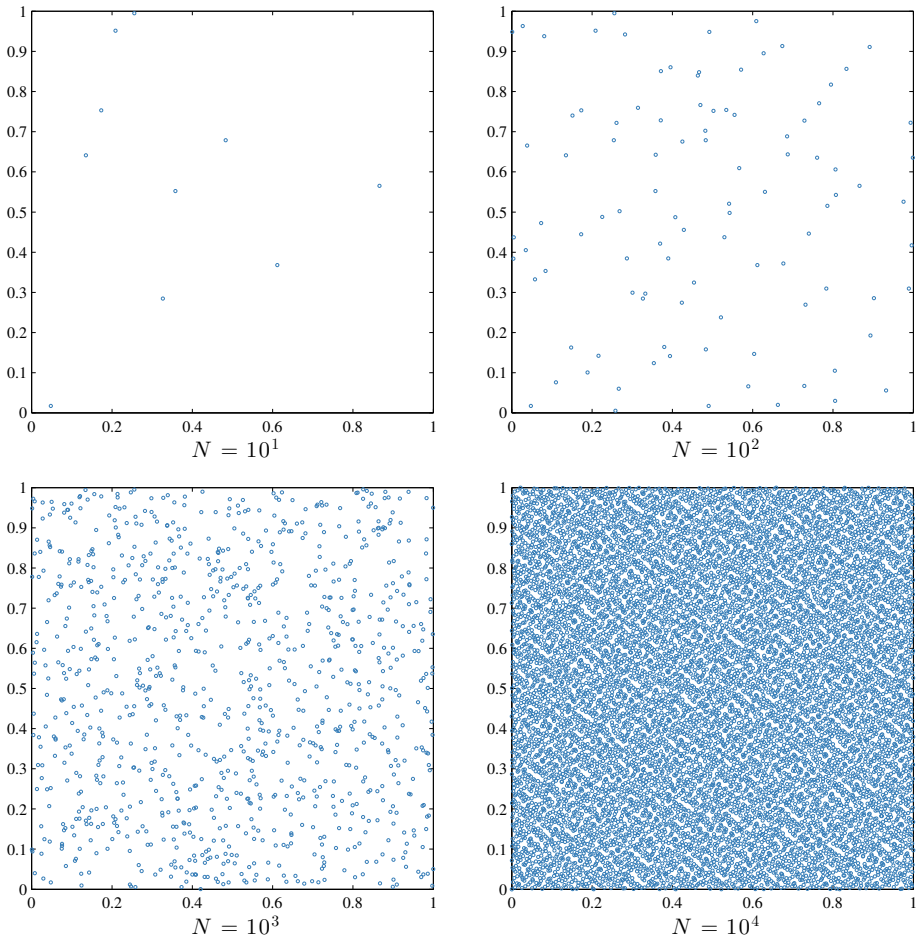

Figure 5.1: Uniformly distributed independent pseudo-random numbers in the unit square. As sample size increases, samples appear to form "clumps".

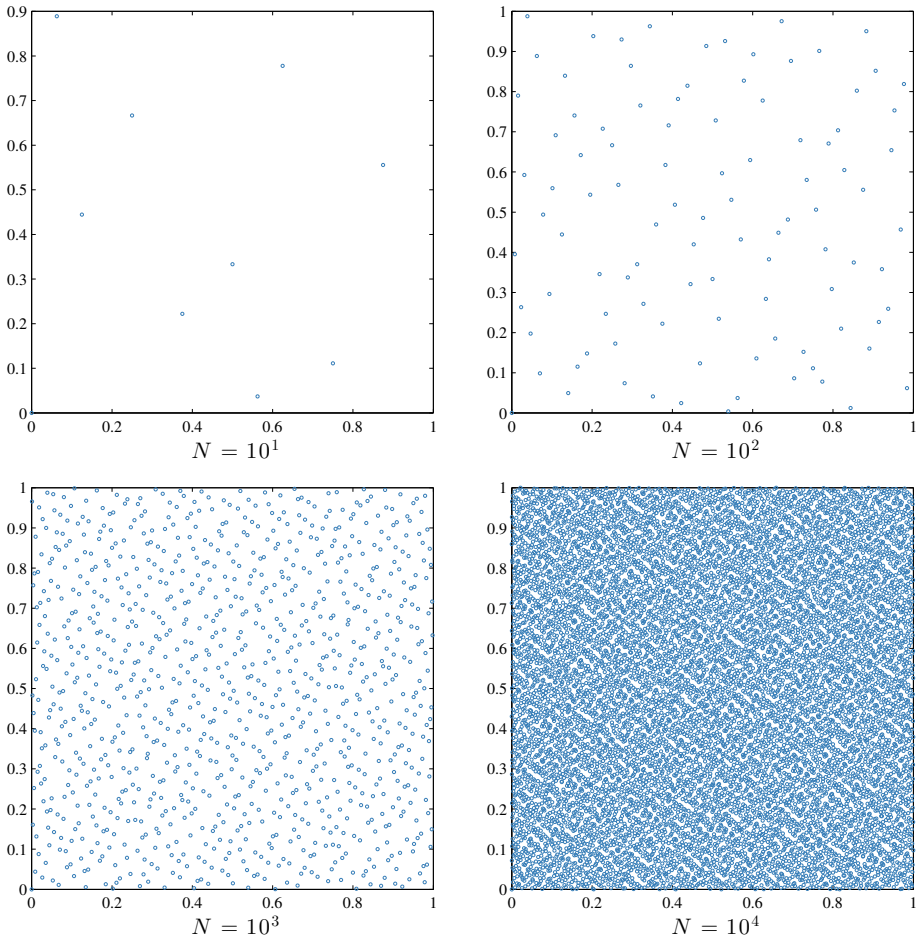

Figure 5.2: The first 1000 terms of the Halton sequence.

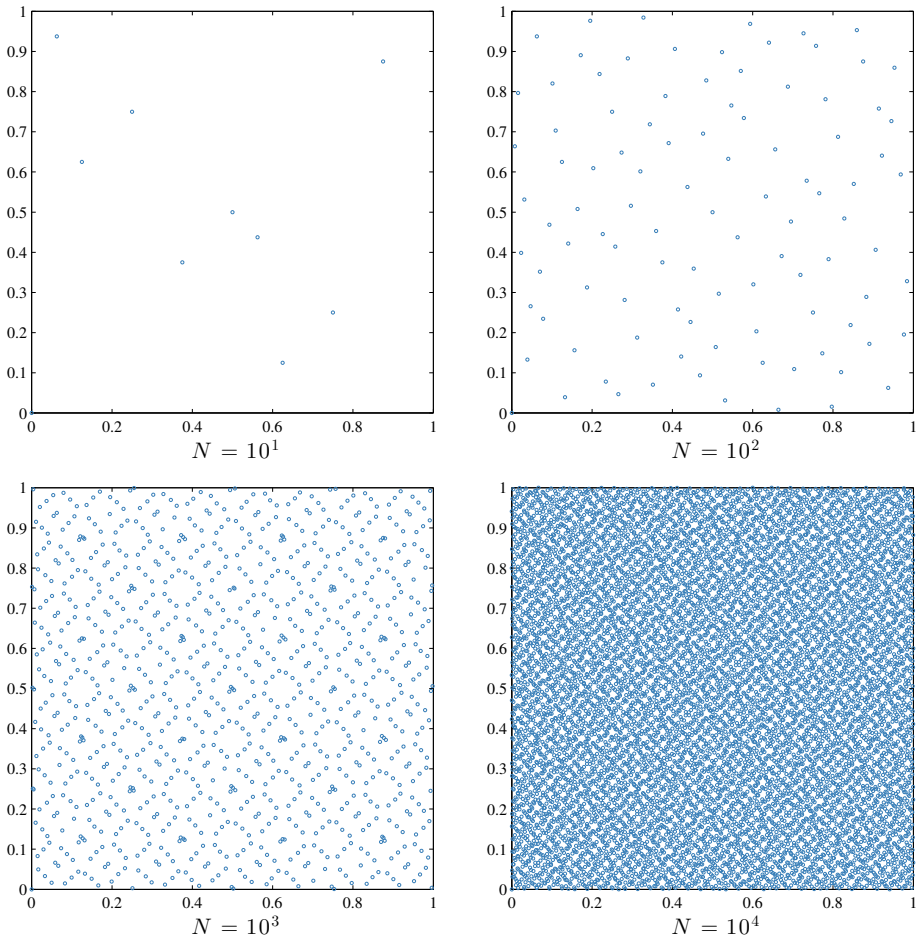

Figure 5.3: The first 1000 terms of the the Sobol sequence.

$$\Psi(\mathbf{v}, t) = \frac{1}{\sqrt{(4\pi t)^d}} \exp\left(-\frac{v^2}{4t}\right), \tag{5.24}$$

and hence the solution is given by the convolution with initial data

$$f(\mathbf{v}, t) = \int_{\mathbb{R}^d} \Psi(\mathbf{v} - \mathbf{y}, t) f_0(\mathbf{y})\, d\mathbf{y}. \tag{5.25}$$

In the last section, we saw that by using low-discrepancy sequences, or quasi-random numbers, it is possible to achieve a greater convergence rate than is possible when naively using uniformly distributed random numbers. In the next section we will describe the method first proposed by Venkiteswaran and Junk [2005a] for solving the diffusion equation by using low-discrepancy sequences, employing a technique they gave the epithet *quasi-random mixing*.

5.3.1 Initialising the particles

In [Venkiteswaran and Junk, 2005a], the authors consider the diffusion equation with a Gaussian initial condition

$$f_0(\mathbf{v}) = (2\pi)^{-d/2} \exp(-|\mathbf{v}|^2/2). \tag{5.26}$$

If the set of points $\{\xi_1, \ldots \xi_n\}$ are a low-discrepancy set in $[0, 1)^d$, then to initialise a set of $\mathbf{V}$ that are distributed according to f_0, we can use the Gaussian cumulative distribution function (CDF)

$$H(x) = \frac{1}{2}\left(1 + \operatorname{erf}\left(x/\sqrt{2}\right)\right), \tag{5.27}$$

to create such a set by setting

$$\mathbf{V}_k^{(i)} = H^{-1}(\xi_k^{(i)}), \tag{5.28}$$

where the index i indexes the particle number and the index k indexes the dimension. In this case the approximation of the initial distribution is

$$f_0(\mathbf{v}) \approx \hat{f}_0(\mathbf{v}) := \frac{1}{N}\sum_{i=1}^{N} \delta\left(\mathbf{v} - \mathbf{V}^{(i)}\right). \tag{5.29}$$

5.3.2 Evolution in time

Given an initial distribution $\hat{f}_0$, it is well known that the solution at a time $t = \Delta t$ can be obtained by convolving the initial condition with the Gaussian kernel

$$G_{\Delta t}(\mathbf{v}) = (4\pi\Delta t)^{-d/2} \exp(-v^2/4\Delta t) \tag{5.30}$$

and so it would be natural estimate $f(\Delta t, \mathbf{v})$ by

$$\hat{f}_1(\mathbf{v}) = \int G_{\Delta t}(\mathbf{v} - \mathbf{v}')\hat{f}_0(\mathbf{v}')\, d\mathbf{v}' = \frac{1}{N}\sum_{i=1}^{N} G_{\Delta t}(\mathbf{v} - \mathbf{V}^{(i)}). \tag{5.31}$$

However this is a continuous distribution, and we would like to retain a particle description of the distribution. That is a new set of M particles, say $\left\{\mathbf{V}_1^i\right\}$ such that

$$\hat{f}_1(\mathbf{v}) \approx \frac{1}{M}\sum_{i=1}^{M} \delta\left(\mathbf{v} - \mathbf{V}^{(i)}\right). \tag{5.32}$$

The quality of the approximation given above is determined by the discrepancy, so for an arbitrary volume $\mathcal{B}$ we would like the approximation

$$\int_{\mathcal{B}} \hat{f}_1(\mathbf{v}) d\mathbf{v} \approx \frac{1}{M}\sum_{i=1}^{M} \chi_{\mathcal{B}}(\mathbf{V}_1^{(i)}) \tag{5.33}$$

where $\chi_{\mathcal{B}}$ is the characteristic function on $\mathcal{B}$, to be as good as possible. Venkiteswaran and Junk [2005a] were able to construct the following argument: taking the expectation of $\chi_{\mathcal{B}}$ using (5.31), gives

$$\int_{\mathbb{R}^d} \chi_{\mathcal{B}}(\mathbf{v})\hat{f}_1(\mathbf{v})\, d\mathbf{v} = \int_{\mathbb{R}^d}\int_{\mathbb{R}^d} \chi_{\mathcal{B}}(\mathbf{v} + \mathbf{v}')\; G_{\Delta t}(\mathbf{v})\hat{f}_0(\mathbf{v}')\, d\mathbf{v}\, d\mathbf{v}'. \tag{5.34}$$

Under the transformation

$$\mathbf{y} = \mathbf{H}(\mathbf{v}/\sqrt{2\Delta t}), \tag{5.35}$$

with $\mathbf{H}(\mathbf{v}) = (H(v_1), H(v_2), \ldots, H(v_d))$, which gives the Jacobian $G_{\Delta t}(\mathbf{v})$, (5.34) can be written as

$$\int_{\mathbb{R}^d} \chi_{\mathcal{B}}(\mathbf{v}) \hat{f}_1(\mathbf{v})\, d\mathbf{v} = \int_{[0,1]^d} \int_{\mathbb{R}^d} \chi_{\mathcal{B}}(\sqrt{2\pi}\mathbf{H}^{-1}(\mathbf{y}) + \mathbf{v}').\hat{f}_0(\mathbf{v}')\, d\mathbf{v}' d\mathbf{y}. \tag{5.36}$$

Now, suppose we have pairs $(\mathbf{V_0}, \xi)$ where $\mathbf{V_0}$ are independently distributed according to f_0 and $\xi \sim U([0,1)^d]$ respectively. Then it is easy to check that

$$\int_{\mathbb{R}^d} \chi_{\mathcal{B}}(\mathbf{v}) \hat{f}_1(\mathbf{v})\, d\mathbf{v} = \mathbb{E}[\chi_{\mathcal{B}}(\sqrt{2\pi}\mathbf{H}^{-1}(\xi) + \mathbf{V_0})]. \tag{5.37}$$

This gives motivation for the creation of new particles

$$\mathbf{V_1}^{(i)} = \mathbf{V_0}^{(i)} + \sqrt{2\pi}\mathbf{H}^{-1}(\xi^{(i)}), \tag{5.38}$$

which is nothing other than the Euler-Marayuma scheme of a discretised simple Brownian motion. Now, If we wish to use a quasi-Monte Carlo estimate of this expectation then the naive approach would lead us to the approximation

$$\mathbb{E}[\phi(\sqrt{2\pi}\mathbf{H}^{-1}(\xi) + \mathbf{V_0})] \approx \sum_{i=1}^{N}\sum_{j=1}^{M} \phi(\mathbf{V_0^{(i)}} + \sqrt{2\pi}\mathbf{H}^{-1}(\xi^{(j)}), \tag{5.39}$$

leading to the creation of NM new particles, which would result in an exponentially growing population of particles. Clearly this would result in a very impractical algorithm. The method [Venkiteswaran and Junk, 2005b] proposed can be justified by considering an arbitrary test function $\psi : \mathbb{R}^d \times [0,1)^d \to \mathbb{R}$:

$$\int_{[0,1)^d} \int_{\mathbb{R}^d} \psi(\mathbf{v}', \mathbf{y}) \hat{f}_0(\mathbf{v}')\, d\mathbf{v}' d\mathbf{y} = \frac{1}{N}\sum_{i=1}^{N} \int_{[0,1)^d} \psi(\mathbf{V_0}^{(i)}, \mathbf{y})\, d\mathbf{y}. \tag{5.40}$$

By tessellating an s-dimensional unit hypercube I^s into N disjoint subsets A_i of volume $1/N$, and defining χ_i to be the characteristic function (or indicator function)

on each set A_i we see that

$$\frac{1}{N} = \int_{I^s} \chi_i(\lambda)\, d\lambda, \tag{5.41}$$

and so,

$$\int_{[0,1)^d} \int_{\mathbb{R}^d} \psi(\mathbf{v}', \mathbf{y}) \hat{f}_0(\mathbf{v}')\, d\mathbf{v}' d\mathbf{y} = \sum_{i=1}^{N} \int_{[0,1)^s} \int_{[0,1)^d} \psi(\mathbf{V_0}^{(i)}, \mathbf{y}) \chi_i(\lambda)\, d\mathbf{y}\, d\lambda. \tag{5.42}$$

It may not be immediately clear why this is a useful observation to make, however if we take a quasi-Monte Carlo approximation of this integral by choosing a set of points (ξ, λ) with a low discrepancy in I^{d+s}

$$\sum_{i=1}^{N} \int_{[0,1)^s} \int_{[0,1)^d} \psi(\mathbf{V_0}^{(i)}, \mathbf{y}) \chi_i(\lambda)\, d\mathbf{y}\, d\lambda \approx \frac{1}{N} \sum_{i=1}^{N} \sum_{k=1}^{N} \psi(\mathbf{V_0}^{(i)}, \xi^{(k)}) \chi_i(\lambda^{(k)}). \tag{5.43}$$

If we are able to choose low discrepancy points so that λ_k lies in exactly one of the tessellated sets A_k then the double sum will have at most N non-zero terms. If the permutation $\sigma : \{1, \ldots, N\} \to \{1, \ldots, N\}$ maps each k to the to the index i for which $\chi_i(\lambda_k) = 1$ then,

$$\frac{1}{N} \sum_{i=1}^{N} \sum_{k=1}^{N} \psi(\mathbf{V_0}^{(i)}, \xi^{(k)}) \chi_i(\lambda^{(k)}) = \frac{1}{N} \sum_{i=1}^{N} \psi(\mathbf{V_0}^{(\sigma(k))}, \xi^{(k)}) \tag{5.44}$$

This property is fulfilled by $(0, m, d+s)-$nets, where the number of particles requires is $N = b^m$, where b is the base of the sequence, which must be greater or equal to the smallest prime number larger than $d + s$. So combining equations (5.43) (5.39) this motivates the quasi-Monte Carlo scheme

$$\mathbf{V_1}^{(i)} = \mathbf{V_0}^{(\sigma(i))} + \sqrt{2\pi}\mathbf{H}^{-1}(\xi^{(i)}) \tag{5.45}$$

which amounts to relabelling the indices of the particles before adding the quasi-random increments. In this way we justify the use of the Euler scheme in producing a low discrepancy estimates. In the same way it is possible to justify the use of other numerical schemes that discretise a Brownian motion.

5.4 Quasi-random sorting and mixing

[Venkiteswaran and Junk, 2005b] found that their mixing method alone was not sufficient for convergence, so in addition Venkiteswaran utilised a technique created by Lécot and El Khettabi [1999] for solving the diffusion equation. The approach that Lécot and El Khettabi [1999] took to remove correlations is a technique called quasi-random sorting. This can be summarised as the sorting of the particles position in each dimension sequentially, to produce a permutation σ which re-indexes the particles. This sorting step occurs once during each time-step. The authors found that the improvement in convergence rate, for the sorting method, degraded in dimensions higher than two, which was the motivation for the creation of the quasi-random mixing algorithm. The final method proposed by Venkiteswaran was to combine sorting in r dimensions and mixing in s dimensions into one algorithm, given the notation QMC(r, s). They found that QMC$(1, 1)$ achieved the best performance.

Instead of including the step where particles are sorted in 1-dimension, the method I propose, which I will refer to as a *randomised QMC* or RQMC, breaks correlations by introducing a random element back into the algorithm.

5.5 Randomised QMC for diffusion

A downside of the QMC method is that its deterministic nature fails to give it the means to provide any information about the error of the outputted estimate. The Koksma-Hlawka inequality provides in a sense, the worst possible error, but actually calculating this is difficult, especially because for the kind of problems we are considering f will be an unknown function and an estimate will be required to find its variational bound $V(f)$. Also, it gives the worse possible error, which might not be representative of the error we expect to see on average. This has led to the development of randomised QMC methods, which reintroduce an element of stochasticity into the calculations, allowing statistical error estimates to be obtained. There are several existing methods to randomise a quasi-Monte Carlo sequence, and we refer the reader to [LEcuyer and Lemieux, 2005] for a comprehensive guide.

The simplest method of introducing randomness was proposed by Cranley and Patterson [1976]. In order to randomise the sequence, during every time step we generate a vector $\mathbf{u} \sim U([0, 1))$ and add it modulo 1 to every point in the sequence, i.e.

$$\xi_i^{(j)} = \xi_i^{(j)} + u_i \mod 1. \tag{5.46}$$

where j indexes the particle number. This method is often referred to as *Cranley Patterson rotation*. The addition of the random uniform vector modulo 1 has the effect of guaranteeing that the estimator is unbiased [Munger et al., 2012]. When a point set $\mathcal{P}_n = \{\xi_1, \ldots, \xi_n\}$ is randomised Niederreiter [1992] showed that

$$\mathrm{Var}\left(\sum_i f(\xi_i)\right) = \mathbb{E}\left[\left(\sum_i f(\xi_i) - \int f(x)dx\right)^2\right] \leq \mathbb{E}[D^2(\mathcal{P}_n)]V^2(f) \tag{5.47}$$

which, so long as $\mathrm{Var}\,(f)$ is finite, means that rate of rate of convergence for the randomised method has the same bound. To test our RQMC method, we first apply to solve the diffusion equation (5.22) in 1-dimension with unit Gaussian initial condition. That is we compare the Euler-Marayuma discretisation, with

$$V_{t+1}^{(i)} = V_t^{(i)} + \sqrt{2\Delta t}\,\xi_i, \tag{5.48}$$

$\xi_i \sim N(0,1)$, for $i = 1 \ldots N$, against the RQMC scheme

$$V_{t+1}^{(i)} = V_t^{\sigma(i)} + \sqrt{2\Delta t}\,H^{-1}\left((\psi_i + u) \mod 1\right) \tag{5.49}$$

where ψ_i are terms from a $(0, m, 2)$-net in $[0,1)^2$ and $u \sim U\left([0,1)\right)$, where $N = b^m$. For our 1-dimensional results, we choose a Faure sequence in base $b = 2$ (with mixing in 1-dimension) which restricts the number particle numbers to powers of 2. Figure (5.4) shows the root-mean-square error in estimating the observable $\mathbb{E}[V_{100}]$ using both methods. The RQMC method displays an increased rate of root mean square error (RMSE) convergence, with an exponent that we estimate to be -0.93.

In figure 5.5 we test the method on a diffusion in 3-dimensions. We use the same procedure with a Faure sequence in base $b = 5$, the rate of convergence is estimated to be on average -0.94. This is a significant improvement to the $-1/2$ exponent. The results demonstrate the convergence of the method. In the next section we apply the method to the Fokker-Planck particle dynamics.

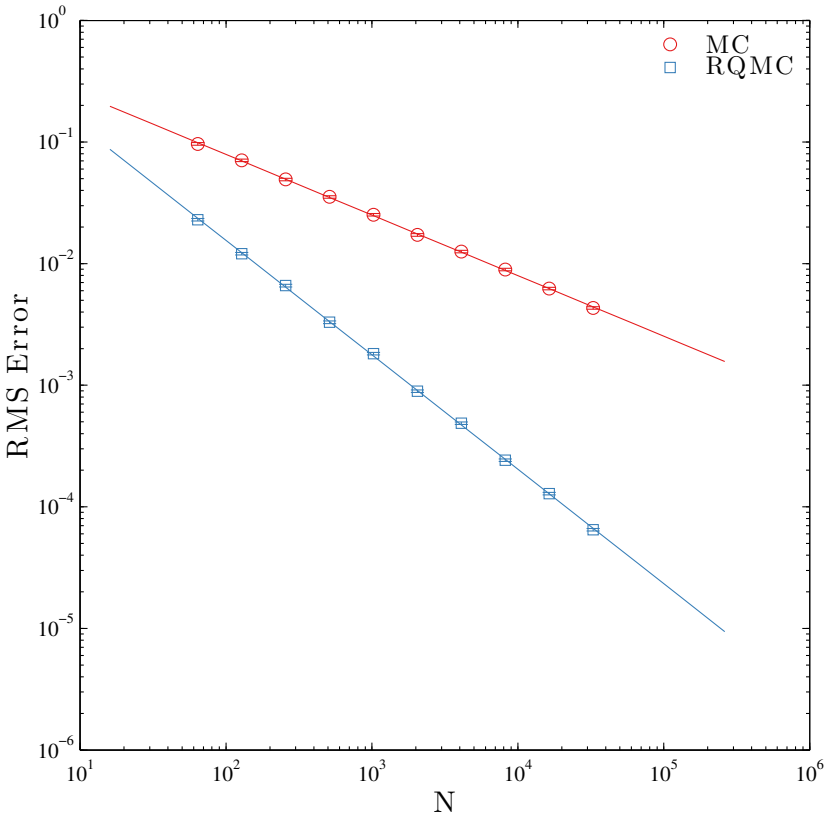

Figure 5.4: Comparison of mean square error, after 1000 time steps of different solutions schemes for the 1D diffusion equation. The RMQC method was implemented with a 1D Faure sequence.

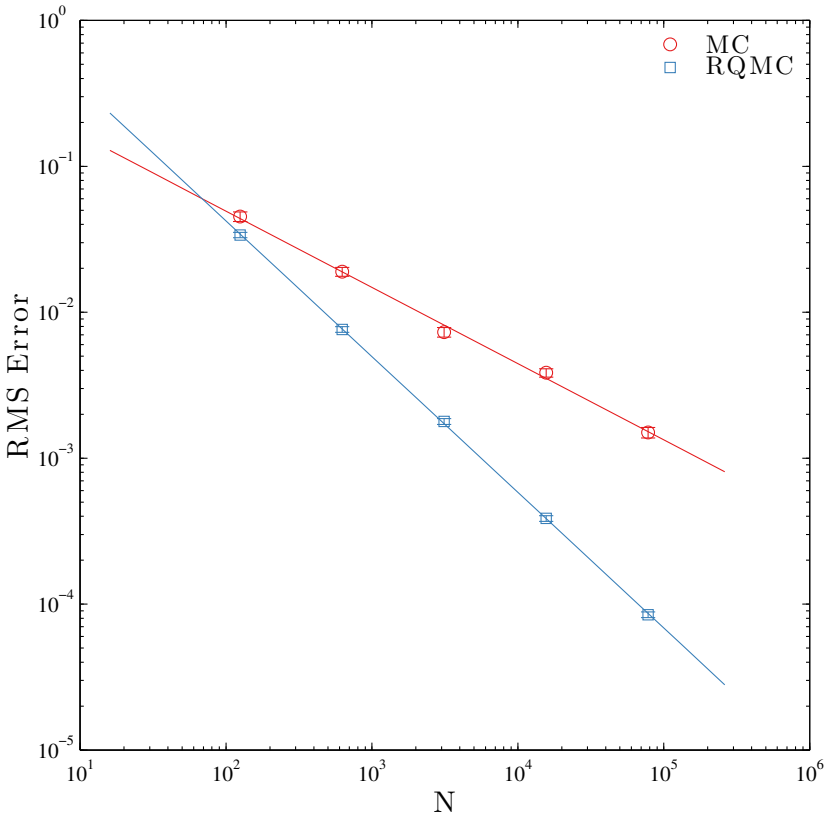

Figure 5.5: Comparison of mean square error, after 1000 time steps of different solutions schemes for the 3D diffusion equation. The RMQC method was implemented with a 3D Faure sequence.

5.5.1 Randomised QMC for a homogeneous Fokker-Planck relaxation

In a subsequent paper [Venkiteswaran and Junk, 2005b] went on to apply their algorithm to solve a Fokker-Planck equation modelling a fluid of polymers, where molecules are modelled as bead-spring chains. When numerically solving the homogeneous in space Fokker-Planck equation with particles, the full advection-diffusion operator can be written as the composition of an advection and diffusion operator. When considered in this way, this lets us substitute in our RQMC scheme for diffusion into the time-discretised approximate dynamics (3.33).

As for the other variance reduction schemes tested in the previous chapter, we test this method with a homogeneous relaxation to equilibrium, that is $f(t, \mathbf{x}, \mathbf{v}) = f(t, \mathbf{v})$ has no spatial component. We start from an initial distribution of particles $f_0(\mathbf{v}) = (1/2)(f_{MB}(v_1, c_0, c_0) + f_{MB}(v_1, -c_0, c_0))f_{MB}(v_2, 0, c_0)f_{MB}(v_3, 0, c_0)$, which will relax towards the Maxwellian distribution $f_{MB}(\mathbf{v}, \mathbf{0}, \sqrt{(4/3)c_0^2})$.

Figure 5.6 shows a comparison of mean results from 100 independent realisations of the MC (blue) and RQMC (red) algorithms with 5^3 computational particles. The shaded areas represent the standard deviation of the estimator of $|v|/c_0$, and we see that the relative uncertainty of the RQMC algorithm is significantly lower than that of the MC algorithm.

5.6 Application to spatially inhomogeneous problems

In spatially homogeneous problems, generally we are interested in estimating an expectation, for example the mean velocity at a location $\mathbf{x}$

$$\mathbf{u}(\mathbf{x}, t) = \int \mathbf{v} f(\mathbf{x}, \mathbf{v}, t)\, d\mathbf{v}, \tag{5.50}$$

and because we have a particle representation of f, we need to discretise the space into cells. This means that for each cell, indexed by i, we are typically estimating

$$\mathbf{u}^i(t) = \int\int \mathbf{v} f(\mathbf{x}, \mathbf{v}, t)\chi_i(\mathbf{x})\, d\mathbf{v}\, d\mathbf{x}, \tag{5.51}$$

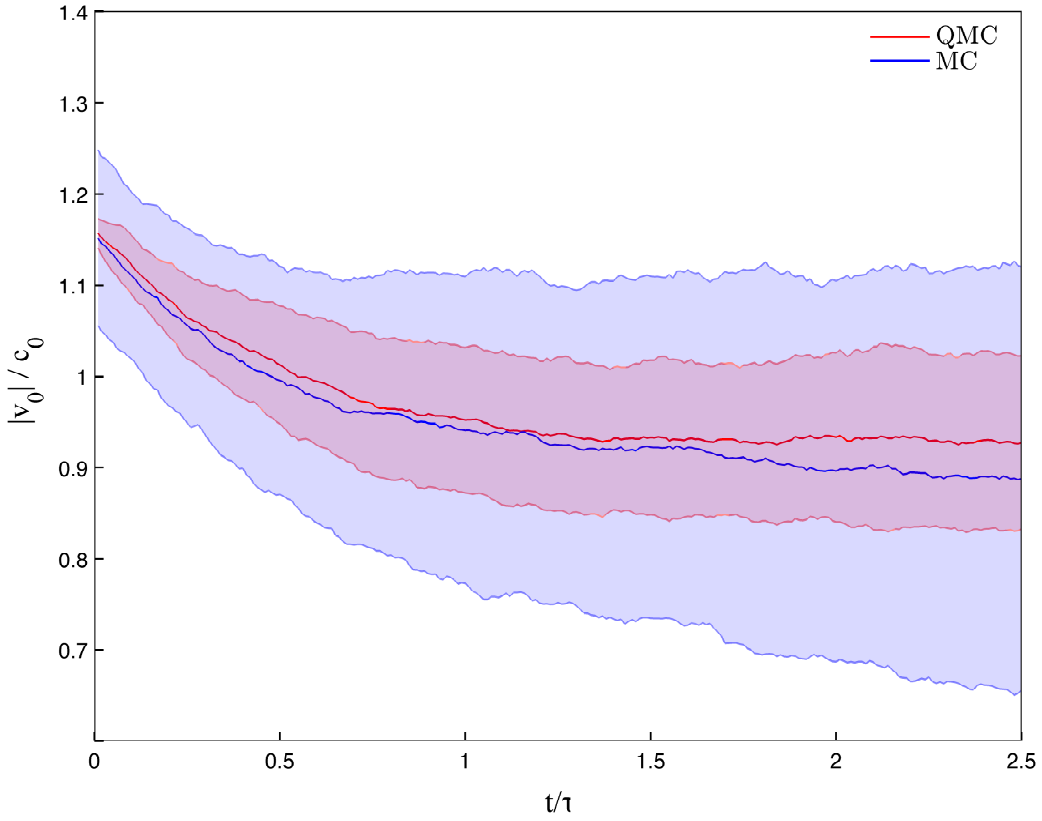

Figure 5.6: Comparison of mean square error, after 1000 time steps of different solutions schemes for the 3D diffusion equation. The RMQC method was implemented with a 5D-Faure sequence.

where the membership function $\chi_i(\mathbf{x})$ returns 1 if $\mathbf{x}$ lies within cell i and 0 otherwise. This function is not differentiable when $\mathbf{x}$ lies on the boundary of a cell, and so if we had a low discrepancy particle approximation of $f(\mathbf{x}, \mathbf{v}, t)$, the Koksma-Hlawka inequality would not guarantee a better than $N^{-1/2}$ rate of convergence. One way to avoid this would be to have a non-strict cell assignment i.e. a differentiable function to replace $\chi_i(\mathbf{x})$ that assigns particles to cells in a soft way, whilst still ensuring that $\mathbf{u}^i$ converges to $\mathbf{u}$ with increasing spatial resolution of the grid of cells. Any attempt at doing this, however, would mean a compromise between spatial resolution, as non-strict cell assignment would have the effect of blurring the estimators, and discrepancy as the stricter the cell assignment, the higher the total-variation of the integrand is likely to be.

Another challenge would be creating the low discrepancy particle approximation of the measure $f(\mathbf{x}, \mathbf{v}, t)$. This is because each particle's position $\mathbf{X}_j$ depends on it's velocity $\mathbf{V}_j$, and vice versa. This creates a challenge because the low discrepancy scheme described in this chapter is designed to solve problems where the diffusion can be decoupled from the drift, so it is unclear how to construct a scheme where the diffusion is spatially dependent. Also, one would need to be address boundary conditions and determine how to ensure that after collision with a boundary, the particles new velocity, contributes to a low-discrepancy approximation. This also makes developing a QMC algorithm with sub $N^{-1/2}$ convergence a much harder task. Addressing these issues will required further research

5.7 Discussion

In this chapter we have adapted a QMC method for solving the diffusion equation with particles, by replacing the sorting step in the QMC(1,1) algorithm with a randomisation technique. We find that the RQMC method achieves a better than $N^{-1/2}$ convergence, and have demonstrated the ability of the method to reduce the variance of estimations of expected quantities for diffusion and a homogeneous relaxation to equilibrium. The randomisation of the method means that averages can be taken over independent ensembles so the error of the method can be measured statistically. The method is simple to implement and doesn't require any major alterations to the basic algorithm.

We have considered applying the method to problems that are not spatially homogeneous, but found that the challenges preventing low-discrepancy particle approximations of the in homogenous distribution are great, and it is possible that QMC is not applicable in such situations. The major problem comes from the coupling of the particles dynamics in space, and velocity space, and could be an avenue for further research in the future.

6

Non-equilibrium steady-states of the Fokker-Planck kinetic equation, for elastic collisions

"Lisa get in here... in this house we obey the laws of thermodynamics!"
– Homer Simpson (*The Simpsons, Episode 124*)

The remaining chapters of this thesis are devoted to answering the following question: what might happen in the Simpsons' household if Homer did not enforce the laws of thermodynamics? Or more precisely, when the 2^{nd} law of thermodynamics does not apply. There are clear reasons why Homer might want his house to obey the laws of thermodynamics, not least that thermodynamic systems, where the state of the system can be adequately described by variables such as entropy, temperature, internal energy and pressure, are well understood. But this theory does not apply for systems which are not isolated, and systems that are observed in nature rarely are. Specifically, we are interested in the non-equilibrium steady states of the Fokker-Planck kinetic model, in cases where the presence of non-zero fluxes of energy and mass prevent the system relaxing to its thermodynamic equilibrium state.

6.1 Motivation

The hard sphere gas [Hansen and McDonald, 1990] is an idealised model of atomic, molecular, granular or colloidal gases. Interactions between particles in real gases are usually strongly repulsive at short separation distances due to volume exclusion and

weakly attractive at large distances due to Van-der-Waals forces. The hard sphere model idealises this behaviour with an interaction which is infinitely repulsive at separations shorter than a characteristic particle core radius and zero for larger separations. Such particles only interact when they collide. If collisions conserve energy, the system is said to be elastic. If energy is lost in collisions it is said to be inelastic (see [Krapivsky et al., 2010b]).

The elastic case is a good model for atomic and molecular gases. An isolated elastic system relaxes to an equilibrium steady state in which the distribution of velocities is Maxwellian. The inelastic case is more appropriate as a model of granular or colloidal gases [Brilliantov and Poschel, 2004] in which particles are macroscopic and can dissipate collisional kinetic energy into their internal degrees of freedom. An isolated inelastic system relaxes to a state in which velocities are zero since collisions dissipate energy. A non-trivial steady state velocity distribution is possible only if energy is continually supplied from an external source as occurs, for example, in vibrated granular gases [Rouyer and Menon, 2000]. Such steady states are inherently far from equilibrium because they result from a balance between two distinct driving and dissipation mechanisms for which detailed balance is not possible. The corresponding velocity distributions are generally not Maxwellian [Olafsen and Urbach, 1999; Kudrolli and Henry, 2000] and, at least in the case of vibrated granular gases, have stretched exponential tails [Rouyer and Menon, 2000].

One might then wonder whether there are circumstances in which a far-from-equilibrium hard sphere gas can exhibit a scale-invariant steady state. This is a natural question since scale invariance is a common property of many other driven dissipative systems including hydrodynamic turbulence [Frisch, 1995; Falkovich et al., 2001], cluster aggregation [Hayakawa, 1987; Takayasu et al., 1991; Connaughton et al., 2005], wave turbulence [Nazarenko, 2011a; Newell and Rumpf, 2011] and non-equilbrium Bose gases [Lacaze et al., 2001; Connaughton and Pomeau, 2004; Spohn, 2010].

This question has been recently addressed by Ben-Naim and co-workers in a series of papers [Ben-Naim and Machta, 2005; Ben-Naim et al., 2005; Kang et al., 2010] on the solutions of the Boltzmann equation for the inelastic hard sphere gas with a source of energy. They have shown that a stationary power-law velocity distribution is possible provided the driving mechanism is such that energy is supplied only to particles having very high velocities. Collisions redistribute this energy in the

phase space to particles having smaller velocities in a scale-invariant step-by-step process referred to as a "cascade" by analogy with scale-to-scale energy transport in turbulence. The cascade process generates a power law velocity distribution for velocities much smaller than the velocity scale of the driving.

These results become puzzling however if one asks what happens in the elastic limit. For the driven elastic hard sphere gas to reach a steady state, one must add an additional dissipation mechanism. This is reflected in the fact that the results of Ben-Naim et al. are singular in the elastic limit. Nevertheless, if this supplementary dissipation mechanism acts at velocities well separated from the velocity scale of the driving, then one might expect that the cascade dynamics identified in the inelastic case could be relevant over an intermediate range of scales and could lead to scaling. In fact, it has been shown by Kats and coworkers [Kats et al., 1975; Kats, 1976] that there are no universal self-consistent steady power-law solutions of the Boltzmann equation in the elastic case. Here, by universal, we mean that such solutions are determined by one parameter only, namely the flux of energy being transported through energy space.

Numerical simulations [Proment et al., 2012] strongly suggest that the steady state is close to Maxwellian. This is somewhat counterintuitive given that the system is strongly out of equilibrium. Analytic insight into this issue to date is restricted to partial solutions of a heuristic model called the differential approximation model [Proment et al., 2011, 2012] which replaces the collision operator with a nonlinear diffusion operator having the same scaling properties. Furthermore, simple arguments based on conservation laws suggest that the energy cascade in the elastic case should be towards higher velocities rather than towards smaller velocities. Therefore, everything that is known about the elastic case seems orthogonal to what is known about the inelastic case. In this chapter I provide some analytic arguments using the Fokker-Planck gas collision operator, supported where appropriate by numerical evidence, which resolve these dichotomies. In particular I investigate the universality of the solutions, with the aim of determining what characterises the stationary non-equilibrium states.

6.2 Kolmogorov-Zakharov spectra

Kolmogorov [1941] derived a formula for the energy spectrum of a high Reynolds number, incompressible turbulent fluid in terms of the wavenumber k, and found it

to be a power-law,

$$E(k) = C\epsilon_0^{2/3} k^{-5/3}, \tag{6.1}$$

where C is a constant, and ϵ_0 is the rate of dissipation. This has become known as *Kolmogorov's* 5/3 *law*. His calculations rely on the observation that turbulent flows consist of vortices which themselves consist of even smaller vortices. The vortices, at the larger scales are generated by an input of energy, for example by a stirring mechanism, and without this input of energy the motion would eventually settle down because of viscous dissipation acting on small length scales.

Kolmogorov postulated that in a statistical steady state, the transport of energy between scales where energy is injected and scales where energy is dissipated, is constant due to a local cascade process, where energy is transferred only between vortices of similar sizes. This range of energy scales is often referred to as the inertial range, as inertial effects are considered to have a much greater effect than viscous ones. By supposing this flux is constant, Kolmogorov deduced that the energy that lies in vortices of a specific size must only depend on the wavenumber k and the rate of dissipation ϵ_0. A simple dimensional analysis then results in the exponents given in equation (6.1). It is a simple argument but remarkably validated experimentally numerous times [Benzi et al., 1993; Frisch, 1980]. Deviations to the $-5/3$ exponent are commonly found and determining what precisely is universal for these transitional turbulence flows is an active area of research.

Almost 20 years later after Kolmogorov's discovery, similar power-law spectra were also found by Zakharov [Zakharov, 1965; Zakharov and Filonenko, 1967] in the field of wave-turbulence (WT). Wave turbulence began as field separate from the study of strong hydrodynamic turbulence, and may be defined as the study of non-equilibrium non-linear kinetic wave equations [Nazarenko, 2011b]. These kinetic wave equations describe how systems of weakly interacting waves evolve according to given resonant interactions, and are called *kinetic* equations in reference to Boltzmann's original kinetic equation where the interaction is between particles and not waves, and the microscopic conservation laws play the role of resonant interactions.

Analogously to the hydrodynamic cascade states, these steady-state cascades are not purely characterised by thermodynamic quantities, such as temperature and

chemical potential, but rather by constant fluxes of conserved quantities through phase space. Up until Zakharov's pioneering work, hydrodynamic turbulence and wave turbulence were distinct lines of enquiry. Such steady state solutions became known as Kolmogorov-Zakharov (KZ) spectra. Areas where the theory of WT has been successfully applied include gravity and capillary waves on the surface of water, waves that occur in planetary atmospheres and oceans, Rossby waves in atomspheric dynamics, Bose-Einstein condensates, non-linear optics, plasma waves, and many more.

6.3 Kolmogorov-Zakharov spectra of the Boltzmann equation

Like other kinetic models that have two conserved quantities, the homogeneous isotropic Boltzmann equation (which conserves energy and mass) might be expected to have two possible solutions that correspond to constant fluxes being transported through phase space. It was Kats et al. [1975] who first found stationary KZ spectra for the Boltzmann equation which correspond to these constant flux solutions. Here, we present the dimensional argument that, under the assumption of locality, results in the scaling exponents of these KZ spectra. We emphasise that the use of notation and methods from wave-turbulence is not due to an assumption that either turbulence, or waves, are present within dilute gases. The analogy originates from the kinetic equations where energy is transferred between scales. We begin with the spatially homogeneous Boltzmann equation (2.8) in the form:

$$\frac{\partial f}{\partial t} = \int W_{12}^{34}(f_3 f_4 - f_2 f_1))\,\mathrm{d}\mathbf{v}_2 \mathrm{d}\mathbf{v}_3 \mathbf{v}_4, \tag{6.2}$$

where

$$W_{12}^{34} = |\Gamma(\mathbf{v}_1\,\mathbf{v}_2;\,\mathbf{v}_3\,\mathbf{v}_4)|^2 \delta(\mathbf{v}_1 + \mathbf{v}_2 - \mathbf{v}_3 - \mathbf{v}_4) \times \delta(|\mathbf{v}_1|^2 + |\mathbf{v}_2|^2 - |\mathbf{v}_2|^2 - |\mathbf{v}_4|^2). \tag{6.3}$$

For the hard sphere gas, $\Gamma = \sigma^2/m$, where σ is the molecular diameter, and m is the molecular mass. If we assume that the gas is statistically isotropic, then it is possible to write the distribution function f in terms of the energy $\omega = |\mathbf{v}|^2$, so that $f(\mathbf{x}, \mathbf{v}, t) = f(\omega, t)$. The use of the notation $\omega = v^2$ originates from the

wave turbulence literature, where ω is a frequency. In three dimensions, the particle distribution in ω-space $F(\omega, t)$ must satisfy $F(\omega, t) = 2\pi\omega^{3/2} f(\omega, t)$ and so the Boltzmann Equation can be simplified into the form of the homogeneous isotropic Boltzmann equation (HIBE) [Proment et al., 2012]:

$$\frac{\partial F_1}{\partial t} = \int_0^\infty \int_0^\infty \int_0^\infty S_{34}^{12}(f_3 f_4 - f_1 f_2)\delta(\omega_1 + \omega_2 - \omega_3 - \omega_4)\,\mathrm{d}\omega_2 \mathrm{d}\omega_3 \mathrm{d}\omega_4, \tag{6.4}$$

where $F_1 = F(\omega_1, t)$, $f_i = f(\omega_i, t)$ and

$$S_{34}^{12} = \frac{2\pi\sigma^2}{m} \min\{\sqrt{\omega_1}, \sqrt{\omega_2}, \sqrt{\omega_3}, \sqrt{\omega_4}\}. \tag{6.5}$$

Boltzmann's H-Theorem leads to the conclusion that any non-zero initial condition must relax to an equilibrium state described by the Maxwell-Boltzmann distribution

$$f_{MB}(\omega) = Ae^{-\omega/T} \tag{6.6}$$

where T is the thermodynamic temperature. Collisions in the gas are assumed to be elastic, resulting in the existence of two invariant quantities, particle density ρ_M and energy density ρ_E which can be found as moments of the distribution:

$$\rho_M = 2\pi \int_0^\infty \omega^{1/2} f(\omega)\,\mathrm{d}\omega \tag{6.7}$$

$$\rho_E = \frac{2\pi}{\rho_M} \int_0^\infty \omega^{3/2} f(\omega)\,\mathrm{d}\omega. \tag{6.8}$$

Without the presence of forcing and dissipation, these thermodynamic quantities will remain constant in time and so the Maxwellian distribution that is relaxed to will have the same particle and energy density as that of the initial condition. The KZ spectra for the Boltzmann equation can be found with the following dimensional argument. We will consider the dimensional quantities in terms of units of energy $[E]$, length $[L]$, time $[t]$. The integral of $F(\omega)$ over ω-space is a density so F has units $[E]^{-1}[L]^{-3}$, and hence $f(\omega)$ has units $[L]^{-3}[E]^{-5/2}$. In general, if we assume

that $S_{34}^{12} = \gamma\Gamma_{34}^{12}$, where $\Gamma_{34}^{12} \sim \omega^{\lambda}$ so has units $[E]^{\lambda}$, and γ is a constant with units designed to keep (6.4) dimensionally consistent, then it is required that:

$$[E]^{-1}[L]^{-3}[t]^{-1} = [\gamma][E]^{\lambda}[L]^{-6}[E]^{-5}[E]^{-1}[E]^{3} \tag{6.9}$$

and so

$$[\gamma] = [L]^{3}[E]^{2-\lambda}[t]^{-1}. \tag{6.10}$$

Now, let us suppose that the steady-state solution with constant energy flux, ϵ, is local, and can be written in terms of only the local quantities η, γ, and ω, i.e.

$$f = \gamma^{a}\eta^{b}\omega^{c}. \tag{6.11}$$

ϵ is the energy flux, so has units $[E][L]^{-3}[t]^{-1}$. Dimensional analysis this requires that

$$[L]^{-3}[E]^{-5/2} = [L]^{3a}[E]^{a(2-\lambda)}[t]^{-a}[t]^{-b}[L]^{-3b}[E]^{b}[E]^{c}. \tag{6.12}$$

Equating powers of $[L]$ gives $-3 = 3a - 3b$, while equating powers of $[t]$ forces $0 = -a - b$, and so $a = -1/2$ and $b = 1/2$. Finally, equating powers of $[E]$

$$-5/2 = -(2-\lambda)/2 + 1/2 + c, \tag{6.13}$$

so

$$c = \frac{-10 + 4 - 2\lambda - 2}{4}. \tag{6.14}$$

For the hard-sphere particle interaction we know that $\lambda = 1/2$, so the exponent $c = -9/4$. The same argument applied to a constant particle flux η results in the exponent $c = -7/4$.

It is simple to check that the exponent $c = -7/4$ corresponds to a constant flux of particles in the positive direction, while the exponent $c = -9/4$ corresponds to

a constant flux of energy in the negative direction. In order for such solutions to be physically relevant, the collision operator must converge when the inertial range is infinite. However, as originally shown by Kats et al. [1975], the collision integral fails to converge for these solutions. Further to this, the directions of the flux given by these solutions do not match up those given by the Fjortoft argument [Fjørtoft, 1953], which we will discuss in the next section.

6.4 The Fjortoft argument

The Fjortoft argument relies on the conservation and the dimensions of conserved quantities to determine wether the conserved quantities are transported predominantly in the positive or negative direction. For the HIBE, it takes the following form. Consider an open system with a forcing scale ω_f and two dissipation scales $\omega_{\min}$ and $\omega_{\max}$ which are widely separated, so that $\omega_{\min} \ll \omega_f \ll \omega_{\max}$. We wish to determine the direction that particles and energy will be transported in. If energy is injected with a rate ϵ at the forcing scale ω_f, then since dimensionally energy density and particle density differ by a factor of ω, the forcing rate of the particles η must have the relationship $\epsilon \sim \omega_f \eta$. If energy is dissipated at the smaller scale $\omega_{\min}$ with a rate of the same order of magnitude as ϵ, then particles here will be dissipated at a rate proportional to $\epsilon/\omega_{\min} \sim \eta\omega_f/\omega_{\min} \gg \eta$. In the steady state we cannot have the dissipation rate greater than the forcing rate, hence it is reasonable to conclude that energy is mostly dissipated at the higher energy scale and so energy flux is predominantly in the positive direction. By an analogous argument it can be concluded that particle flux must be predominantly in the negative direction. An alternative argument that relies on applying the Cauchy-Schwartz inequality to certain centroids of the distribution is given by Nazarenko [2011a].

When KZ spectra have the alternate flux direction to that predicted by the Fjortoft argument, this is generally interpreted as there is no possible forcing and dissipation mechanism that can be applied in order for these solutions to be realised. From this it can be concluded that the KZ spectra are not physically relevant solutions for the Boltzmann equation.

6.5 The Boltzmann differential approximation model

Instead it has been proposed that mixed-state cascades, or so called "warm cascades" must exist for the Boltzmann equation [Proment et al., 2012]. Using a lattice based

algorithm to numerically solve the HIBE, Proment and co-authors were able to show that when forcing within a narrow band of energies around a scale ω_f, and dissipation in the form of a filter which removes particles with energies below a minimum $\omega_{\min}$ and above a maximum energy $\omega_{\min}$, were present, solutions to the HIBE occur that appear very close to the Maxwellian distribution with a well defined temperature.

To investigate such mixed-state solutions, Proment et al. postulated a differential approximation model (DAM) for the Boltzmann equation. DAMs are simplified models of kinetic equations which are constructed in order to preserve the scalings of the original equation, and their solutions. As such, they are a very useful tool for providing qualitative and quantitative knowledge of the underlying physical system. For example, such simplified models have been created for the non-linear Schrodinger equation, the kinetic equations that model Kelvin-waves in quantum turbulence Nazarenko [2006], a model for water gravity WT [Hasselmann et al., 1985] and models of cluster aggregation.

In order to simplify the collision operator, Proment et al. made the assumption that the interactions of the system in it's steady state are *strongly local*, that is the integrand of the collision operator only makes a significant contribution when $\omega_1 \approx \omega_2 \approx \omega_3 \approx \omega_4$. By making this assumption, the HIBE can be used to derive the following DAM.

$$\partial_t F(\omega, t) = -\partial_{\omega\omega} R[f(\omega, t)], \tag{6.15}$$

where

$$R[f(\omega, t)] = -S\omega^{13/2} f^2(\omega, t) \partial_{\omega\omega} \log f(\omega, t). \tag{6.16}$$

The above DAM has the form of dual conservation law, and it is trivial to check that the KZ spectra with the exponents $\alpha = 9/4$, $\alpha = 7/4$ are solutions that represent constant energy flux and constant particle flux solutions respectively. By using this DAM, and matching the front solutions near to the cut offs $\omega_{\min}$ and $\omega_{\max}$ to a Kats-Kontorovic correction of the form $f = f_M(1 + f_d)$, Proment et al. were then able to make the prediction

$$T = \frac{2\omega_{\max}}{\frac{7}{2}\log\frac{\omega_{\max}}{\omega_{\min}} + \log\frac{\omega_{\max}}{\omega_f} - 2\log\frac{9}{2}}. \tag{6.17}$$

Surprisingly, they found that their results predicted a temperature of the steady-state that is independent of the forcing rate ϵ and that the solution scales linearly with ϵ. This is significant as it departs from the dimensional analysis that, due to the quadratic non-linearity of the collision operator, leads to the scaling $f \sim \epsilon^{1/2}$. They compared this prediction to numerical results from the HIBE numerical code, and found that their prediction agreed qualitatively with the numerics.

6.6 Steady-states of the isotropic Fokker-Planck equation

We now use of the Fokker-Planck equation to study the same problem. In 3-dimensions and homogeneous in space it takes the following form

$$\partial_t f = \frac{1}{\tau}\nabla_{\mathbf{v}} \cdot \{(\mathbf{v} - \mathbf{U})f + T\,\nabla_{\mathbf{v}} f\}\,. \tag{6.18}$$

where τ is a relaxation time. When $f = f(\omega)$ is isotropic, the equation becomes:

$$\partial_t f = \frac{2\pi}{\tau\omega^{1/2}}\frac{\partial}{\partial\omega}\left\{\omega^{3/2}\left(f + T\frac{\partial f}{\partial\omega}\right)\right\} := I_{FP}(f). \tag{6.19}$$

Since the collision operator conserves mass and energy, we can write (6.19) in conservative forms for mass and energy:

$$\partial_t \omega^{1/2} f = -\frac{\partial}{\partial\omega} J_p \tag{6.20}$$

$$\partial_t \omega^{3/2} f = -\frac{\partial}{\partial\omega} J_E \tag{6.21}$$

where J_p and J_E are the fluxes of mass and energy respectively, and are related by

$$J_E = \omega J_p - \int_0^\omega J_p(\omega')\,d\omega'. \tag{6.22}$$

The fluxes are defined so that a positive flux means that the flux moves in the direction of higher energies. As in Proment et al. [2012], we introduce forcing in our system by adding a source term into the equation governing the evolution of the distribution of energy $F = \omega^{3/2} f$,

$$\frac{\partial F}{\partial t} = \omega^{3/2} I_{FP}(f) + \mathcal{F}(\omega). \tag{6.23}$$

If we add a source term $\mathcal{F}(\omega) = \epsilon\delta(\omega - \omega_f)$ where ϵ is the rate of energy forcing, and ω_f is the forcing scale, then the solution to the steady state ODE is a Greens function from which solutions to arbitrary forms of forcing may be found. This form of forcing can be considered to be a constant flux of particles entering the system with energy ω_f. Dissipation is introduced by enforcing Dirichlet boundary conditions $f(\omega_{\max}) = f(\omega_{\min}) = 0$ for a lower energy cut-off $\omega_{\min}$ and higher energy cut-off $\omega_{\max}$ allowing energy and particles to freely leave the system.

Explicitly solving (6.23) for its steady state requires the solution of a non-linear integro-differential equation. Such equations normally are intractable analytically, but here we are able to exploit the fact that the equation is transformed into a linear PDE by supposing T is known. We are then able to find T self-consistently. The self-consistency assumption leads us to the following Dirichlet problem

$$\begin{cases} I_{\mathrm{FP}}(f(\omega)) = 0 \quad \forall\, \omega \in (\omega_{\min}, \omega_f) \cup (\omega_f, \omega_{\max}), \\ f(\omega_{\min}) = 0, \\ f(\omega_{\max}) = 0, \\ J_p(\omega_{\max}) - J_p(\omega_{\min}) = \epsilon/\omega_f \end{cases} \tag{6.24}$$

with the self consistency condition

$$\begin{aligned} T &= \psi[f(\omega; T)] \\ &= \frac{2}{3} \frac{\int \omega^{3/2} f(\omega; T)\, d\omega}{\int \omega^{1/2} f(\omega; T)\, d\omega}\,. \end{aligned} \tag{6.25}$$

With the ansatz

$$f(\omega) = e^{-\omega/T} f_d(\omega), \tag{6.26}$$

where f_d is a correction to a Maxwellian distribution, an analytic solution can be found (see Appendix D), and is given by

$$f(\omega) = \begin{cases} \tau f_M(\omega) J_p(\omega) \left(\hat{f}(\omega_{\min}) - \hat{f}(\omega) \right) & : \omega < \omega_f \\ \tau f_M(\omega) J_p(\omega) \left(\hat{f}(\omega_{\max}) - \hat{f}(\omega) \right) & : \omega \geq \omega_f, \end{cases}$$

where

$$\hat{f}(\omega) = \frac{2\sqrt{\pi}\mathrm{erfi}(\sqrt{\omega/T})}{\sqrt{T}} - \frac{2e^{\omega/T}}{\omega^{1/2}}, \tag{6.27}$$

and the particle flux J_p is given by

$$J_p = \begin{cases} \dfrac{-\epsilon}{\omega_f}\theta & : \omega < \omega_f \\ \dfrac{\epsilon}{\omega_f}(1-\theta) & : \omega \geq \omega_f \,, \end{cases}$$

where,

$$\theta(\omega_{\max}, \omega_{\min}, \omega_f, T) = \frac{\hat{f}(\omega_{\max}) - \hat{f}(\omega_f)}{\hat{f}(\omega_{\max}) - \hat{f}(\omega_{\min})} \in (0,1), \tag{6.28}$$

and we notice that when we have $\omega_{\min} \ll \omega_f \ll \omega_{\max}$, the predictions given by the Fjortoft argument are recovered (see Figure (6.6)). The analytic form of the solution (6.27) illustrates how arbitrarily large fluxes are able to be carried by solutions that appear close to Maxwellian. The derivative of the deviation f_d is

$$\frac{d\, f_d}{d\, \omega} = \omega^{-3/2} e^{\omega/T}, \tag{6.29}$$

so for $\omega \ll T$ and $\omega \gg T$, the derivative is dominated by the polynomial and exponential terms, and the derivative is large. However, for $\omega \sim \mathcal{O}(T)$, the derivative becomes small, with a minimum occurring at $\omega = 3T/2$. It is in this region where the

deviation appears to be constant and the solution appears to be close to Maxwellian.

6.7 Time dependent solutions

Time dependent solutions were found numerically using the NDsolve function within the software package *Mathematica*, which uses the method of lines to discretize the problem in all but one direction, and then integrates the resulting system of ODEs. Figures 6.1-6.2 show the direct cascade, while figures 6.3-6.4 show the inverse cascade.

6.8 Parameter dependence of the effective temperature in the non-equilibrium steady state

Given the general solution to the Dirichlet problem, the temperature can be found self consistently as the solution to (7.19). In agreement with the differential approximation model, we can see immediately that the temperature is independent of the forcing rate ϵ, and therefore must only depend on the forcing scale ω_{f} and dissipation scales ω_{min} and ω_{max}, see Fig 6.5.

We compare our predictions from the Fokker-Planck model to numerical results from the HIBE with the numerical solver created by Asinari [2010], and with predictions from the DAM model. The Asinari algorithm solves the HIBE by discretising the ω space up to a certain energy scale ω_{cutoff}, and integration is performed over a pre-determined set of resonant energies. Dissipation is included by setting the distribution above ω_{max} and below ω_{min} to zero during each timestep. To prevent ultraviolet bottleneck effects, we ensure that $\omega_{\mathrm{cutoff}} > 2\,\omega_{\mathrm{max}}$.

In Fig 6.7, we set $\omega_{\mathrm{min}} = 450$, $\omega_{\mathrm{max}} = 9850$ and $\omega_f = 1500$, and compare the distributions produced by the Fokker-Planck and HIBE models. Due to differences in boundary conditions and forcing mechanisms, we observe differences in these regions, but in general the distributions show the same qualitative behaviour. We then observe the effect of changing the forcing and dissipation scales on the temperature, while keeping the other parameters fixed. Fig 6.8 and Fig 6.9 show the effect of varying the dissipation scales, and Fig 6.10 shows the effect of varying the forcing scale on the effective temperature. Our results show that there is a good agreement between the HIFP and the HIBE effective temperate, and an improvement to the predictions generated from the DAM approximation.

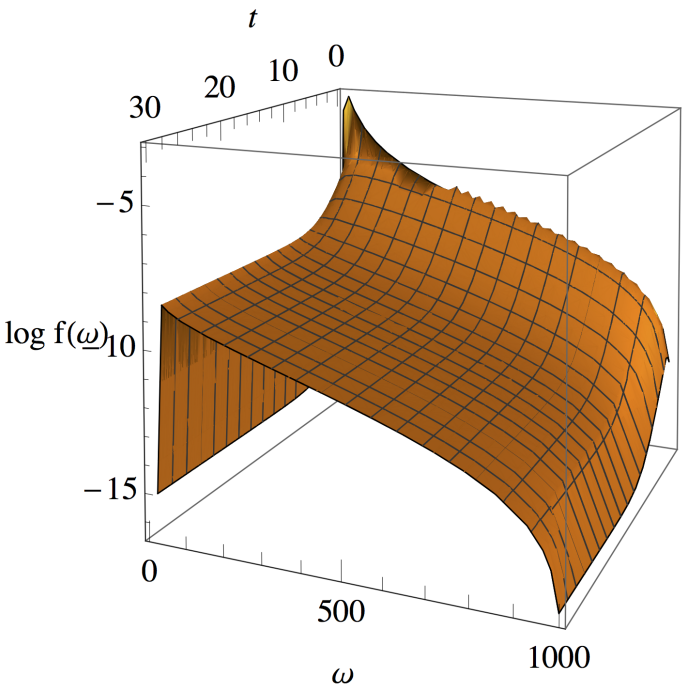

Figure 6.1: Time dependent solutions to HIFP, $\omega_{\min} = 10$, $\omega_{\max} = 1000$, $\omega_f = 15$.

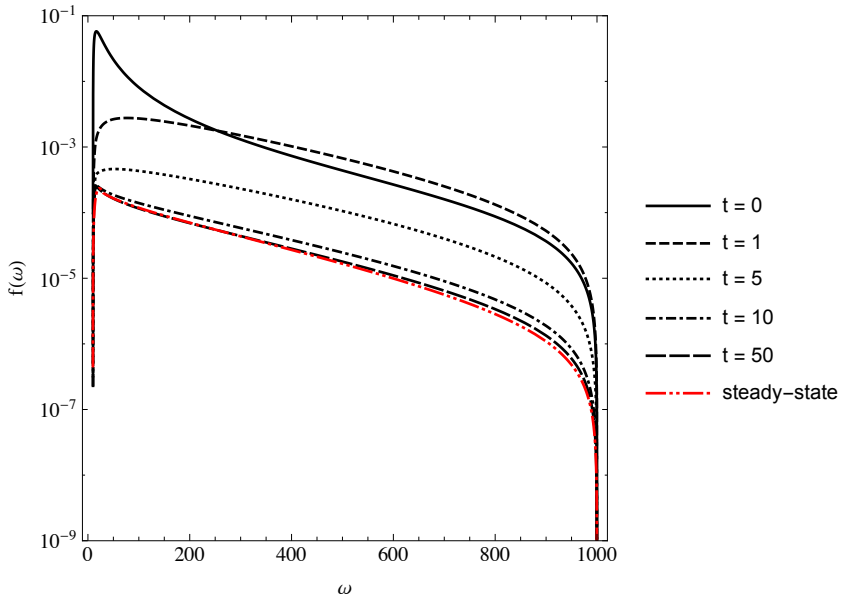

Figure 6.2: Time dependent solutions to HIFP, $\omega_{\min} = 10$, $\omega_{\max} = 1000$, $\omega_f = 15$

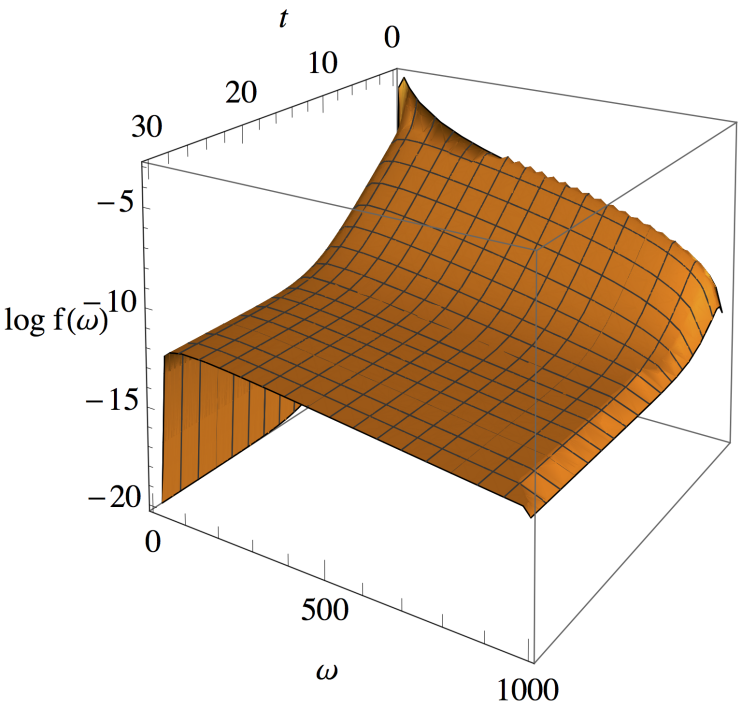

Figure 6.3: Time dependent solutions to HIFP, $\omega_{\min} = 10$, $\omega_{\max} = 1000$, $\omega_f = 990$

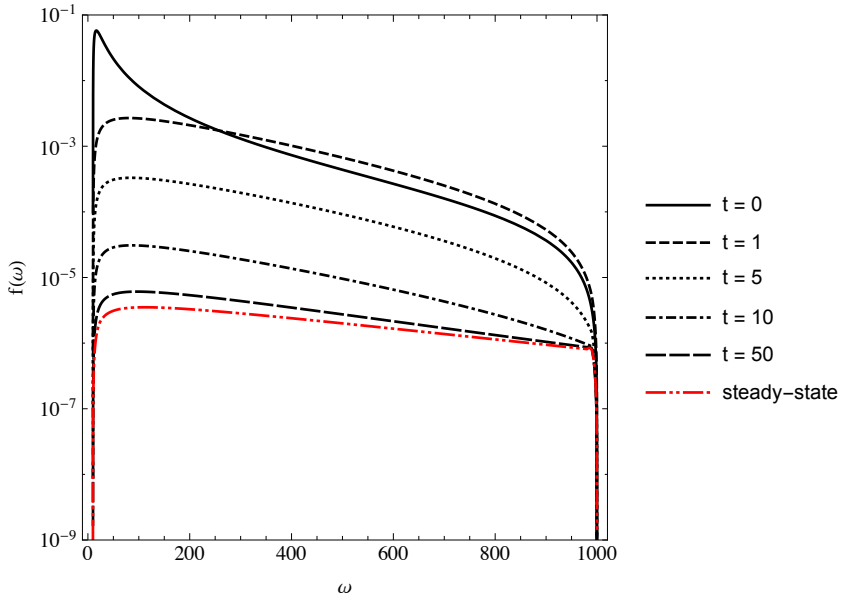

Figure 6.4: Time dependent solutions to HIFP, $\omega_{\min} = 10$, $\omega_{\max} = 1000$, $\omega_f = 990$

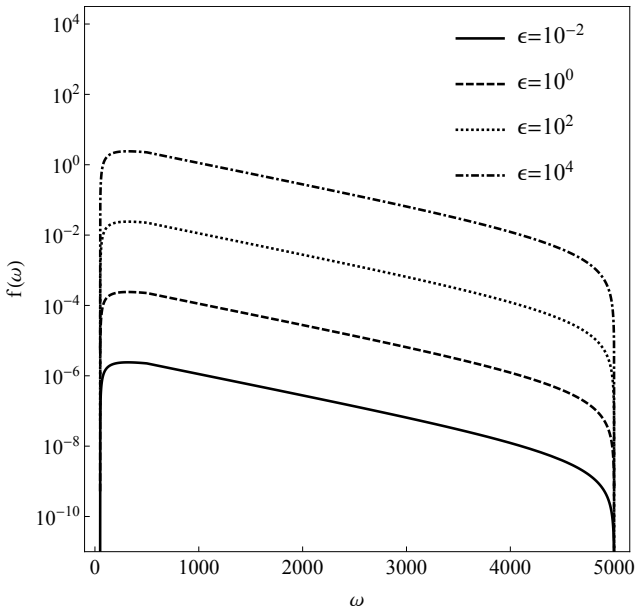

Figure 6.5: Steady state solutions with varying forcing rates, $\omega_{\min} = 50$, $\omega_f = 500$, $\omega_{\max} = 5000$, $\tau = 1$. $T = 746.6$ found self consistently.

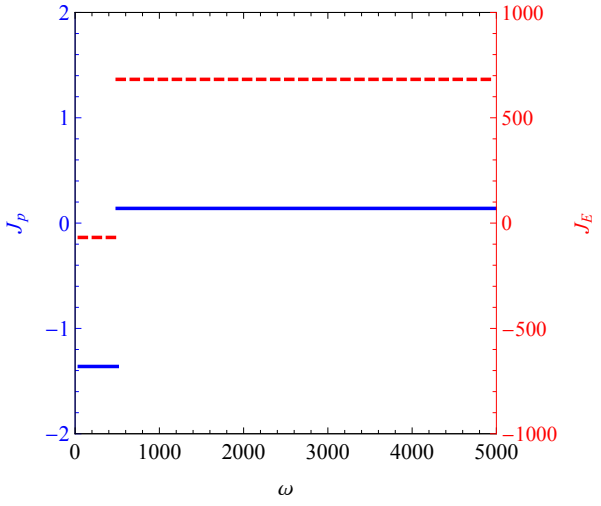

Figure 6.6: Particle flux (blue, solid line, left axis), and energy flux (red, dashed line, right axis) with parameters $\omega_{\min} = 50$, $\omega_f = 500$, $\omega_{\max} = 5000$, $\tau = 1$. $T = 746.6$.

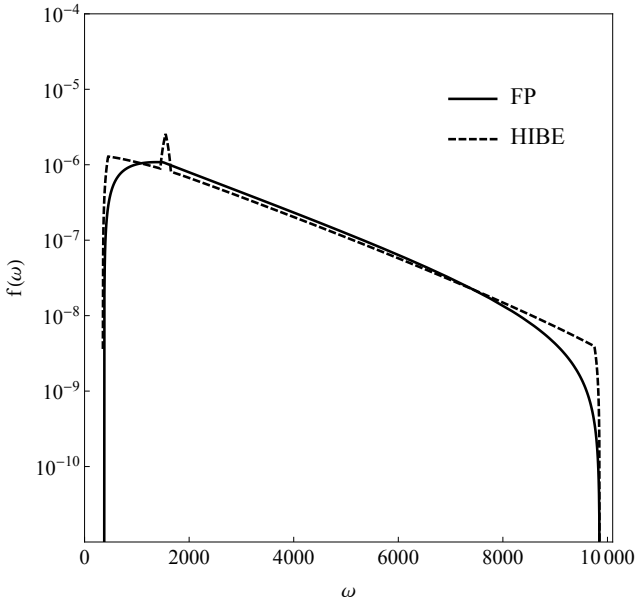

Figure 6.7: Fokker-Planck solution (solid) and HIBE solution (dashed) with parameters $\omega_{\min} = 450$, $\omega_f = 1500$, $\omega_{\max} = 9850$, $\tau = 1$. $T = 1442.6$

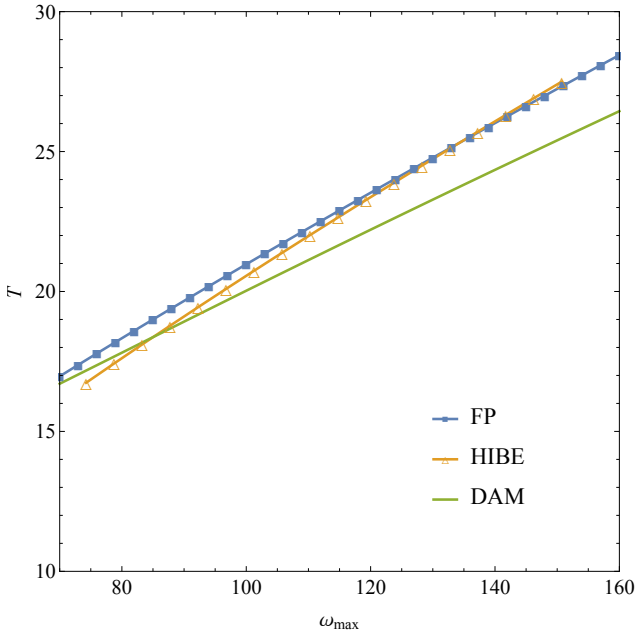

Figure 6.8: Comparison of effective temperature, when varying $\omega_{\max}$ and keeping other parameters fixed: $\omega_{\min} = 4.5$, $\omega_f = 22.5$.

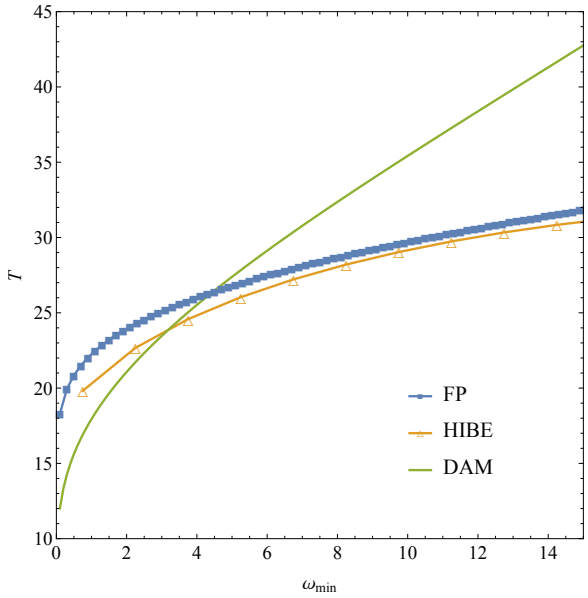

Figure 6.9: Comparison of effective temperature, when varying $\omega_{\min}$ and keeping other parameters fixed: $\omega_f = 22.5$, $\omega_{\max} = 148.5$.

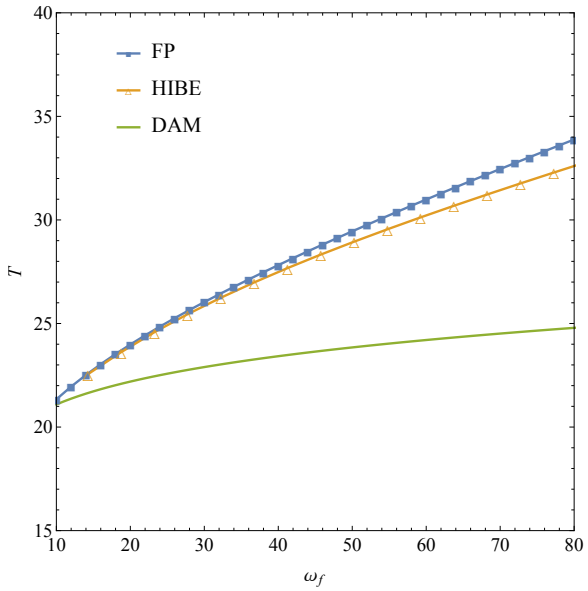

Figure 6.10: Comparison of effective temperature, when varying ω_f and keeping other parameters fixed: $\omega_{\min} = 4.5$, $\omega_{\max} = 148.5$.

As well as finding the temperature numerically, we observe that for any choice of parameter values, the solution to $T = \psi(T)$ appears close to the limit

$$\begin{aligned} T^* &= \lim_{T\to\infty} \psi(T) \\ &= \frac{\omega_{\min}^{3/2}\omega_f^{1/2} + \omega_{\min}^{1/2}\omega_f^{3/2} + \omega_{\min}(\omega_{\min}+\omega_f)}{5\left(\sqrt{\omega_{\min}\omega_f} + \omega_{\min} - \sqrt{\omega_{\max}\omega_f} - \omega_{\max}\right)} \\ &\quad + \frac{-\omega_{\max}^{3/2}\omega_f^{1/2} - \omega_{\max}^{1/2}\omega_f^{3/2} - \omega_{\max}(\omega_{\max}+\omega_f)}{5\left(\sqrt{\omega_{\min}\omega_f} + \omega_{\min} - \sqrt{\omega_{\max}\omega_f} - \omega_{\max}\right)}. \end{aligned} \tag{6.30}$$

See figures 6.11-6.12. This gives us the following predictions:

$$\lim_{\omega_{\max}\to\infty} \frac{T}{\omega_{\max}} = c_1 \tag{6.31}$$

and

$$\lim_{\omega_{\min}\to 0} \frac{T}{\sqrt{\omega_{\min}}} = c_2 \tag{6.32}$$

for positive constants c_1 and c_2. This predictions appear to be in agreement with the numerical evidence provided by Figures 6.9 - 6.8.

6.9 Locality

The concept of the locality of the energy spectra is one that has its origins in the wave turbulence literature [Nazarenko, 2011b]. An energy spectrum is considered *local* if in the so-called inertial range, that is, the energy range between forcing and dissipation scales which are widely separated, the solution is independent of the details of the source and sink. In particular, this means that if we take the inertial range to be infinite, the solution will be non-zero and finite. Formally, a spectrum is local if the collision operator converges when the inertial range is infinite.

The assumption of locality is important, because as a consequence one can assume that the collision operator converges without a compact support. This allows the order of integration to swapped for an integral collision operator, and is a key step in the dimensional analysis technique that allows KZ spectra to be found. When a Kolmogorov spectrum is found, one can then check in a self consistent manner that the solution satisfies the criteria of locality. This is the case for the

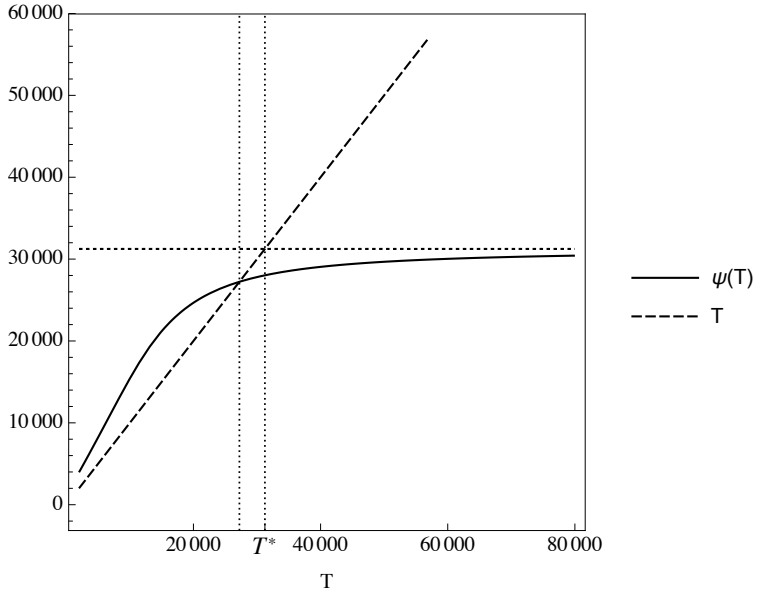

Figure 6.11: Comparison of solution to $T = \psi(T)$ and T^*, with $\omega_{\min} = 1000$, $\omega_f = 2000$, $\omega_{\max} = 10^5$.

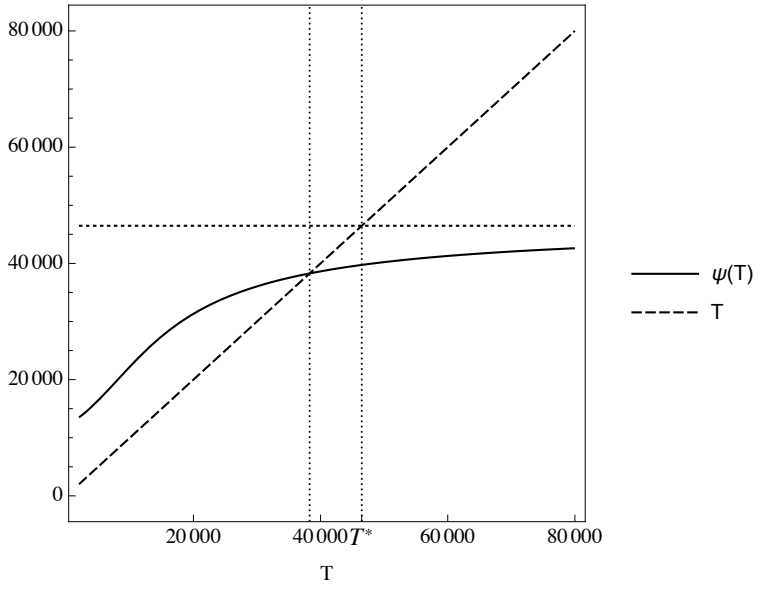

Figure 6.12: Comparison of solution to $T = \psi(T)$ and T^*, with $\omega_{\min} = 1000$, $\omega_f = 20000$, $\omega_{\max} = 10^5$.

Boltzmann equation. KZ spectra can be found for the Boltzmann equation under the assumption of locality, but these power-law spectra have exponents which mean the collision integral does not converge for an infinite inertial range, and so they are not relevant solutions.

Locality is a somewhat broadly defined property. A stricter definition is provided by *strong locality*, which is the assumption that allows the construction of differential approximation models commonly used in wave turbulence to analyse cascades. The DAM for the Boltzmann equation, first proposed by Proment et al, is one such model, directly obtained by assuming that particles with energy ω are assumed to only interact with particles $\omega+\Delta\omega$ where $\Delta\omega$ is small, allowing the Taylor expansion of the Boltzmann integrand.

The Fokker-Planck collision operator is an integro-differential operator, and so it possible that steady-state solutions to the equation could be either local or non-local. First we consider the direct cascade, and begin by observing the effect on the solution by increasing the upper dissipation scale, $\omega_{\max}$. Figures 6.13, 6.14 demonstrate that as we take $\omega_{\max} \to \infty$ and keeping the other parameters fixed, the solution loses dependence on $\omega_{\max}$. We then observe in figure 6.15 the effect of decreasing the forcing scale ω_f, and find that as we decrease ω_{f} the solution scales like $f \sim \omega_f^{-1}$. This is a non-local dependence of the forcing scale on the solution.

Next, we test the locality of the the inverse cascade, which represents a constant flux of particles. If we want to keep the particle flux constant as we increase the forcing scale ω_f then since $\eta = \epsilon/\omega_f$, we need the energy forcing to scale like $\epsilon \sim \omega_f$. This means that as we increase ω_f, the solution loses it's dependence on the forcing scale. So just like the direct cascade, the inverse cascade has a solution in the inertial range that does not depend on the upper energy scale. Next, we check the effect on the solution of decreasing the lower cut-off $\omega_{\min}$, whilst keeping the forcing scale and upper-dissipation scale fixed. Figure 6.16 clearly shows the effect of the lower dissipation scale on the solution. Again, we conclude that this cascade has a non-local dependence on the $\omega_{\min}$ and so the inverse cascade is also non-local.

6.10 Discussion

In this chapter we have reviewed the existing literature regarding the non-equilibrium steady-states of the Boltzmann equation. Th KZ spectra that are possible to derive

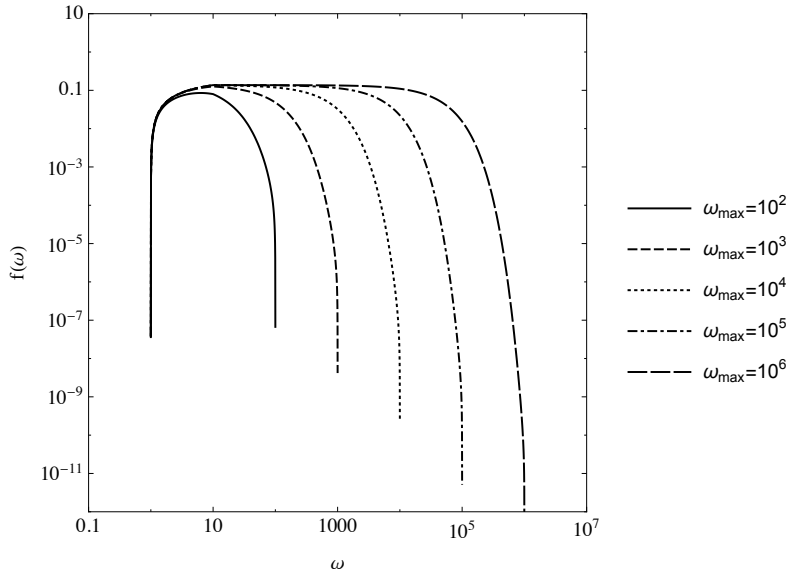

Figure 6.13: Comparison of solutions when keeping $\omega_{\min} = 1$, $\omega_f = 10$ fixed, and increasing $\omega_{\max}$. We find that as we keep increasing $\omega_{\max}$, the solution at a fixed ω no longer depends on $\omega_{\max}$.

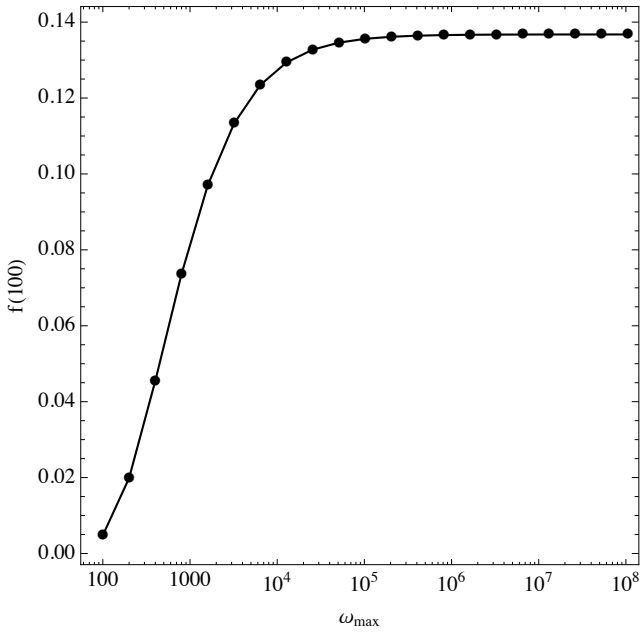

Figure 6.14: The effect on the solution f, at $\omega = 50$ when keeping $\omega_{\min} = 1$, $\omega_f = 10$ fixed, and increasing $\omega_{\max}$. We find that as we keep increasing $\omega_{\max}$, the solution at a fixed ω no longer depends on $\omega_{\max}$.

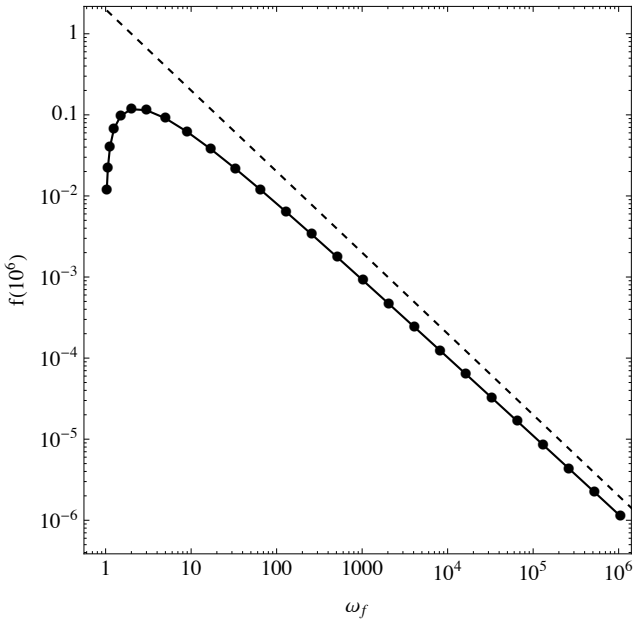

Figure 6.15: The effect on the solution f, at $\omega = 2 \times 10^6$ when keeping $\omega_{\min} = 1$, $\omega_{\max} = 10^7$ fixed, and varying ω_f. We find that the solution scales with the inverse of the forcing scale.

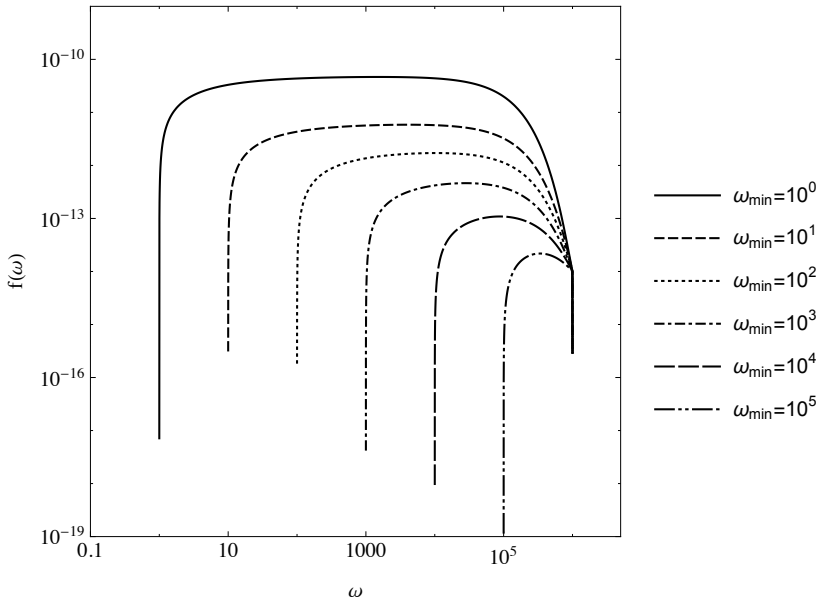

Figure 6.16: Comparison of solutions when keeping $\omega_{\max} = 10^6$, $\omega_f = 9.999 \times 10^5$ fixed, and decreasing $\omega_{\min}$. We find that the solution has a strong dependence on the lower dissipation scale.

by using dimensional analysis, under the assumption of locality, do not match up with the flux directions obtained form the Fjortoft argument and also result in a diverging collision operator, and so are not relevant. We derived a homogeneous isotropic Fokker-Planck approximation and find self consistent analytic solutions in the presence of a specific form of forcing and dissipation, and find them to be close to a Maxwellian distribution. These solutions appear to be qualitatively similar to the warm cascades found by Proment et al.

Our work suggests that in the steady-state, the both direct and inverse cascades are non-local. The direct cascade has a solution that depends on the forcing scale within the inertial range, whereas the inverse cascade has a non-vanishing dependence on the lower cut-off with a solution in the inertial range that depends on the both dissipation and forcing scales. We have used numerics to compare the solutions of the HIFP and HIBE, and their temperatures dependence on the forcing and dissipation scales, and find they are in good agreement. Although the results from the Fokker-Planck model are able to reproduce the behaviour of the Boltzmann equation more closely than those from the DAM, it is still interesting that the DAM is able to reproduce the same qualitative behaviour. The fundamental difference between the two models is that the DAM assumes strong locality of interaction, whereas the Fokker-Planck model includes a non-local diffusion coefficient. It appears that the local interactions dominate the behaviour as both models exhibit qualitatively similar steady states, but that there is a non-negligible contribution to the dynamics of the Boltzmann equation from non-local interactions which the Fokker-Planck model, due to its non-local diffusion coefficient is able to approximate to a greater degree.

In the next chapter, we will see how the Fokker-Planck model behaves in the elastic limit of an inelastic Maxwell gas, to see if it aligns with what knowledge we have from existing studies of the Boltzmann equation.

7

Steady state solutions for an inelastic gas in 1D with Maxwell molecules

"I am conscious of being only an individual struggling weakly against the stream of time. But it still remains in my power to contribute in such a way that, when the theory of gases is again revived, not too much will have to be rediscovered"

– Ludwig Edward Boltzmann

7.1 Introduction

So far we have only considered gases where the collisions between particles are elastic. That is, when the total kinetic energy of particles is conserved during binary collisions. However, when wishing to model a granular gas, the loss of energy during each collision needs to be taken into account. This is achieved in the following way. Supposing again that $\mathbf{v}$ and $\mathbf{v}_*$ are the velocities of two molecules pre-collision, and $\mathbf{n}$ is the impact direction, then the post collision velocities $\mathbf{v}'$ $\mathbf{v}'_*$ must satisfy

$$\left(\mathbf{v}' - \mathbf{v}'_*\right) \cdot \mathbf{n} = -e\left(\mathbf{v} - \mathbf{v}_*\right) \cdot \mathbf{n}, \tag{7.1}$$

where $e \in [0, 1]$ is the inelasticity parameter. $e = 1$ corresponds to no loss of energy and collisions are said to be *elastic*, $e = 0$ corresponds to complete loss of energy and collisions are said to be *sticky*. Often this is written equivalently as

$$\mathbf{v}' = \mathbf{v} - p\left((\mathbf{v} - \mathbf{v}_*) \cdot \mathbf{n}\right)\mathbf{n} \tag{7.2}$$

$$\mathbf{v}'_* = \mathbf{v}_* + p\left((\mathbf{v} - \mathbf{v}_*) \cdot \mathbf{n}\right)\mathbf{n}, \tag{7.3}$$

with $p = 1 - q = (1 + e)/2$. Perhaps surprisingly, with even the smallest amount of inelasticity the long-time dynamics of such systems are vastly different to the elastic case. Without the conservation of energy, the governing physical laws allow rich behaviours such as large-scale clustering and inelastic collapse, which are not possible for gases that obey the conservation of energy [Krapivsky et al., 2010a]. The physics literature of granular gases is extensive, and we direct the reader to [Brilliantov and Poschel, 2004] which provides an accomplished overview. We will summarise some of the major results without going into too many details.

When such systems are left to their own devices, it is clear that energy will dissipate from the system and asymptotically the distribution of velocities will decay towards a delta function centred on the mean velocity. Such freely cooling systems are well understood [Villani, 2006]. For example, it can be shown that from a dimensional argument that

$$\frac{dT}{dt} \simeq T^{-3/2}. \tag{7.4}$$

This is known as Haff's law [Haff, 1983], and suggests that the temperature will decay like $O(t^{-2})$ with time and that the solution at time t lies a distance of $O(t^{-1})$ away from the Dirac delta function.

Later it was postulated by Ernst and Brito [2002] that such freely cooling systems at large but finite times, are characterised by their temperature $T(t)$ and an invariant velocity distribution after rescaling, given by

$$f(v,t) = T(t)^{-d/2}\tilde{f}\left(v/T(t)^{1/2}, t\right) \tag{7.5}$$

where, the transformed or *rescaled* distribution $\tilde{f}$ in the coupled limit $t \to \infty$, $v \to 0$ with $v/T(t)^{1/2} = c$ kept constant,

$$\lim_{t\to\infty} \tilde{f}\,(c,t) = \lim_{t\to\infty} T(t)^{d/2} f(cT(t)^{1/2},t) := \tilde{f}\,(c) \tag{7.6}$$

is in general a heavy-tailed function, which depends on the collision model, inelasticity and dimension. For Maxwell molecules is in 1-dimension, Baldassarri et al. [2002] showed that the invariant scaling function has the form

$$\tilde{f}(c) = \frac{2}{\pi}\left(\frac{1}{1+c^2}\right)^2, \tag{7.7}$$

and later, using different methods it was shown by Krapivsky and Ben-Naim [2001] that for Maxwell molecules ($\lambda = 0$)in d-dimensions, the tail of the scaling function behaves like $\tilde{f}(c) \sim c^{-\sigma}$ where $\sigma = \sigma(d,e)$. The analysis is harder for the hard-sphere interaction, as the Fourier transform of the collision operator does not lend itself towards analytical methods so easily. However Mischler and Mouhot [2006] were able to prove that for hard-sphere interactions the self-similar solutions have a scaling function that satisfies

$$a_1 \exp\left(-a_2\left|v\right|\right) \leq \tilde{f}(\mathbf{v}) \leq A_1 \exp\left(-A_2\left|v\right|\right) \qquad \forall\, \mathbf{v} \in \mathbb{R}^d \tag{7.8}$$

for constants a_1, a_2, A_1, $A_2 > 0$. This gives the behaviour of the distribution in the tail. Another question we can ask, as we did in previous chapter, is what happens when we introduce a source of energy into the system. Will the system reach a non-trivial steady state, and if so how are these steady states characterised? It turns out that, the answer to this, again, can depend on the type of forcing, amount of inelasticity and dimension.

There are clearly many different ways to introduce forcing into the system. One of the most common methods, where energy is injected at all scales, is to introduce a *heat bath* into the system, which is done by the addition of a term such as $T_e\Delta_v f$, where $T_e > 0$ is some external temperature. This type of forcing is sometimes called *white noise forcing*. In the hard-sphere case, Van Noije and Ernst [1998] found that the steady state solution has a tail that behaves like

$$f(\mathbf{v}) \sim \exp\left(-Av^{3/2}\right), \tag{7.9}$$

where $A \sim 1/\sqrt{e}$ with the elasticity e. Later it was shown by Ernst et al. [2006] that in fact, for general collision models there is a steady state that has a tail that behaves like $f(\mathbf{v}) \sim e^{-Av^{1+\lambda/2}}$, where λ is homogeneity degree of the collision kernel. Other ways to introduce forcing include introducing a *negative friction* term (see Trizac et al. [2007]), and an extreme forcing mechanism we will describe in the next section.

7.2 The extreme forcing limit

A surprising result was found by Ben-Naim and Machta [Ben-Naim and Machta, 2005; Ben-Naim et al., 2005; Kang et al., 2010]. By considering the tail of the Boltzmann equation with a variable hard-sphere collision kernel, they found stationary power-law solutions to a linearised collision operator of the form

$$f(\omega) \sim v^{-\alpha}, \tag{7.10}$$

where α is the solution of the following transcendental equation,

$$\frac{1 -_2 F_1\left(\frac{d+\lambda-\alpha}{2}, \frac{\lambda+1}{2}, \frac{d+\lambda}{2}, 1-p^2\right)}{(1-p)^{\alpha-d-\lambda}} = \frac{\Gamma\left(\frac{\alpha-d+1}{2}\right)\Gamma\left(\frac{d+\lambda}{2}\right)}{\Gamma\left(\frac{\alpha}{2}\right)\Gamma\left(\frac{\lambda+1}{2}\right)}, \tag{7.11}$$

from which they deduce the bounds

$$1 + d + \lambda \leq \alpha \leq 2 + d + \lambda, \tag{7.12}$$

where the lower bound is approached in the inelastic limit and the upper bound is approached in the quasi-elastic limit. The linearised Boltzmann equation they derive is found by assuming that in the tail the interaction is non-local, that is, high energy particles only interact with particles of much smaller energies. What makes these solutions puzzling is that these are non-trivial stationary solutions to a dissipative system with no explicit forcing term. The authors interpret these solutions heavy tailed solutions that in effect act as their own heat bath, by a mechanism they call *extreme driving*. In effect, these are solutions where the forcing scale has been taken to infinity. Physically, this is equivalent to particles being given large amounts of energy at very low rate. These predictions were then verified with stochastic numerical experiments, for Maxwell molecules ($\lambda = 0$) and hard sphere molecules

($\lambda = 1$). In these numerical experiments particles collide in-elastically, with the total number of particles kept fixed. With a rate γ, small compared to the collision rate particles, a particle is randomly selected and reassigned a velocity, so that the total energy lost between this time and the previous selection, is injected back into the system.

One of the features of these solutions is that the direction of energy flux is towards smaller scales. This is the opposite direction to what is known for flux direction of the energy cascade in the inertial range for the elastic case. The question we will now answer is whether this is a feature of inelastic gases or could be caused by the form of the forcing mechanism. Let us recall the form of the flux that was found for the Fokker-Planck model in the previous chapter

$$J_p = \begin{cases} -\dfrac{\epsilon}{\omega_f}\theta & : \omega < \omega_f \\ \dfrac{\epsilon}{\omega_f}(1-\theta) & : \omega \geq \omega\,, \end{cases}$$

with $\theta = \theta(\omega_{\max}, \omega_{\min}, \omega_f) \in (0,1)$. The pure inverse cascade of particles and direct cascade of mass can be obtained by taking the limit $\omega_{\max} \to \infty$ with $\omega_{\min}\omega_{\max} = k$ kept constant and ω_f fixed, which results in the particle flux:

$$J_p \simeq \begin{cases} \dfrac{-\epsilon}{\omega_f} & : \omega < \omega_f \\ 0 & : \omega \geq \omega_f\,, \end{cases}$$

and energy flux

$$J_E \simeq \begin{cases} 0 & : \omega < \omega_f \\ \epsilon & : \omega \geq \omega_f\,. \end{cases}$$

θ, which is a function of the forcing and dissipation scales, in effect controls the direction of the particle flux, with $\theta = 1$ representing a negative cascade of particles, and $\theta = 0$ representing a direct cascade. Now, if we consider an "extreme driving" mechanism for the inverse cascade, which we consider to be found by taking the limit $\omega_{\max} \to \infty$ with $\omega_f/\omega_{\max} = k < 1$ kept constant, and $\omega_{\min}$ fixed. In this limit $\theta = 0$, and so the direction of the fluxes found in the inertial range is reversed. This is consistent with the direction of energy flux in the non-universal power-

law solutions found by Ben-Naim and Machta under the "extreme driving" forcing mechanism that they considered. However, in the extreme forcing limit we consider, our solutions remain close to Maxwellian, and the non-universal power-law solutions like those found by Ben-Naim and Machta are not possible. It is clear then, that the extreme forcing limits and elastic limit do not commute. One more question one can ask is to what extent simple Fokker-Planck approximations are relevant for an inelastic granular gas, in particular we seek to determine if a Fokker-Planck model is able to model the "extreme driving" mechanism.

7.3 Self-similar solutions of the 1D Fokker-Planck Maxwell gas

In this section we consider in one-dimension the Maxwell gas ($\lambda = 0$). We choose to study Maxwell molecules because the independence of the relative velocity on the collision rate makes the analysis simpler, and we restrict our analysis to a 1D gas to remove the complication of angular integration. Using the non-dimensionalisation given in equation (7.6), in the freely cooling case Pareschi and Toscani [2006] derived a Fokker-Planck collision operator from the Boltzmann equation and found self-similar power-law solutions which in the quasi-elastic limit agree with the exponents found in [Baldassarri et al., 2002] .

We take a similar approach, except we do not non-dimensionalise using the thermal velocity, and seek stationary solutions that can be interpreted as non-trivial steady states under the mechanism of extreme forcing, in a similar way to Ben-Naim and Machta. By considering all smooth functions $\phi : \mathbb{R} \to \mathbb{R}$, one can write the Boltzmann equation for Maxwell molecules in its weak form

$$\frac{d}{dt}\int_{\mathbb{R}} \phi(v) f(v,t)\, dv = \gamma \int_{\mathbb{R}^2} f(v,t) f(w,t) \left(\phi(v^*) - \phi(v)\right) dv dw, , \tag{7.13}$$

where γ is a parameter that makes the equation dimensionally consistent, and post collision velocities

$$v^* = pv + qw, \quad w^* = qv + pw, \quad p, q \geq 0 \tag{7.14}$$

are generated by binary collisions between particles of velocity v and w. The second order Taylor expansion of $\phi(v^*)$ around v

$$\begin{aligned}\phi(v^*) - \phi(v) = &\left(qv + (p-1)w\right)\phi'(v) \\ &+ \frac{1}{2}\left(qv + (p-1)w\right)^2 \phi''(\tilde{v}),\end{aligned} \tag{7.15}$$

where $\tilde{v} = \theta v^* + (1-\theta)v$, for some $0 \leq \theta \leq 1$, allows equation (7.13) to be written as

$$\begin{aligned}&\frac{d}{dt}\int_{\mathbb{R}} \phi(v) f(v,t)\, dv = \\ &\quad \gamma\left(\int_{\mathbb{R}^2} f(v,t)f(w,t)\left(qv + (p-1)w\right)\phi'(v)\, dv\, dw\right. \\ &\quad + \frac{1}{2}\int_{\mathbb{R}^2} f(v,t)f(w,t)\left(\left(qv + (p-1)w\right)^2 \phi''(v)\, dv\, dw\right. \\ &\quad \left.\left. + R(p,q)\right)\right)\end{aligned} \tag{7.16}$$

where

$$\begin{aligned}&R(p,q) = \\ &\frac{1}{2}\int_{\mathbb{R}^2} f(v,t)f(w,t)\left(\phi''(\tilde{v}) - \phi''(v)\right)\left(qv + (p-1)w\right)^2 dv\, dw.\end{aligned} \tag{7.17}$$

Defining the macroscopic quantities

$$\rho(t) = \int_{\mathbb{R}} f(v,t)\, dv \tag{7.18}$$

$$\rho E(t) = \int_{\mathbb{R}} v^2 f(v,t)\, dv \tag{7.19}$$

and enforcing zero bulk momentum

$$\int_{\mathbb{R}} v f(v,t)\, dv = 0, \tag{7.20}$$

allows (7.16) to be simplified as

$$\frac{d}{dt}\int_{\mathbb{R}}\phi(v)f(v,t)\,dv = \gamma\rho\left(q\int_{\mathbb{R}}f(v,t)v\phi'(v)\,dv \right.$$
$$\left. + \int_{\mathbb{R}}f(v,t)\left(q^2v^2+(p-1)^2E\right)\phi''(v)\,dv\,dw + \rho^{-1}R(p,q)\right). \tag{7.21}$$

Without forcing, we know that the mass is conserved, and so for all t, $\rho(t) = \rho_0$, the density of the initial condition. If we suppose that the remainder term $R(p,q)$ is small in comparison to ρ, then (7.21) is just the weak form of the Fokker-Planck equation

$$\frac{\partial f}{\partial t} = \gamma\rho_0\left(q\frac{\partial}{\partial v}\left(f(v,t)v\right) + \frac{\partial^2}{\partial v^2}\left(\left(q^2v^2+(p-1)^2E\right)f(v,t)\right)\right). \tag{7.22}$$

As in the elastic case, we can rewrite this equation in terms of the energy $\omega = v^2$, with $f(\omega,t) = f(v^2,t)$. We define a new relaxation time $\tau = \gamma\rho_0 t$, and search for driven steady-states, where the driving is provided by a delta function centred on an energy scale $\omega_f = v_f^2$. Hence the equation we are considering becomes

$$\frac{\partial f}{\partial \tau} = 2\left(q\omega^{1/2}\frac{\partial}{\partial\omega}\left(\omega^{1/2}f(\omega,t)\right) + \frac{\partial}{\partial\omega}\left(\left(q^2\omega+(p-1)^2E\right)f(\omega,t)\right)\right.$$
$$\left. +2\omega\frac{\partial^2}{\partial\omega^2}\left(\left(q^2\omega+(p-1)^2E\right)f(\omega,t)\right)\right) + \eta\delta(\omega-\omega_f), \tag{7.23}$$

where η is the forcing rate. Now, supposing that the long-time behaviour of the system does not depend on the initial condition, and that there is a unique non-trivial stationary state, we define

$$\rho^*(\omega_f) = \lim_{t\to\infty}\rho(t) < \infty$$
$$E^*(\omega_f) = \lim_{t\to\infty}E(t) < \infty, \tag{7.24}$$

where E and ρ are found as solutions to (7.23) with forcing at the scale ω_f. Letting $q = 1-p$, we find the steady states by solving the following ODE

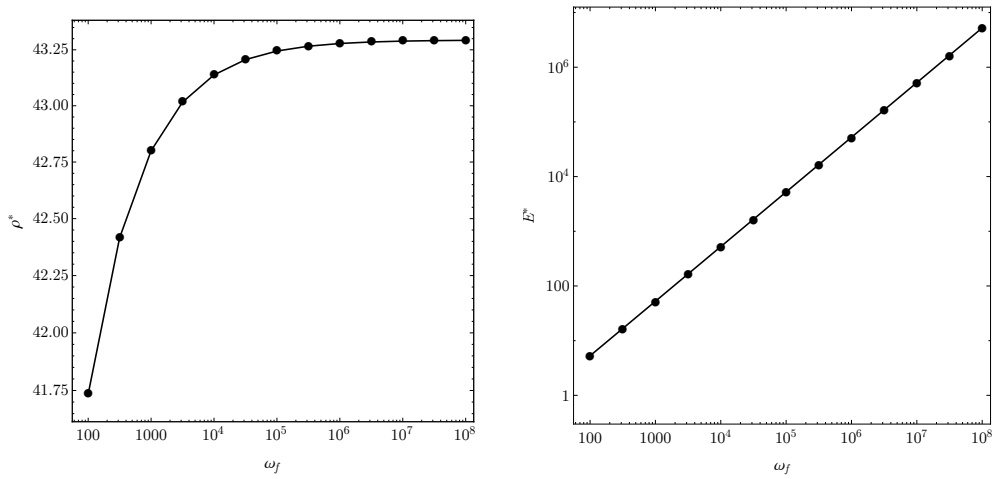

(a) Density, ρ^* (b) Energy, E^*

Figure 7.1: Density and energy of the steady-state, as the forcing scale $\omega_f \to \infty$. The upper-cut off $\omega_{max} = 2\omega_f$, $q = 0.9$. We find that the density converges to a finite value, but the energy diverges, growing linearly with the forcing scale.

$$2q\omega^{1/2}\frac{\partial}{\partial\omega}\left(\omega^{1/2}f(\omega,t)\right) + 2q^2\frac{\partial}{\partial\omega}\left(\left(\omega + E^*\right)f(\omega,t)\right) + 4q^2\omega\frac{\partial^2}{\partial\omega^2}\left(\left(\omega + E^*\right)f(\omega,t)\right) + \eta\delta(\omega - \omega_f) = 0, \quad (7.25)$$

supplemented with the boundary conditions

$$f(\omega_{\max}) = 0, \quad (7.26)$$

$$f'(\omega_{\max}) = \frac{-\eta}{2\omega_{\max}^{1/2}(E^* + \omega_{\max})}, \quad (7.27)$$

the first of which allows energy and mass to dissipate from the system, and the second enforces that the mass injected into the system is equal to the mass flow out, which is a necessary condition for the existence of a steady state. This solution is supplemented with the self-consistency conditions given by (E.1). This equation admits a stationary solution which can be written in terms of hypergeometric and Meijer-G functions, which we supply in Appendix F. We are interested in an extreme forcing limit, that is the behaviour as $\omega_f \to \infty$. For convenience, we set the the upper cut-off $\omega_{\max} = 2\omega_f$. For finite ω_f, solutions to this equation are self-consistent (see Figures 7.1a-7.1b), i.e. we are able find finite density and energy numerically.

In the point-wise limit $\omega_f \to \infty$, with $\eta\omega_f^{1/2}$ held constant (so the forcing rate $\eta \to 0$), before checking for self-consistency, we find that

$$f(\omega) \to \left(\frac{1}{2q(E^* + \omega)}\right)^{-(1+\frac{1}{2q})}, \tag{7.28}$$

which in the quasi-elastic limit, $q = 1$, agrees with the exponents that Ben-Naim and Machta found for the exponents of their extreme driving steady-state solutions. This asymptotic solution is not self-consistent, as although it possesses finite density, it does not have finite energy E. This is significant, because the analysis performed by Ben-Naim and Machta was unable to find the constant coefficient in front of their power-laws, i.e.

$$f(v) = Av^{-\alpha}, \tag{7.29}$$

with A unknown. Our work suggests that in the limiting regime they are considering, the coefficient A decays to 0.

7.4 Discussion

In this chapter we have reviewed what is known about the steady-state and self-similar distributions of inelastic granular gases, including a family of distributions that are stationary solutions of a system that is forced by a mechanism termed extreme driving. These non-universal solutions give rise to an inverse flux of energy, the opposite direction of flux to the known warn cascade solutions of the elastic Boltzmann equation. We have shown that the steady solutions of the Fokker-Planck approximation are also able to generate an inverse energy cascade under the extreme driving mechanism. We conclude that the quasi-elastic limit of an inelastic gas is in general not commutative, and this limit is not able to be reached from an elastic gas. Finally, we show how a Fokker-Planck equation can be obtained from the 1D Boltzmann equation for Maxwell molecules, and show that in the quasi-elastic limit it exhibits power-law stationary states with exponents that are consistent with those obtained for the extreme forced Boltzmann equation.

8

Conclusions and outlook

"All that most maddens and torments; all that stirs up the lees of things; all truth with malice in it; all that cracks the sinews and cakes the brain; all the subtle demonisms of life and thought; all evil, to crazy Ahab, were visibly personified, and made practically assailable in Moby Dick."

– Herman Melville, *Moby Dick*

The research presented in this thesis contributes to both the methods and theory of rarefied gases, where specifically this thesis focusses on the Fokker-Planck approximation to the Boltzmann equation for dilute gases. Our main contributions are the following:

- In Chapter 3 we have provided an H-Theorem for the Fokker-Planck gas kinetic model, which under some assumptions regarding the smoothness of the solution, shows that in the spatially homogeneous setting the solution will eventually relax towards the equilibrium Maxwellian distribution. To our knowledge, this result was missing from the existing literature.

- We have proposed two methods for reducing the variance of a stochastic particle solution method for the Fokker-Planck model. The first we present in this thesis is the common random number scheme, which is able to work in geometries where the correlated equilibrium solution is able to keep individual particle positions strongly correlated. We find the for the planar Couette flow, the method is able to reduce the noise of statistical samples by a factor of close to 10. While writing this thesis, the author was made aware that this method has been published independently [Gorji et al., 2015].

- The second is an importance sampling scheme. The method is similar to the variance reduction scheme used in the VRDSMC method, in that weights

are attached to the computational particles. We presented a novel method that uses the conditional distributions which are known Gaussians to update the weights during each time-step. We tested the method on a homogeneous relaxation, a planar Couette flow and a lid-driven cavity flow. In each case, the variance of the estimators was greatly reduced, and results indicate for low-speed flows the noise-to-signal ratio of the method is independent of the Mach number.

- In Chapter 5 a randomised quasi-Monte Carlo scheme was created for solving the diffusion equation with low-discrepancy sequences. We showed that in 1 and 3 dimensions the scheme has a sub $N^{-1/2}$ convergence rate, and have no reason to believe that it degrades significantly for higher dimensional problems. We applied the method to a homogeneous relaxation and found the method was able to reduce the variance, however our attempts to apply the method to inhomogeneous problems were not successful. Nonetheless, it may be possible to apply the method to other problems where the solution can be written in terms of an integral of a Greens function, for example reaction-diffusion equations.

- In Chapter 6 we have presented analytical steady-states to a forced/dissipated Fokker-Planck gas, where the temperature has to be found self-consistently. Our results agree qualitatively with numerical evidence found previously using a differential approximation model. We have shown that the cascades in this model are non-local. We have also shown that the direction of the fluxes given by the Fjortoft argument can be reversed, which answers how it is possible for the quasi-elastic limit of solutions to the inelastic Boltzmann equation to have an inverse cascade of energy when the forcing mechanism is one of an "extreme driving" type.

It was the intention when this body of work began, that the research would be conducted with an interdisciplinary spirit, with ideas and concepts brought in from a wide range of areas, and then developed, and I hope this has come across in this thesis. An example of this are the variance reduction chapters. As more applications for rarefied gas calculations have arisen, interest into developing suitable numerical methods has grown. Reducing the noise for low-speed flows is one of the challenges involved in this greater effort. Variance reduction for increasing the precision of estimates obtained from random samples, is a well developed area of applied probability, separate from the numerical study of rarefied gases which tends

to be conducted within engineering departments, and so it is natural that knowledge from this area has so far diffused slowly into the rarefied gas methods. The variance reduction techniques that have been proposed in this thesis are an attempt to help bridge this gap. The proposed methods, namely the common random number technique and importance sampling technique, are two relatively simple methods. The advantage of this is that they are relatively easy to understand and implement, but it is possible that other refined techniques such as introducing stratified and antithetic sampling could be applied, and this is certainly a possible avenue of future research.

The work we have presented is significant, as it shows that for low-speed flows the Fokker-Planck kinetic model has the potential to be a viable alternative to DSMC which is currently the preferred method of choice. Further research to fully evaluate how a variance reduced Fokker-Planck method performs in comparison to the variance reduced DSMC is now needed. Gorji and Jenny [2015] have shown how the Fokker-Planck particle method can be coupled to DSMC. Another future avenue of research could be to couple to the model to continuum methods, such as a NSF solver, for applications where there are multiple length scales that are significant for the flow field. In such multi-scale problems, a local Knudsen number can be defined. Using particle methods where the local Knudsen number is close to zero is very inefficient in comparison to using NSF solvers, and so it is desirable to have methods that decompose the domain into regions where the different gas models are valid, and a way to couple the solutions so that information is able to pass from one to the other. The Fokker-Planck particle scheme may have an advantage over DSMC for this type of coupling, because the thermodynamic fields can be fed directly into equations of motion for the particles without having to use thermostats.

In Chapters 6 and 7 we have showed that the Fokker-Planck model, as well being well suited for practical purposes, is able to give answers to theoretical questions too. One criticism of the work could be to what extent the Fokker-Planck model is an approximation to the Boltzmann equation. It is not an approximation in the sense that you can obtain the Fokker-Planck model directly from the Boltzmann equation from an expansion in terms of a small parameter. In the derivation in Appendix A this is what is attempted, but crucially it assumes collisions are between large and small molecules, whereas of course, we are using this model for a one species gas. This is a fair criticism, but we would not put it into the same class of purely phenomenological models that, for example, the BGK collision operator

inhabits and where no attempt can be made to justify the functional form from the underlying collision process. The Fokker-Planck equation retains the non-linear quadratic dependence on the distribution function and has been shown to produce results that agree well with particle solutions of the Boltzmann equation, which we argue gives weight to the claim that the solutions we find in these chapters mimic the real solutions of the homogeneous isotropic Boltzmann equation.

The questions addressed in the final chapters were primarily theoretical, in the sense that quite heavy simplifying assumptions of homogeneity in space and statistical isotropy were made. Nevertheless, there is a connection between these steady-state solutions and the practical steady-state solutions of physical flows in the earlier chapters, e.g. the Couette flow. We can interpret the collisions of a particle with the wall in the non-equilibrium boundary layer as a source of energy and a particular energy scale. There will also be an upper-cut off, with fast moving particles more likely to leave the non-equilibrium layer. Our results suggest that it may be possible in this non-equilibrium layer for the velocity distribution to appear close to Maxwellian, but still retaining the ability to transport energy in a non-equilibrium manner. This is a connection that could be investigated using the DSMC methods.

Finally, it is worth remarking that within the non-equilibrium steady-state chapters we are implicitly assuming the Boltzmann equation, and in particular its assumption that velocities of particles pre-collision are uncorrelated (molecular chaos), is valid in such strongly out of equilibrium situations, which is a comment I have encountered discussing this topic on conferences. Whilst there certainly are non-equilibrium systems that do display correlations that decay slowly, for example the Ising model (in dimensions greater than 2) close to its phase transition, flocking models of birds [Vicsek and Zafeiris, 2012], and chemical reaction-diffusion systems, there are plenty of examples of non-equilibrium systems where correlations do decay quickly, for example the Ising model far from its phase transition. A particularly good example of a toy model which highlights this is the East model [Faggionato et al., 2012], whose stationary distribution can be written as a product of independent Bernoulli measures despite non-trivial kinetically constrained microscopic dynamics. This emphasises the need to check the validity of assumptions in models we use with experiments.

Appendix A

Derivation of the Fokker-Planck collision operator from the Boltzmann equation: the Raleigh gas

This derivation can be found in Chang et al. [1970]; Ferrari [1982] in the setting of a Raleigh gas, in which a particles of mass m are surrounded by particles of mass M, against which they collide. The surrounding gas is supposed to be at equilibrium at temperature T, and the equilibrium is not disturbed by the collisions with particles m. Given this description, the Boltzmann collision operator is given by

$$Q(f) = \int\int \left(f'F' - fF\right) |\mathbf{v} - \mathbf{V}| \, d\mathbf{V} d\Omega, \tag{A.1}$$

where

$$F(\mathbf{V}) = N \left(\frac{M}{2\pi kT}\right)^{3/2} e^{-MV^2/2kT} \tag{A.2}$$

is the Maxwellian equilibrium distribution of surrounding gas. The primes refer to the post collision velocity variables: $(\mathbf{v}, \mathbf{V}) \to (\mathbf{v}', \mathbf{V}')$. If the particle m is very heavy in comparison the mass M ($m/M \gg 1$) and the velocity v/V is always of order $(m/M)^{1/2}$ (satisfied when the velocities are not far from equipartition) then we can expand the collision operator in powers of the small parameter M/m. This

occurs in the following manner. First we let

$$f(\mathbf{v}) = f_{MB}(v)h(\mathbf{v}), \tag{A.3}$$

where h describes the deviation from equilibrium. By using conservation of energy it follows that

$$Q(f) = f_{MB}(v) \int F(\mathbf{V}) \int \left(h' - h\right) |\mathbf{v} - \mathbf{V}| \, d\Omega d\mathbf{V} \tag{A.4}$$

$$= f_{MB}(v) I(h). \tag{A.5}$$

If we let $\mathbf{g} = \mathbf{V} - \mathbf{v}$ and $\mathbf{g}' = \mathbf{V}' - \mathbf{v}'$, then conservation of momentum gives

$$\mathbf{v}' - \mathbf{v} = -\frac{M}{M+m}\left(\mathbf{g}' - \mathbf{g}\right) \approx -\frac{M}{m}\left(\mathbf{g}' - \mathbf{g}\right), \tag{A.6}$$

and since M/m is small, this means $\mathbf{v}$ and $\mathbf{v}'$ are close to each other. This allows $h(\mathbf{v}', t)$ to be expanded around $\mathbf{v}$, so we can write

$$h(\mathbf{v}', t) - h(\mathbf{v}, t) \approx \sum_{i=1}^{3} \left(v_i' - v_i\right) \frac{\partial h}{\partial v_i} + \frac{1}{2} \sum_{i,j=1}^{3} \left(v_i' - v_i\right)\left(v_j' - v_j\right) \frac{\partial^2 h}{\partial v_i v_j}. \tag{A.7}$$

We can also make use of the identity

$$g = V\left(1 - 2\frac{v}{V}\cos\phi + \frac{v^2}{V^2}\right)^{1/2}, \tag{A.8}$$

which can be expanded up to order $(m/M)^{1/2}$ as

$$g \approx V\left(1 - \frac{v}{V}\cos\phi\right). \tag{A.9}$$

The next step is to write the solid angle as $d\Omega = \sin\theta d\theta d\phi$, and consider $\mathbf{V}$ written in a spherical coordinate system. By using the following verifiable identity:

$$\int (A_i - B_i) d\Phi = 2\pi \left(\frac{A}{B} \cos\Theta - 1 \right) B_i, \tag{A.10}$$

$$\int (A_i - B_i)(A_j - B_j) d\Phi = 2\pi \left\{ B_i B_j \left[\left(\frac{A}{B} \cos\Theta - 1 \right)^2 - \frac{1}{2} \frac{A^2}{B^2} \sin^2\Theta \right] + \frac{1}{2} A^2 \sin^2\Theta \delta_{ij} \right\} \tag{A.11}$$

(where $\mathbf{B}$ is a fixed vector and Θ, Φ are the polar angles of $\mathbf{A}$ with respect to $\mathbf{B}$) one can integrate over the azimuthal angle. If we use the dimensionless variables

$$\mathbf{c} = \sqrt{\frac{m}{2kT}} \mathbf{v}, \qquad \mathbf{C} = \sqrt{\frac{M}{2kT}} \mathbf{V} \tag{A.12}$$

the resulting integral can be written

$$\begin{aligned} I(h) = {} & 4\pi^2 \frac{M}{m} \left(\frac{2kT}{M} \right)^2 \int d\theta \sin\theta (1 - \cos\theta) \int dC C^3 e^{-C^2} \\ & \times \int d\phi \sin\phi \left[1 - \sqrt{\frac{M}{m}} \frac{c}{C} \cos\phi \right] \left\{ \sqrt{\frac{m}{M}} \cos\phi \frac{C}{c} c_i \frac{\partial h}{\partial c_i} - \left[c_i \frac{\partial h}{\partial c_i} + \frac{1}{8} (3\cos\theta - 1) \right. \right. \\ & \left. \left. \times \left(3\cos^2\theta - 1 \right) \frac{C^2}{c^2} c_i c_j \frac{\partial^2 h}{\partial c_i c_j} + \frac{1}{8} \left(\cos^2\phi - 3 - \cos\theta \left(3\cos\phi - 1 \right) \right) C^2 \frac{\partial^2 h}{\partial c_i c_i} \right] \right\}. \end{aligned} \tag{A.13}$$

Performing the integration over the angle ϕ results in

$$I(h) = \frac{8\pi^2}{3} \frac{M\sigma}{m} \left(\frac{2kT}{M} \right)^2 \int d\theta \sin\theta \left(1 - \cos\theta \right) \int dC e^{-C^2} C^5 \left(\frac{\partial^2 h}{\partial c_i c_i} - 2 c_i \frac{\partial h}{\partial c_i} \right). \tag{A.14}$$

Recombining this with A.5, and reverting back to dimensional coordinates results in the collision operator

$$J(f) = \frac{1}{\tau} \frac{\partial}{\partial v_i} \left\{ v_i f + \frac{kT}{m} \frac{\partial f}{\partial v_i} \right\}, \tag{A.15}$$

where for hard spheres the integration gives the relaxation time

$$\tau = \frac{3}{8\sqrt{\pi}} \frac{m}{NM\sigma^2} \sqrt{\frac{M}{2kT}}. \tag{A.16}$$

Appendix B

Derivation of Fokker-Planck equation from Brownian particle dynamics

This is a different approach to deriving a Fokker-Planck gas kinetic equation, where we follow the deviation described by [Green, 1951]. Here we consider the motion of a Brownian hard-sphere particle in a gas whose molecules interact the particle, but not with each other. As in Appendix A, it also assumed that the mass of the gas which the Brownian particle is suspended in is small in comparison to the mass of the Brownian particle, and that the immersive gas is at equilibrium with temperature T.

Again, we suppose the $f(\mathbf{v}, t)$ is the distribution of the velocity of Brownian particle at time t. We will mechanically consider how the distribution changes when the Brownian particle collides with a gas particle. That is, we will equate the rate of change of the distribution function to the difference of probability of a particle entering and leaving an elementary volume of phase $d\mathbf{v}$.

We assume that the change of momentum of both the Brownian and gas particle occurs only in the direction of the normal of the point of contact. If $\mathbf{v}$ and $\mathbf{v}'$ are the pre and post-collision velocity of the Brownian particle of mass m, and $\mathbf{V}$, $\mathbf{V}'$ are the pre and post collision velocities of the gas particle of mass M, then conservation of energy and momentum require

$$\mathbf{v}' = \mathbf{v} + \frac{2Mm}{M+m}(\mathbf{V}-\mathbf{v})\cdot\mathbf{nn} \tag{B.1}$$

$$\mathbf{V}' = \mathbf{V} - \frac{2Mm}{M+m}(\mathbf{V}-\mathbf{v})\cdot\mathbf{nn}. \tag{B.2}$$

To calculate the number of molecules entering $d\mathbf{v}'$, one needs to know what initial velocities $\mathbf{v}$ are able to collide with a particle of initial velocity $\mathbf{V}$ so that the final velocity is $\mathbf{v}'$. That is, we require $\mathbf{v}$ in terms of $\mathbf{V}$ and $\mathbf{v}'$, which can be obtained from equation (B.1):

$$\mathbf{v} = \mathbf{v}' - \frac{2Mm}{m-M}\left(\mathbf{V}-\mathbf{v}'\right)\cdot\mathbf{nn}. \tag{B.3}$$

Next, the probability that a Brownian particle enters the region $d\mathbf{v}'$ in a time element dt because of collisions with a gas molecule in the velocity range $d\mathbf{v}$, which occurs in the neighbourhood dA of its surface, is the product of the probability of the Brownian particle having a suitable velocity, and that there is a gas particle available to give the desired collision in a time dt. If such a gas molecule has velocity $\mathbf{V}$ then the normal component to the relative velocity must be such that it encounters the Brownian particle at dA, and the probability of this occurring for a large number of particles will approach the expectation. Therefore the probability that a Brownian particle enters the region $d\mathbf{v}$ is given by

$$-f(\mathbf{v},t)\mathbf{n}\cdot(V-v)\,NM(2\pi kT)^{-3/2}e^{-MV^2/2kT}d\mathbf{v}\,d\mathbf{V}\,dA\,dt. \tag{B.4}$$

A similar argument gives the probability for a particle leaving the region $d\mathbf{v}'$ in a time dt as

$$-f(\mathbf{v}',t)\mathbf{n}\cdot\left(V-v'\right)NM(2\pi kT)^{-3/2}e^{-MV^2/2kT}d\mathbf{v}\,d\mathbf{V}\,dA\,dt. \tag{B.5}$$

Now, from B.3 we have

$$d\mathbf{v} = \frac{m+M}{m-M}d\mathbf{v}' \tag{B.6}$$

and B.1 and B.3 together give:

$$\mathbf{n}\cdot(\mathbf{V}-\mathbf{v}) = \frac{m+M}{m-M}\mathbf{n}\cdot\left(\mathbf{V}-\mathbf{v}'\right). \tag{B.7}$$

Putting this together with gain and loss in probability, gives the overall change of probability as

$$-\left[\left(\frac{m+M}{m-M}\right)^2 f(\mathbf{v},t) - f(\mathbf{v}',t)\right]\mathbf{n}\cdot\left(\mathbf{V}-\mathbf{v}'\right) NM\left(2\pi kT\right)^{-3/2} e^{-MV^2/2kT} d\mathbf{v}'\, d\mathbf{V}\, dA\, dt, \tag{B.8}$$

where we require $\mathbf{n}\cdot(\mathbf{V}-\mathbf{v}') < 0$. To get the total change in probability we integrate over all such $\mathbf{V}$ and surface elements dA, resulting in the rate of change

$$\begin{aligned}\frac{\partial f}{\partial t} =& - NM(2\pi kT)^{-3/2} \\ & \int\int\left[\left(\frac{m+M}{m-M}\right)^2 f(\mathbf{v},t) - f(\mathbf{v}',t)\right]\mathbf{n}\cdot\left(\mathbf{V}-\mathbf{v}'\right) e^{-MV^2/2kT} d\mathbf{v}'\, d\mathbf{V}\, d\mathbf{A} \quad .\end{aligned} \tag{B.9}$$

Now, if f is smooth enough to be approximated by a power series, then expanding the integrand of equation (B.9) around $\mathbf{v}$, truncating at the first term and completing the integration gives

$$\frac{\partial f}{\partial t} = \left[\left(\frac{m+M}{m-M}\right)^2 - 1\right] Af + \left(\frac{m+M}{m-M}\right)\mathbf{B}\cdot\nabla f + \left(\frac{m+M}{m-M}\right)^2 \mathbf{C}:\Delta f, \tag{B.10}$$

where

$$A = \frac{2}{MN\sigma^2}\left(2\pi kT\right)^{1/2} \tag{B.11}$$

$$B = \frac{8}{3mN\sigma^2}\left(2\pi kT\right)^{1/2}\mathbf{v} \tag{B.12}$$

$$C = \frac{8}{3N\sigma^2}\left(2\pi kT\right)^{1/2} kT\mathbf{I} \tag{B.13}$$

where $\mathbf{I}$ is the unit dyadic. Substitution of these values into B.10, and retaining only the lowest orders of M/m gives the same result given by Wang-Chang and

Uhlenbeck in Appendix A.

Appendix C

Finding KZ spectra: Balks argument

The KZ spectra for the Boltzmann can be found with the following argument presented by outline the method presented by Balk [2000] showing (under the assumption of locality) the existence of these KZ spectra. If we write the collision integral as

$$I(f_1) = \int_0^\infty \int_0^\infty \int_0^\infty S_{34}^{12}(f_3 f_4 - f_1 f_2)\delta(\omega_1 + \omega_2 - \omega_3 - \omega_4)\,\mathrm{d}\omega_2 \mathrm{d}\omega_3 \mathrm{d}\omega_4, \tag{C.1}$$

and we substitute in power-law solutions of the form $f = A\omega^{-\alpha}$, then

$$I(f_1) = A^2\omega_1^{-1} \int_0^\infty \int_0^\infty \int_0^\infty S_{34}^{12}\left(\omega_3^{-\alpha}\omega_4^{-\alpha} - \omega_1^{-\alpha}\omega_2^{-\alpha}\right)\omega_1\omega_2\omega_3\omega_4\,\delta\left(\omega_1 + \omega_2 - \omega_3 - \omega_4\right)\frac{\mathrm{d}\omega_2}{\omega_2}\frac{\mathrm{d}\omega_3}{\omega_3}\frac{\mathrm{d}\omega_4}{\omega_4}. \tag{C.2}$$

Now if we define

$$\mu = -\frac{1}{2} + 2\alpha - 4 + 1, \tag{C.3}$$

and include a factor of ω_1^μ inside the integral, then the homogeneity degree of the integrand is zero, and we can write the integral as

$$I(f_1) = A^2\omega_1^{-1-\mu}\int_0^\infty\int_0^\infty\int_0^\infty S_{34}^{12}\left(\omega_3^{-\alpha}\omega_4^{-\alpha}-\omega_1^{-\alpha}\omega_2^{-\alpha}\right)\omega_1\omega_2\omega_3\omega_4\,\delta(\omega_1+\omega_2-\omega_3 - \omega_4)\omega_1^\mu\,\frac{\mathrm{d}\omega_2}{\omega_2}\frac{\mathrm{d}\omega_3}{\omega_3}\frac{\mathrm{d}\omega_4}{\omega_4}$$
$$= \frac{A^2\omega_1^{-1-\mu}}{4}\int_0^\infty\int_0^\infty\int_0^\infty S_{34}^{12}\left(\omega_3^{-\alpha}\omega_4^{-\alpha}-\omega_1^{-\alpha}\omega_2^{-\alpha}\right)\omega_1\omega_2\omega_3\omega_4\,\delta\left(\omega_1+\omega_2-\omega_3 - \omega_4\right)\left(\omega_1^\mu+\omega_2^\mu-\omega_3^\mu+\omega_4^\mu\right)\,\frac{\mathrm{d}\omega_2}{\omega_2}\frac{\mathrm{d}\omega_3}{\omega_3}\frac{\mathrm{d}\omega_4}{\omega_4} \tag{C.4}$$

where, crucially, we have implicitly assumed the integrand converges in order to swap the order of integration, and used symmetry properties of the collision operator. Now, it is clear that the integrand vanishes precisely when $\mu = 1$ or $\mu = 0$, which corresponds to the exponents

$$\alpha = 9/4, \qquad \alpha = 7/4. \tag{C.5}$$

Appendix D

Non-equilibrium steady-state solutions of the Fokker-Planck collision operator

In this appendix, we derive the non-equilibrium steady states of the Fokker-Planck equation. We begin by factorising out a Maxwellian distribution from f,

$$f(\omega) = e^{-\omega/T} f_d(\omega). \tag{D.1}$$

Now, the particle flux J_p is given by

$$J_p = -\frac{\omega^{3/2}}{\tau}\left(f + T\partial_\omega f\right) \tag{D.2}$$

$$= -\frac{\omega^{3/2}}{\tau}\left(e^{-\omega/T} f_d(\omega) + e^{-\omega/T}\left(T\partial_\omega f_d - f_d(\omega)\right)\right) \tag{D.3}$$

$$= -\frac{T}{\tau}\omega^{3/2} e^{-\omega/T}\partial_\omega f_d. \tag{D.4}$$

Supposing that particles are injected at the forcing scale ω_f, which induces a constant flux of particles $-\eta_-$ to lower energies, and a positive particle flux η_+ then the deviation from equilibrium solves the following ODE

$$\frac{df_d(\omega)}{d\omega} = \begin{cases} \dfrac{\tau e^{\omega/T}\eta_-}{T\omega^{3/2}} & \omega \in (\omega_{\min}, \omega_f) \\ \dfrac{-\tau e^{\omega/T}\eta_+}{T\omega^{3/2}} & \omega \in (\omega_f, \omega_{\min}). \end{cases} \tag{D.5}$$

Integrating the above ODEs results in a general solution with four unknown constants, η_-, η_+ and two constants of integration. These can be found by supplementing the ODE with the boundary conditions $f(\omega_{\min}) = f(\omega_{\max}) = 0$, the continuity condition

$$\lim_{\omega \to \omega_f^-} f(\omega) = \lim_{\omega \to \omega_f^+} f(\omega) \tag{D.6}$$

and the steady state condition that the particle flux in must be equal to the particle flux out, that is, $\epsilon/\omega_f = \eta_- + \eta_+$.

Appendix E

Temperature function

The temperature function

$$\begin{aligned} T &= \psi[f(\omega;T)] \\ &= \frac{2}{3}\frac{\int \omega^{3/2} f(\omega;T)\, d\omega}{\int \omega^{1/2} f(\omega;T)\, d\omega}\,, \end{aligned} \tag{E.1}$$

at the steady state can be found to be equal to the expression below, found using Mathematica with the change of notation $\omega_{\min} = a$, $\omega_{\max} = b$, $\omega_f = s$. It was not possible to simplify this expression further.

$$
\begin{aligned}
\psi(T) = & \frac{e^{\frac{a+b}{T}}\left(-\sqrt{\pi}\sqrt{T}\operatorname{erf}\left(\sqrt{\frac{a}{T}}\right)+2\sqrt{a}e^{-\frac{a}{T}}+\sqrt{\pi}\sqrt{T}\operatorname{erf}\left(\sqrt{\frac{s}{T}}\right)-2e^{-\frac{s}{T}}\sqrt{s}\right)T^{3/2}}{s\left(\sqrt{T}\left(\sqrt{a}e^{b/T}-\sqrt{b}e^{a/T}\right)+\sqrt{ab}\sqrt{\pi}\operatorname{erfi}\left(\sqrt{\frac{a}{T}}\right)-\sqrt{ab}\sqrt{\pi}\operatorname{erfi}\left(\sqrt{\frac{b}{T}}\right)\right)} \\
& + \frac{e^{\frac{a+b}{T}}\left(\sqrt{\pi}\sqrt{T}\operatorname{erf}\left(\sqrt{\frac{b}{T}}\right)-2\sqrt{b}e^{-\frac{b}{T}}-\sqrt{\pi}\sqrt{T}\operatorname{erf}\left(\sqrt{\frac{s}{T}}\right)+2e^{-\frac{s}{T}}\sqrt{s}\right)T^{3/2}}{s\left(\sqrt{T}\left(\sqrt{a}e^{b/T}-\sqrt{b}e^{a/T}\right)+\sqrt{ab}\sqrt{\pi}\operatorname{erfi}\left(\sqrt{\frac{a}{T}}\right)-\sqrt{ab}\sqrt{\pi}\operatorname{erfi}\left(\sqrt{\frac{b}{T}}\right)\right)} \\
& + \frac{\sqrt{b}\sqrt{\pi}\left(-e^{a/T}\sqrt{\pi}\sqrt{T}\operatorname{erf}\left(\sqrt{\frac{a}{T}}\right)+e^{a/T}\sqrt{\pi}\sqrt{T}\operatorname{erf}\left(\sqrt{\frac{s}{T}}\right)+2\sqrt{a}-2e^{\frac{a-s}{T}}\sqrt{s}\right)\operatorname{erfi}\left(\sqrt{\frac{s}{T}}\right)T}{s\left(\sqrt{T}\left(\sqrt{a}e^{b/T}-\sqrt{b}e^{a/T}\right)+\sqrt{ab}\sqrt{\pi}\operatorname{erfi}\left(\sqrt{\frac{a}{T}}\right)-\sqrt{ab}\sqrt{\pi}\operatorname{erfi}\left(\sqrt{\frac{b}{T}}\right)\right)} \\
& + \frac{\sqrt{a}\sqrt{\pi}\left(e^{b/T}\sqrt{\pi}\sqrt{T}\operatorname{erf}\left(\sqrt{\frac{b}{T}}\right)-e^{b/T}\sqrt{\pi}\sqrt{T}\operatorname{erf}\left(\sqrt{\frac{s}{T}}\right)-2\sqrt{b}+2e^{\frac{b-s}{T}}\sqrt{s}\right)\operatorname{erfi}\left(\sqrt{\frac{s}{T}}\right)T}{s\left(\sqrt{T}\left(\sqrt{a}e^{b/T}-\sqrt{b}e^{a/T}\right)+\sqrt{ab}\sqrt{\pi}\operatorname{erfi}\left(\sqrt{\frac{a}{T}}\right)-\sqrt{ab}\sqrt{\pi}\operatorname{erfi}\left(\sqrt{\frac{b}{T}}\right)\right)} \\
& - \frac{\sqrt{a}e^{b/T}\sqrt{\pi}\left(-\sqrt{\pi}\sqrt{T}\operatorname{erf}\left(\sqrt{\frac{a}{T}}\right)+2\sqrt{a}e^{-\frac{a}{T}}+\sqrt{\pi}\sqrt{T}\operatorname{erf}\left(\sqrt{\frac{s}{T}}\right)-2e^{-\frac{s}{T}}\sqrt{s}\right)\operatorname{erfi}\left(\sqrt{\frac{a}{T}}\right)T}{s\left(\sqrt{T}\left(\sqrt{a}e^{b/T}-\sqrt{b}e^{a/T}\right)+\sqrt{ab}\sqrt{\pi}\operatorname{erfi}\left(\sqrt{\frac{a}{T}}\right)-\sqrt{ab}\sqrt{\pi}\operatorname{erfi}\left(\sqrt{\frac{b}{T}}\right)\right)} \\
& - \frac{\sqrt{a}\sqrt{\pi}\left(e^{b/T}\sqrt{\pi}\sqrt{T}\operatorname{erf}\left(\sqrt{\frac{b}{T}}\right)-e^{b/T}\sqrt{\pi}\sqrt{T}\operatorname{erf}\left(\sqrt{\frac{s}{T}}\right)-2\sqrt{b}+2e^{\frac{b-s}{T}}\sqrt{s}\right)\operatorname{erfi}\left(\sqrt{\frac{a}{T}}\right)T}{s\left(\sqrt{T}\left(\sqrt{a}e^{b/T}-\sqrt{b}e^{a/T}\right)+\sqrt{ab}\sqrt{\pi}\operatorname{erfi}\left(\sqrt{\frac{a}{T}}\right)-\sqrt{ab}\sqrt{\pi}\operatorname{erfi}\left(\sqrt{\frac{b}{T}}\right)\right)} \\
& - \frac{\sqrt{b}\sqrt{\pi}\left(-e^{a/T}\sqrt{\pi}\sqrt{T}\operatorname{erf}\left(\sqrt{\frac{a}{T}}\right)+e^{a/T}\sqrt{\pi}\sqrt{T}\operatorname{erf}\left(\sqrt{\frac{s}{T}}\right)+2\sqrt{a}-2e^{\frac{a-s}{T}}\sqrt{s}\right)\operatorname{erfi}\left(\sqrt{\frac{b}{T}}\right)T}{s\left(\sqrt{T}\left(\sqrt{a}e^{b/T}-\sqrt{b}e^{a/T}\right)+\sqrt{ab}\sqrt{\pi}\operatorname{erfi}\left(\sqrt{\frac{a}{T}}\right)-\sqrt{ab}\sqrt{\pi}\operatorname{erfi}\left(\sqrt{\frac{b}{T}}\right)\right)} \\
& - \frac{\sqrt{b}e^{a/T}\sqrt{\pi}\left(\sqrt{\pi}\sqrt{T}\operatorname{erf}\left(\sqrt{\frac{b}{T}}\right)-2\sqrt{b}e^{-\frac{b}{T}}-\sqrt{\pi}\sqrt{T}\operatorname{erf}\left(\sqrt{\frac{s}{T}}\right)+2e^{-\frac{s}{T}}\sqrt{s}\right)\operatorname{erfi}\left(\sqrt{\frac{b}{T}}\right)T}{s\left(\sqrt{T}\left(\sqrt{a}e^{b/T}-\sqrt{b}e^{a/T}\right)+\sqrt{ab}\sqrt{\pi}\operatorname{erfi}\left(\sqrt{\frac{a}{T}}\right)-\sqrt{ab}\sqrt{\pi}\operatorname{erfi}\left(\sqrt{\frac{b}{T}}\right)\right)} \\
& + \frac{\pi\sqrt{\frac{ab}{T}}\left(-\sqrt{\pi}\sqrt{T}\operatorname{erf}\left(\sqrt{\frac{a}{T}}\right)+2\sqrt{a}e^{-\frac{a}{T}}+\sqrt{\pi}\sqrt{T}\operatorname{erf}\left(\sqrt{\frac{s}{T}}\right)-2e^{-\frac{s}{T}}\sqrt{s}\right)\operatorname{erfi}\left(\sqrt{\frac{a}{T}}\right)\operatorname{erfi}\left(\sqrt{\frac{b}{T}}\right)T}{s\left(\sqrt{T}\left(\sqrt{a}e^{b/T}-\sqrt{b}e^{a/T}\right)+\sqrt{ab}\sqrt{\pi}\operatorname{erfi}\left(\sqrt{\frac{a}{T}}\right)-\sqrt{ab}\sqrt{\pi}\operatorname{erfi}\left(\sqrt{\frac{b}{T}}\right)\right)} \\
& + \frac{\pi\sqrt{\frac{ab}{T}}\left(\sqrt{\pi}\sqrt{T}\operatorname{erf}\left(\sqrt{\frac{b}{T}}\right)-2\sqrt{b}e^{-\frac{b}{T}}-\sqrt{\pi}\sqrt{T}\operatorname{erf}\left(\sqrt{\frac{s}{T}}\right)+2e^{-\frac{s}{T}}\sqrt{s}\right)\operatorname{erfi}\left(\sqrt{\frac{a}{T}}\right)\operatorname{erfi}\left(\sqrt{\frac{b}{T}}\right)T}{s\left(\sqrt{T}\left(\sqrt{a}e^{b/T}-\sqrt{b}e^{a/T}\right)+\sqrt{ab}\sqrt{\pi}\operatorname{erfi}\left(\sqrt{\frac{a}{T}}\right)-\sqrt{ab}\sqrt{\pi}\operatorname{erfi}\left(\sqrt{\frac{b}{T}}\right)\right)}
\end{aligned}
\tag{E.2}
$$

$$
\begin{aligned}
&- \frac{2\sqrt{ab}\sqrt{\pi}(b-s)\operatorname{erfi}\left(\sqrt{\frac{s}{T}}\right)}{s\left(\sqrt{T}\left(\sqrt{a}e^{b/T}-\sqrt{b}e^{a/T}\right)+\sqrt{ab}\sqrt{\pi}\operatorname{erfi}\left(\sqrt{\frac{a}{T}}\right)-\sqrt{ab}\sqrt{\pi}\operatorname{erfi}\left(\sqrt{\frac{b}{T}}\right)\right)} \\
&- \frac{2\sqrt{ab}\sqrt{\pi}(s-a)\operatorname{erfi}\left(\sqrt{\frac{s}{T}}\right)}{s\left(\sqrt{T}\left(\sqrt{a}e^{b/T}-\sqrt{b}e^{a/T}\right)+\sqrt{ab}\sqrt{\pi}\operatorname{erfi}\left(\sqrt{\frac{a}{T}}\right)-\sqrt{ab}\sqrt{\pi}\operatorname{erfi}\left(\sqrt{\frac{b}{T}}\right)\right)} \\
&- \frac{2\sqrt{ab}\sqrt{\pi}\operatorname{erfi}\left(\sqrt{\frac{a}{T}}\right)\left(-{}_2F_2\left(1,1;\frac{1}{2},2;-\frac{b}{T}\right)b+b-s+s\,{}_2F_2\left(1,1;\frac{1}{2},2;-\frac{s}{T}\right)\right)}{s\left(\sqrt{T}\left(\sqrt{a}e^{b/T}-\sqrt{b}e^{a/T}\right)+\sqrt{ab}\sqrt{\pi}\operatorname{erfi}\left(\sqrt{\frac{a}{T}}\right)-\sqrt{ab}\sqrt{\pi}\operatorname{erfi}\left(\sqrt{\frac{b}{T}}\right)\right)} \\
&- \frac{2\sqrt{ab}\sqrt{\pi}\operatorname{erfi}\left(\sqrt{\frac{b}{T}}\right)\left({}_2F_2\left(1,1;\frac{1}{2},2;-\frac{a}{T}\right)a-a+s-s\,{}_2F_2\left(1,1;\frac{1}{2},2;-\frac{s}{T}\right)\right)}{s\left(\sqrt{T}\left(\sqrt{a}e^{b/T}-\sqrt{b}e^{a/T}\right)+\sqrt{ab}\sqrt{\pi}\operatorname{erfi}\left(\sqrt{\frac{a}{T}}\right)-\sqrt{ab}\sqrt{\pi}\operatorname{erfi}\left(\sqrt{\frac{b}{T}}\right)\right)} \\
&- \frac{2e^{b/T}(s-a)\sqrt{aT}}{s\left(\sqrt{T}\left(\sqrt{a}e^{b/T}-\sqrt{b}e^{a/T}\right)+\sqrt{ab}\sqrt{\pi}\operatorname{erfi}\left(\sqrt{\frac{a}{T}}\right)-\sqrt{ab}\sqrt{\pi}\operatorname{erfi}\left(\sqrt{\frac{b}{T}}\right)\right)} \\
&- \frac{2e^{a/T}(b-s)\sqrt{bT}}{s\left(\sqrt{T}\left(\sqrt{a}e^{b/T}-\sqrt{b}e^{a/T}\right)+\sqrt{ab}\sqrt{\pi}\operatorname{erfi}\left(\sqrt{\frac{a}{T}}\right)-\sqrt{ab}\sqrt{\pi}\operatorname{erfi}\left(\sqrt{\frac{b}{T}}\right)\right)} \\
&- \frac{2e^{s/T}\sqrt{abT}\left(-{}_2F_2\left(1,1;\frac{1}{2},2;-\frac{b}{T}\right)b+b-s+s\,{}_2F_2\left(1,1;\frac{1}{2},2;-\frac{s}{T}\right)\right)}{s^{3/2}\left(\sqrt{T}\left(\sqrt{a}e^{b/T}-\sqrt{b}e^{a/T}\right)+\sqrt{ab}\sqrt{\pi}\operatorname{erfi}\left(\sqrt{\frac{a}{T}}\right)-\sqrt{ab}\sqrt{\pi}\operatorname{erfi}\left(\sqrt{\frac{b}{T}}\right)\right)} \\
&- \frac{2e^{s/T}\sqrt{abT}\left({}_2F_2\left(1,1;\frac{1}{2},2;-\frac{a}{T}\right)a-a+s-s\,{}_2F_2\left(1,1;\frac{1}{2},2;-\frac{s}{T}\right)\right)}{s^{3/2}\left(\sqrt{T}\left(\sqrt{a}e^{b/T}-\sqrt{b}e^{a/T}\right)+\sqrt{ab}\sqrt{\pi}\operatorname{erfi}\left(\sqrt{\frac{a}{T}}\right)-\sqrt{ab}\sqrt{\pi}\operatorname{erfi}\left(\sqrt{\frac{b}{T}}\right)\right)} \\
&+ \frac{2e^{s/T}(b-s)\sqrt{abT}}{s^{3/2}\left(\sqrt{T}\left(\sqrt{a}e^{b/T}-\sqrt{b}e^{a/T}\right)+\sqrt{ab}\sqrt{\pi}\operatorname{erfi}\left(\sqrt{\frac{a}{T}}\right)-\sqrt{ab}\sqrt{\pi}\operatorname{erfi}\left(\sqrt{\frac{b}{T}}\right)\right)} \\
&+ \frac{2e^{s/T}(s-a)\sqrt{abT}}{s^{3/2}\left(\sqrt{T}\left(\sqrt{a}e^{b/T}-\sqrt{b}e^{a/T}\right)+\sqrt{ab}\sqrt{\pi}\operatorname{erfi}\left(\sqrt{\frac{a}{T}}\right)-\sqrt{ab}\sqrt{\pi}\operatorname{erfi}\left(\sqrt{\frac{b}{T}}\right)\right)}
\end{aligned}
\tag{E.3}
$$

$$
\begin{aligned}
&-\frac{\pi\sqrt{\frac{ab}{T}}\left(-\sqrt{\pi}\sqrt{T}\mathrm{erf}\left(\sqrt{\frac{a}{T}}\right)+2\sqrt{a}e^{-\frac{a}{T}}+\sqrt{\pi}\sqrt{T}\mathrm{erf}\left(\sqrt{\frac{s}{T}}\right)-2e^{-\frac{s}{T}}\sqrt{s}\right)\mathrm{erfi}\left(\sqrt{\frac{a}{T}}\right)\mathrm{erfi}\left(\sqrt{\frac{s}{T}}\right)T}{s\left(\sqrt{T}\left(\sqrt{a}e^{b/T}-\sqrt{b}e^{a/T}\right)+\sqrt{ab}\sqrt{\pi}\mathrm{erfi}\left(\sqrt{\frac{a}{T}}\right)-\sqrt{ab}\sqrt{\pi}\mathrm{erfi}\left(\sqrt{\frac{b}{T}}\right)\right)}\\
&-\frac{\pi\sqrt{\frac{ab}{T}}\left(\sqrt{\pi}\sqrt{T}\mathrm{erf}\left(\sqrt{\frac{b}{T}}\right)-2\sqrt{b}e^{-\frac{b}{T}}-\sqrt{\pi}\sqrt{T}\mathrm{erf}\left(\sqrt{\frac{s}{T}}\right)+2e^{-\frac{s}{T}}\sqrt{s}\right)\mathrm{erfi}\left(\sqrt{\frac{b}{T}}\right)\mathrm{erfi}\left(\sqrt{\frac{s}{T}}\right)T}{s\left(\sqrt{T}\left(\sqrt{a}e^{b/T}-\sqrt{b}e^{a/T}\right)+\sqrt{ab}\sqrt{\pi}\mathrm{erfi}\left(\sqrt{\frac{a}{T}}\right)-\sqrt{ab}\sqrt{\pi}\mathrm{erfi}\left(\sqrt{\frac{b}{T}}\right)\right)}\\
&-\frac{\sqrt{bT}\left(-e^{\frac{a+s}{T}}\sqrt{\pi}\sqrt{T}\mathrm{erf}\left(\sqrt{\frac{a}{T}}\right)+2\sqrt{a}e^{s/T}+e^{\frac{a+s}{T}}\sqrt{\pi}\sqrt{T}\mathrm{erf}\left(\sqrt{\frac{s}{T}}\right)-2e^{a/T}\sqrt{s}\right)T}{s^{3/2}\left(\sqrt{T}\left(\sqrt{a}e^{b/T}-\sqrt{b}e^{a/T}\right)+\sqrt{ab}\sqrt{\pi}\mathrm{erfi}\left(\sqrt{\frac{a}{T}}\right)-\sqrt{ab}\sqrt{\pi}\mathrm{erfi}\left(\sqrt{\frac{b}{T}}\right)\right)}\\
&-\frac{\sqrt{aT}\left(e^{\frac{b+s}{T}}\sqrt{\pi}\sqrt{T}\mathrm{erf}\left(\sqrt{\frac{b}{T}}\right)-2\sqrt{b}e^{s/T}-e^{\frac{b+s}{T}}\sqrt{\pi}\sqrt{T}\mathrm{erf}\left(\sqrt{\frac{s}{T}}\right)+2e^{b/T}\sqrt{s}\right)T}{s^{3/2}\left(\sqrt{T}\left(\sqrt{a}e^{b/T}-\sqrt{b}e^{a/T}\right)+\sqrt{ab}\sqrt{\pi}\mathrm{erfi}\left(\sqrt{\frac{a}{T}}\right)-\sqrt{ab}\sqrt{\pi}\mathrm{erfi}\left(\sqrt{\frac{b}{T}}\right)\right)}\\
&+\frac{\sqrt{ab}\sqrt{\pi}\left(-e^{s/T}\sqrt{\pi}\sqrt{T}\mathrm{erf}\left(\sqrt{\frac{a}{T}}\right)+2\sqrt{a}e^{\frac{s-a}{T}}+e^{s/T}\sqrt{\pi}\sqrt{T}\mathrm{erf}\left(\sqrt{\frac{s}{T}}\right)-2\sqrt{s}\right)\mathrm{erfi}\left(\sqrt{\frac{a}{T}}\right)T}{s^{3/2}\left(\sqrt{T}\left(\sqrt{a}e^{b/T}-\sqrt{b}e^{a/T}\right)+\sqrt{ab}\sqrt{\pi}\mathrm{erfi}\left(\sqrt{\frac{a}{T}}\right)-\sqrt{ab}\sqrt{\pi}\mathrm{erfi}\left(\sqrt{\frac{b}{T}}\right)\right)}\\
&+\frac{\sqrt{ab}\sqrt{\pi}\left(e^{s/T}\sqrt{\pi}\sqrt{T}\mathrm{erf}\left(\sqrt{\frac{b}{T}}\right)-2\sqrt{b}e^{\frac{s-b}{T}}-e^{s/T}\sqrt{\pi}\sqrt{T}\mathrm{erf}\left(\sqrt{\frac{s}{T}}\right)+2\sqrt{s}\right)\mathrm{erfi}\left(\sqrt{\frac{b}{T}}\right)T}{s^{3/2}\left(\sqrt{T}\left(\sqrt{a}e^{b/T}-\sqrt{b}e^{a/T}\right)+\sqrt{ab}\sqrt{\pi}\mathrm{erfi}\left(\sqrt{\frac{a}{T}}\right)-\sqrt{ab}\sqrt{\pi}\mathrm{erfi}\left(\sqrt{\frac{b}{T}}\right)\right)}\\
&+\frac{2e^{a/T}\sqrt{bT}\left(-{}_2F_2\left(1,1;\frac{1}{2},2;-\frac{b}{T}\right)b+b-s+s\,{}_2F_2\left(1,1;\frac{1}{2},2;-\frac{s}{T}\right)\right)}{s\left(\sqrt{T}\left(\sqrt{a}e^{b/T}-\sqrt{b}e^{a/T}\right)+\sqrt{ab}\sqrt{\pi}\mathrm{erfi}\left(\sqrt{\frac{a}{T}}\right)-\sqrt{ab}\sqrt{\pi}\mathrm{erfi}\left(\sqrt{\frac{b}{T}}\right)\right)}\\
&+\frac{2\sqrt{ab}\sqrt{\pi}\mathrm{erfi}\left(\sqrt{\frac{s}{T}}\right)\left(-{}_2F_2\left(1,1;\frac{1}{2},2;-\frac{b}{T}\right)b+b-s+s\,{}_2F_2\left(1,1;\frac{1}{2},2;-\frac{s}{T}\right)\right)}{s\left(\sqrt{T}\left(\sqrt{a}e^{b/T}-\sqrt{b}e^{a/T}\right)+\sqrt{ab}\sqrt{\pi}\mathrm{erfi}\left(\sqrt{\frac{a}{T}}\right)-\sqrt{ab}\sqrt{\pi}\mathrm{erfi}\left(\sqrt{\frac{b}{T}}\right)\right)}\\
&+\frac{2e^{b/T}\sqrt{aT}\left({}_2F_2\left(1,1;\frac{1}{2},2;-\frac{a}{T}\right)a-a+s-s\,{}_2F_2\left(1,1;\frac{1}{2},2;-\frac{s}{T}\right)\right)}{s\left(\sqrt{T}\left(\sqrt{a}e^{b/T}-\sqrt{b}e^{a/T}\right)+\sqrt{ab}\sqrt{\pi}\mathrm{erfi}\left(\sqrt{\frac{a}{T}}\right)-\sqrt{ab}\sqrt{\pi}\mathrm{erfi}\left(\sqrt{\frac{b}{T}}\right)\right)}\\
&+\frac{2\sqrt{ab}\sqrt{\pi}\mathrm{erfi}\left(\sqrt{\frac{s}{T}}\right)\left({}_2F_2\left(1,1;\frac{1}{2},2;-\frac{a}{T}\right)a-a+s-s\,{}_2F_2\left(1,1;\frac{1}{2},2;-\frac{s}{T}\right)\right)}{s\left(\sqrt{T}\left(\sqrt{a}e^{b/T}-\sqrt{b}e^{a/T}\right)+\sqrt{ab}\sqrt{\pi}\mathrm{erfi}\left(\sqrt{\frac{a}{T}}\right)-\sqrt{ab}\sqrt{\pi}\mathrm{erfi}\left(\sqrt{\frac{b}{T}}\right)\right)}\\
&+\frac{2\sqrt{ab}\sqrt{\pi}(b-s)\mathrm{erfi}\left(\sqrt{\frac{a}{T}}\right)}{s\left(\sqrt{T}\left(\sqrt{a}e^{b/T}-\sqrt{b}e^{a/T}\right)+\sqrt{ab}\sqrt{\pi}\mathrm{erfi}\left(\sqrt{\frac{a}{T}}\right)-\sqrt{ab}\sqrt{\pi}\mathrm{erfi}\left(\sqrt{\frac{b}{T}}\right)\right)}\\
&+\frac{2\sqrt{ab}\sqrt{\pi}(s-a)\mathrm{erfi}\left(\sqrt{\frac{b}{T}}\right)}{s\left(\sqrt{T}\left(\sqrt{a}e^{b/T}-\sqrt{b}e^{a/T}\right)+\sqrt{ab}\sqrt{\pi}\mathrm{erfi}\left(\sqrt{\frac{a}{T}}\right)-\sqrt{ab}\sqrt{\pi}\mathrm{erfi}\left(\sqrt{\frac{b}{T}}\right)\right)}
\end{aligned}
\tag{E.4}
$$

Appendix F

Inelastic steady-state

The solution to the inelastic Fokker-Planck steady state equation

$$2q\omega^{1/2}\frac{\partial}{\partial\omega}\left(\omega^{1/2}f(\omega,t)\right)+2q^2\frac{\partial}{\partial\omega}\left(\left(\omega+E^*\right)f(\omega,t)\right) + 4q^2\omega\frac{\partial^2}{\partial\omega^2}\left(\left(\omega+E^*\right)f(\omega,t)\right)+\eta\delta(\omega-\omega_f)=0, \quad \text{(F.1)}$$

with boundary conditions

$$f(\omega_{\max})=0, \quad \text{(F.2)}$$

$$f'(\omega_{\max})=\frac{-\eta}{2\omega_{\max}^{1/2}(E^*+\omega_{\max})}, \quad \text{(F.3)}$$

can be found using the Mathematica software package, and are given by

$$
\begin{aligned}
f(\omega) = & \\
& - \frac{2^{-1-\frac{1}{2q}}\sqrt{\omega}(e+\omega)^{\frac{1}{2q}-1}\left(\frac{e+\omega}{e}\right)^{-\frac{1}{2q}}(q(e+\omega))^{-\frac{1}{2q}}\,{}_2F_1\left(\frac{1}{2},-\frac{1}{2q};\frac{3}{2};-\frac{\omega}{e}\right)(e+\omega_{\max})^{-\frac{1}{2q}}\left(\frac{e+\omega_{\max}}{e}\right)^{\frac{1}{2q}}}{q\,{}_2F_1\left(\frac{1}{2},-\frac{1}{2q};\frac{3}{2};-\frac{\omega_{\max}}{e}\right)\sqrt{\omega_{\max}}} \\
& + \frac{\left(\frac{e+\omega}{e}\right)^{-\frac{1}{2q}}\eta(e+\omega)^{\frac{1}{2q}-1}(q(e+\omega))^{-\frac{1}{2q}}\,{}_2F_1\left(\frac{1}{2},-\frac{1}{2q};\frac{3}{2};-\frac{\omega}{e}\right)\sqrt{\omega}\,(e+\omega_{\max})^{-\frac{1}{2q}}\,(q\,(e+\omega_{\max}))^{\frac{1}{2q}}}{2\sqrt{\omega_f}} \\
& + \frac{2^{-1-\frac{1}{2q}}(q(e+\omega))^{-\frac{1}{2q}}}{q(e+\omega)} \\
& + q\eta\sqrt{\omega}(e+\omega)^{\frac{1}{2q}-1}\left(\frac{e+\omega}{e}\right)^{-\frac{1}{2q}}(q(e+\omega))^{-\frac{1}{2q}}\,{}_2F_1\left(\frac{1}{2},-\frac{1}{2q};\frac{3}{2};-\frac{\omega}{e}\right)\times \\
& \frac{{}_2F_1\left(-\frac{1}{2q},-\frac{1}{2q};1-\frac{1}{2q};-\frac{e}{\omega_{\max}}\right)(e+\omega_{\max})^{-\frac{1}{2q}}\left(\frac{e+\omega_{\max}}{e}\right)^{\frac{1}{2q}}(q\,(e+\omega_{\max}))^{\frac{1}{2q}}\left(\frac{e+\omega_{\max}}{\omega_{\max}}\right)^{-\frac{1}{2q}}}{2\,{}_2F_1\left(\frac{1}{2},-\frac{1}{2q};\frac{3}{2};-\frac{\omega_{\max}}{e}\right)\sqrt{\omega_{\max}}} \\
& + \eta\sqrt{\omega}(e+\omega)^{\frac{1}{2q}-1}\left(\frac{e+\omega}{e}\right)^{-\frac{1}{2q}}(q(e+\omega))^{-\frac{1}{2q}}\,{}_2F_1\left(\frac{1}{2},-\frac{1}{2q};\frac{3}{2};-\frac{\omega}{e}\right)\times \\
& \frac{G^{2,2}_{3,3}\left(\frac{\omega_{\max}}{e}\middle|\begin{matrix}\frac{1}{2},1+\frac{1}{2q},1\\0,0,-\frac{1}{2}\end{matrix}\right)(e+\omega_{\max})^{-\frac{1}{2q}}\,(q\,(e+\omega_{\max}))^{\frac{1}{2q}}}{8\Gamma\left(-\frac{1}{2q}\right)\,{}_2F_1\left(\frac{1}{2},-\frac{1}{2q};\frac{3}{2};-\frac{\omega_{\max}}{e}\right)\sqrt{\omega_{\max}}} \\
& - \frac{\eta\sqrt{\omega}(e+\omega)^{\frac{1}{2q}-1}\left(\frac{e+\omega}{e}\right)^{-\frac{1}{2q}}(q(e+\omega))^{-\frac{1}{2q}}\,{}_2F_1\left(\frac{1}{2},-\frac{1}{2q};\frac{3}{2};-\frac{\omega}{e}\right)(e+\omega_{\max})^{-\frac{1}{2q}}\,(q\,(e+\omega_{\max}))^{\frac{1}{2q}}}{2\sqrt{\omega_{\max}}} \\
& - q\eta\sqrt{\omega}(e+\omega)^{\frac{1}{2q}-1}\left(\frac{e+\omega}{e}\right)^{-\frac{1}{2q}}(q(e+\omega))^{-\frac{1}{2q}}\,{}_2F_1\left(\frac{1}{2},-\frac{1}{2q};\frac{3}{2};-\frac{\omega}{e}\right)\times \\
& \frac{{}_2F_1\left(-\frac{1}{2q},-\frac{1}{2q};1-\frac{1}{2q};-\frac{e}{\omega_f}\right)\left(\frac{e+\omega_f}{e}\right)^{\frac{1}{2q}}\left(\frac{e+\omega_f}{\omega_f}\right)^{-\frac{1}{2q}}(e+\omega_{\max})^{-\frac{1}{2q}}\,(q\,(e+\omega_{\max}))^{\frac{1}{2q}}}{2\,{}_2F_1\left(\frac{1}{2},-\frac{1}{2q};\frac{3}{2};-\frac{\omega_{\max}}{e}\right)\sqrt{\omega_{\max}}} \\
& - \eta\sqrt{\omega}(e+\omega)^{\frac{1}{2q}-1}\left(\frac{e+\omega}{e}\right)^{-\frac{1}{2q}}(q(e+\omega))^{-\frac{1}{2q}}\,{}_2F_1\left(\frac{1}{2},-\frac{1}{2q};\frac{3}{2};-\frac{\omega}{e}\right)\times \\
& \frac{G^{2,2}_{3,3}\left(\frac{\omega_f}{e}\middle|\begin{matrix}\frac{1}{2},1+\frac{1}{2q},1\\0,0,-\frac{1}{2}\end{matrix}\right)(e+\omega_{\max})^{-\frac{1}{2q}}\,(q\,(e+\omega_{\max}))^{\frac{1}{2q}}}{8\Gamma\left(-\frac{1}{2q}\right)\,{}_2F_1\left(\frac{1}{2},-\frac{1}{2q};\frac{3}{2};-\frac{\omega_{\max}}{e}\right)\sqrt{\omega_{\max}}}.
\end{aligned}
\tag{F.4}
$$

Bibliography

Husain A Al-Mohssen and Nicolas G Hadjiconstantinou. Low-variance direct monte carlo simulations using importance weights. *ESAIM: Mathematical Modelling and Numerical Analysis*, 44(05):1069–1083, 2010.

Radjesvarane Alexandre, Yoshinori Morimoto, Seiji Ukai, C-J Xu, and Tong Yang. Global existence and full regularity of the boltzmann equation without angular cutoff. *Communications in Mathematical Physics*, 304(2):513–581, 2011.

Leif Arkeryd. On the boltzmann equation. *Archive for Rational Mechanics and Analysis*, 45(1):1–16, 1972.

Pietro Asinari. Nonlinear Boltzmann equation for the homogeneous isotropic case: minimal deterministic Matlab program. *Comput. Phys. Comm.*, 181(10):1776–1788, 2010. ISSN 0010-4655. doi: 10.1016/j.cpc.2010.06.041. URL `http://dx.doi.org/10.1016/j.cpc.2010.06.041`. Associated computer program available online.

Lowell L Baker and Nicolas G Hadjiconstantinou. Variance reduction for monte carlo solutions of the boltzmann equation. *Physics of Fluids (1994-present)*, 17 (5):051703, 2005.

Andrea Baldassarri, Andrea Puglisi, and Umberto Marini Bettolo Marconi. Kinetics models of inelastic gases. *Mathematical Models and Methods in Applied Sciences*, 12(07):965–983, 2002.

AM Balk. On the kolmogorov–zakharov spectra of weak turbulence. *Physica D: Nonlinear Phenomena*, 139(1):137–157, 2000.

Richard Bellman, Richard Ernest Bellman, Richard Ernest Bellman, and Richard Ernest Bellman. *Adaptive control processes: a guided tour*, volume 4. Princeton university press Princeton, 1961.

E. Ben-Naim and J. Machta. Stationary states and energy cascades in inelastic gases. *Phys. Rev. Lett.*, 94(13):138001, 2005.

E. Ben-Naim, B. Machta, and J. Machta. Power-law velocity distributions in granular gases. *Physical Review E*, 72(2):021302, August 2005. doi: 10.1103/PhysRevE.72.021302. URL `http://link.aps.org/doi/10.1103/PhysRevE.72.021302`.

R Benzi, S Ciliberto, R Tripiccione, C Baudet, F Massaioli, and S Succi. Extended self-similarity in turbulent flows. *Physical review E*, 48(1):R29, 1993.

Prabhu Lal Bhatnagar, Eugene P Gross, and Max Krook. A model for collision processes in gases. i. small amplitude processes in charged and neutral one-component systems. *Physical review*, 94(3):511, 1954.

GA Bird. Monte carlo simulation of gas flows. *Annual Review of Fluid Mechanics*, 10(1):11–31, 1978.

Graeme Austin Bird. Molecular gas dynamics. *NASA STI/Recon Technical Report A*, 76:40225, 1976.

Graeme Austin Bird. Molecular gas dynamics and the direct simulation of gas flows. 1994.

AV Bobylev. The chapman-enskog and grad methods for solving the boltzmann equation. In *Akademiia Nauk SSSR Doklady*, volume 262, pages 71–75, 1982.

SV Bogomolov and LV Dorodnitsyn. Equations of stochastic quasi-gas dynamics: Viscous gas case. *Mathematical Models and Computer Simulations*, 3(4):457–467, 2011.

L Boltzmann. Weitere studien über das wärme gleichgenicht unfer gasmoläkuler. sitzungsberichte der akademie der wissenschaften 66 (1872), 275–370. translation: Further studies on the thermal equilibrium of gas molecules. *Kinetic Theory*, 2: 88–174, 1872.

Paul Bratley, Bennett L Fox, and Linus E Schrage. *A guide to simulation*, volume 2. Springer-Verlag New York, 1983.

Nikolai V. Brilliantov and Thorsten Poschel. *Kinetic Theory of Granular Gases*. Oxford University Press, Oxford ; New York, September 2004. ISBN 9780198530381.

Mark Broadie and Paul Glasserman. Estimating security price derivatives using simulation. *Management science*, 42(2):269–285, 1996.

Torsten Carleman. Sur la théorie de l'équation intégrodifférentielle de boltzmann. *Acta Mathematica*, 60(1):91–146, 1933.

Carlo Cercignani and David H Sattinger. *Scaling limits and models in physical processes*, volume 28. Springer, 1998.

Carlo Cercignani, Reinhard Illner, and Mario Pulvirenti. *The mathematical theory of dilute gases*. Springer, 1994.

Subrahmanyan Chandrasekhar. Stochastic problems in physics and astronomy. *Reviews of modern physics*, 15(1):1, 1943.

CS Wang Chang, George E Uhlenbeck, George W Ford, and James D Foch. *The kinetic theory of gases*. North-Holland, 1970.

Gang Chen. Nanoscale energy transport and conversion, 2005.

FG Cheremisin. Solving the boltzmann equation in the case of passing to the hydrodynamic flow regime. In *Doklady Physics*, volume 45, pages 401–404. Springer, 2000.

Kai-Lai Chung. An estimate concerning the kolmogroff limit distribution. *Transactions of the American Mathematical Society*, pages 36–50, 1949.

C. Connaughton and Y. Pomeau. Kinetic theory and bose-einstein condensation. *C. R. Phys.*, 5(1):91–106, 2004.

C. Connaughton, R. Rajesh, and O. Zaboronski. Breakdown of kolmogorov scaling in models of cluster aggregation. *Phys. Rev. Lett.*, 94:194503, 2005.

TG Cowling and Sydney Chapman. *The mathematical theory of non-uniform gases*. University Press, 1960.

R Cranley and TNL Patterson. Randomization of number theoretic methods for multiple integration. *SIAM Journal on Numerical Analysis*, 13(6):904–914, 1976.

Masoud Dahmardeh, Alireza Nojeh, and Kenichi Takahata. Possible mechanism in dry micro-electro-discharge machining of carbon-nanotube forests: A study of the effect of oxygen. *Journal of Applied Physics*, 109(9):093308, 2011.

Josef Dick and Friedrich Pillichshammer. *Digital nets and sequences: Discrepancy Theory and Quasi–Monte Carlo Integration*. Cambridge University Press, 2010.

Ronald J DiPerna and Pierre-Louis Lions. On the cauchy problem for boltzmann equations: global existence and weak stability. *Annals of Mathematics*, pages 321–366, 1989.

AH Epstein, SD Senturia, O Al-Midani, G Anathasuresh, A Ayon, K Breuer, KS Chen, PP Ehrich, E Esteve, L Frechette, et al. Micro-heat engines, gas turbines and rocket engines œ the mit microengine project. *American Institute of Aeronautics and Astronautics*, pages 1–12, 1997.

MH Ernst and R Brito. Scaling solutions of inelastic boltzmann equations with over-populated high energy tails. *Journal of Statistical Physics*, 109(3-4):407–432, 2002.

MH Ernst, E Trizac, and A Barrat. The boltzmann equation for driven systems of inelastic soft spheres. *Journal of statistical physics*, 124(2-4):549–586, 2006.

Alessandra Faggionato, Fabio Martinelli, Cyril Roberto, and Cristina Toninelli. The east model: recent results and new progresses. *arXiv preprint arXiv:1205.1607*, 2012.

G. Falkovich, K. Gaw\cedzki, and M. Vergassola. Particles and fields in fluid turbulence. *Rev. Mod. Phys.*, 73(4):913–975, 2001.

Jing Fan, Iain D Boyd, Chun-Pei Cai, Konstantinos Hennighausen, and Graham V Candler. Computation of rarefied gas flows around a naca 0012 airfoil. *AIAA journal*, 39(4):618–625, 2001.

Leonardo Ferrari. On the velocity relaxation of a rayleigh gas: I. assumptions and approximations in the derivation of the usual kinetic equation. *Physica A: Statistical Mechanics and its Applications*, 115(1):232–246, 1982.

Francis Filbet and Giovanni Russo. Accurate numerical methods for the boltzmann equation. In *Modeling and computational methods for kinetic equations*, pages 117–145. Springer, 2004.

Ragnar Fjørtoft. On the changes in the spectral distribution of kinetic energy for twodimensional, nondivergent flow. *Tellus*, 5(3):225–230, 1953.

U. Frisch. *Turbulence: the legacy of A. N. Kolmogorov*. Cambridge University Press, Cambridge, 1995.

Uriel Frisch. Fully developed turbulence and intermittency. *Annals of the New York Academy of Sciences*, 357(1):359–367, 1980.

Mohamed Gad-el Hak. Comments on critical view on new results in micro-fluid mechanics. *International journal of heat and mass transfer*, 46(20):3941–3945, 2003.

Mohamed Gad-el Hak. *The MEMS handbook*. CRC press, 2010.

D Goldstein, B Sturtevant, and JE Broadwell. Investigations of the motion of discrete-velocity gases. *Progress in Astronautics and Aeronautics*, 117:100–117, 1989.

Anna Górecka-Drzazga. Miniature and mems-type vacuum sensors and pumps. *Vacuum*, 83(12):1419–1426, 2009.

Hossein Gorji and Patrick Jenny. A kinetic model for gas mixtures based on a fokker-planck equation. In *Journal of Physics: Conference Series*, volume 362, page 012042. IOP Publishing, 2012.

M. H. Gorji, M. Torrilhon, and P. Jenny. Fokkerplanck model for computational studies of monatomic rarefied gas flows. *Journal of Fluid Mechanics*, 680:574–601, 8 2011. ISSN 1469-7645. doi: 10.1017/jfm.2011.188. URL `http://journals.cambridge.org/article_S0022112011001881`.

M Hossein Gorji and Patrick Jenny. A fokker–planck based kinetic model for diatomic rarefied gas flows. *Physics of Fluids (1994-present)*, 25(6):062002, 2013.

M Hossein Gorji and Patrick Jenny. Fokker–planck–dsmc algorithm for simulations of rarefied gas flows. *Journal of Computational Physics*, 287:110–129, 2015.

M Hossein Gorji, Nemanja Andric, and Patrick Jenny. Variance reduction for fokker-planck based particle monte carlo schemes. *Journal of Computational Physics*, 2015.

Harold Grad. On the kinetic theory of rarefied gases. *Communications on pure and applied mathematics*, 2(4):331–407, 1949.

Melville S Green. Brownian motion in a gas of noninteracting molecules. *The Journal of Chemical Physics*, 19(8):1036–1046, 1951.

Philip Gressman and Robert Strain. Global classical solutions of the boltzmann equation without angular cut-off. *Journal of the American Mathematical Society*, 24(3):771–847, 2011.

Marek Grzelczak, Jan Vermant, Eric M Furst, and Luis M Liz-Marzán. Directed self-assembly of nanoparticles. *ACS nano*, 4(7):3591–3605, 2010.

Xiao-Jun Gu, D Emerson, et al. Cylindrical couette flow in the transition regime by the method of moments. 2014.

Nicolas G. Hadjiconstantinou. The limits of navier-stokes theory and kinetic extensions for describing small-scale gaseous hydrodynamics. *Physics of Fluids (1994-present)*, 18(11):111301, 2006. doi: http://dx.doi.org/10.1063/1.2393436. URL `http://scitation.aip.org/content/aip/journal/pof2/18/11/10.1063/1.2393436`.

Nicolas G Hadjiconstantinou, Alejandro L Garcia, Martin Z Bazant, and Gang He. Statistical error in particle simulations of hydrodynamic phenomena. *Journal of Computational Physics*, 187(1):274–297, 2003.

Nicolas G Hadjiconstantinou, Gregg A Radtke, and Lowell L Baker. On variance-reduced simulations of the boltzmann transport equation for small-scale heat transfer applications. *Journal of Heat Transfer*, 132(11):112401, 2010.

PK Haff. Grain flow as a fluid-mechanical phenomenon. *Journal of Fluid Mechanics*, 134:401–430, 1983.

Jean-Pierre Hansen and Ian R. McDonald. *Theory of Simple Liquids*. Elsevier, September 1990. ISBN 9780080571010.

S Hasselmann, K Hasselmann, JH Allender, and TP Barnett. Computations and parameterizations of the nonlinear energy transfer in a gravity-wave specturm. part ii: Parameterizations of the nonlinear energy transfer for application in wave models. *Journal of Physical Oceanography*, 15(11):1378–1391, 1985.

H. Hayakawa. Irreversible kinetic coagulations in the presence of a source. *J. Phys. A*, 20:L801–L805, 1987.

Martin Hoffmann and Edgar Voges. Bulk silicon micromachining for mems in optical communication systems. *Journal of Micromechanics and Microengineering*, 12(4): 349, 2002.

Thomas MM Homolle and Nicolas G Hadjiconstantinou. A low-variance deviational simulation monte carlo for the boltzmann equation. *Journal of Computational Physics*, 226(2):2341–2358, 2007.

Adam Huang, James Lew, Yong Xu, Yu-Chong Tai, and Chih-Ming Ho. Microsensors and actuators for macrofluidic control. *Sensors Journal, IEEE*, 4(4):494–502, 2004.

Patrick Jenny, Manuel Torrilhon, and Stefan Heinz. A solution algorithm for the fluid dynamic equations based on a stochastic model for molecular motion. *J. Comput. Phys.*, 229(4):1077–1098, 2010a. ISSN 0021-9991. doi: 10.1016/j.jcp.2009.10.008. URL `http://dx.doi.org/10.1016/j.jcp.2009.10.008`.

Patrick Jenny, Manuel Torrilhon, and Stefan Heinz. A solution algorithm for the fluid dynamic equations based on a stochastic model for molecular motion. *Journal of Computational Physics*, 229(4):1077–1098, February 2010b. ISSN 0021-9991. doi: 10.1016/j.jcp.2009.10.008. URL `http://www.sciencedirect.com/science/article/pii/S0021999109005531`.

W. Kang, J. Machta, and E. Ben-Naim. Granular gases under extreme driving. *EPL (Europhysics Letters)*, 91(3):34002, August 2010. ISSN 0295-5075. doi: 10.1209/0295-5075/91/34002. URL `http://iopscience.iop.org/0295-5075/91/3/34002`.

George Karniadakis, Ali Beskok, and Narayan Aluru. *Microflows and nanoflows: fundamentals and simulation*, volume 29. Springer, 2006.

A. V. Kats, V. M. Kontorovich, S. S. Moiseev, and V. E. Novikov. Power-law solutions of the boltzmann kinetic equation, describing the spectral distribution of particles with fluxes. *JETP Lett.*, 1975.

A.V. Kats. Direction of transfer of energy and quasi-particle number along the spectrum in stationary power-law solutions of the kinetic equations for waves and particles. *Sov. Phys. JETP*, 44:1106, 1976.

Nathan L Kleinman, James C Spall, and Daniel Q Naiman. Simulation-based optimization with stochastic approximation using common random numbers. *Management Science*, 45(11):1570–1578, 1999.

Andrey Nikolaevich Kolmogorov. Dissipation of energy in locally isotropic turbulence. In *Dokl. Akad. Nauk SSSR*, volume 32, pages 16–18, 1941.

Pavel L Krapivsky, Sidney Redner, and Eli Ben-Naim. *A kinetic view of statistical physics*. Cambridge University Press, 2010a.

PL Krapivsky and E Ben-Naim. Nontrivial velocity distributions in inelastic gases. *arXiv preprint cond-mat/0111044*, 2001.

P.L. Krapivsky, S. Redner, and E. Ben-Naim. *A Kinetic View of Statistical Physics*. Cambridge University Press, Cambridge, 2010b.

A. Kudrolli and J. Henry. Non-gaussian velocity distributions in excited granular matter in the absence of clustering. *Physical Review E*, 62(2):R1489–R1492, August 2000. doi: 10.1103/PhysRevE.62.R1489. URL `http://link.aps.org/doi/10.1103/PhysRevE.62.R1489`.

R Lacaze, P Lallemand, Y Pomeau, and S Rica. Dynamical formation of a bose-einstein condensate. *Physica D*, 152-153:779–786, 2001.

JL Lebowitz, HL Frisch, and E Helfand. Nonequilibrium distribution functions in a fluid. *Physics of Fluids (1958-1988)*, 3(3):325–338, 1960.

Christian Lécot and Faysal El Khettabi. Quasi-monte carlo simulation of diffusion. *Journal of complexity*, 15(3):342–359, 1999.

Che-Hsin Lin, Gwo-Bin Lee, Bao-Wen Chang, and Guan-Liang Chang. A new fabrication process for ultra-thick microfluidic microstructures utilizing su-8 photoresist. *Journal of Micromechanics and Microengineering*, 12(5):590, 2002.

Duncan A. Lockerby, Jason M. Reese, David R. Emerson, and Robert W. Barber. Velocity boundary condition at solid walls in rarefied gas calculations. *Phys. Rev. E*, 70:017303, Jul 2004. doi: 10.1103/PhysRevE.70.017303. URL `http://link.aps.org/doi/10.1103/PhysRevE.70.017303`.

Sergey Edward Lyshevski. *MEMS and NEMS: systems, devices, and structures*. CRC Press, 2013.

Pierre LEcuyer and Christiane Lemieux. Recent advances in randomized quasi-monte carlo methods. In *Modeling uncertainty*, pages 419–474. Springer, 2005.

L Marino. Experiments on rarefied gas flows through tubes. *Microfluidics and nanofluidics*, 6(1):109–119, 2009.

James Clerk Maxwell. V. illustrations of the dynamical theory of gases.part i. on the motions and collisions of perfectly elastic spheres. *The London, Edinburgh, and Dublin Philosophical Magazine and Journal of Science*, 19(124):19–32, 1860.

P Miao, PD Mitcheson, AS Holmes, EM Yeatman, TC Green, and BH Stark. Mems inertial power generators for biomedical applications. *Microsystem Technologies*, 12(10-11):1079–1083, 2006.

Stéphane Mischler and Clément Mouhot. Cooling process for inelastic boltzmann equations for hard spheres, part ii: Self-similar solutions and tail behavior. *Journal of statistical physics*, 124(2-4):703–746, 2006.

Stéphane Mischler and Clément Mouhot. Kacs program in kinetic theory. *Inventiones mathematicae*, 193(1):1–147, 2013.

William J Morokoff and Russel E Caflisch. Quasi-random sequences and their discrepancies. *SIAM Journal on Scientific Computing*, 15(6):1251–1279, 1994.

Clément Mouhot, Lorenzo Pareschi, and Thomas Rey. Convolutive decomposition and fast summation methods for discrete-velocity approximations of the boltzmann equation. *ESAIM: Mathematical Modelling and Numerical Analysis*, 47 (05):1515–1531, 2013.

David Munger, Pierre LEcuyer, Fabian Bastin, Cinzia Cirillo, and Bruno Tuffin. Estimation of the mixed logit likelihood function by randomized quasi-monte carlo. *Transportation Research Part B: Methodological*, 46(2):305–320, 2012.

S. V. Nazarenko. *Wave Turbulence: 825 (Lecture Notes in Physics)*. Springer, Heidelberg, 2011a.

Sergey Nazarenko. Differential approximation for kelvin wave turbulence. *Journal of Experimental and Theoretical Physics Letters*, 83(5):198–200, 2006.

Sergey Nazarenko. *Wave turbulence*, volume 825. Springer Science & Business Media, 2011b.

A. C. Newell and B. Rumpf. Wave turbulence. *Ann. Rev. Fluid Mech.*, 43(1):59–78, 2011.

Harald Niederreiter. Low-discrepancy and low-dispersion sequences. *Journal of number theory*, 30(1):51–70, 1988.

Harald Niederreiter. *Random number generation and quasi-Monte Carlo methods*, volume 63. SIAM, 1992.

J. S. Olafsen and J. S. Urbach. Velocity distributions and density fluctuations in a granular gas. *Physical Review E*, 60(3):R2468–R2471, September 1999. doi: 10.1103/PhysRevE.60.R2468. URL `http://link.aps.org/doi/10.1103/PhysRevE.60.R2468`.

ES Oran, CK Oh, and BZ Cybyk. Direct simulation monte carlo: Recent advances and applications 1. *Annual Review of Fluid Mechanics*, 30(1):403–441, 1998.

Lorenzo Pareschi and Giuseppe Toscani. Self-similarity and power-like tails in non-conservative kinetic models. *Journal of statistical physics*, 124(2-4):747–779, 2006.

D. Proment, S. Nazarenko, P. Asinari, and M. Onorato. Warm turbulence in the boltzmann equation. *EPL (Europhysics Letters)*, 96(2):24004, October 2011. ISSN 0295-5075. doi: 10.1209/0295-5075/96/24004. URL `http://iopscience.iop.org/0295-5075/96/2/24004`.

Davide Proment, Miguel Onorato, Pietro Asinari, and Sergey Nazarenko. Warm cascade states in a forced-dissipated boltzmann gas of hard spheres. *Physica D: Nonlinear Phenomena*, 241(5):600–615, March 2012. ISSN 0167-2789. doi: 10.1016/j.physd.2011.11.019. URL `http://www.sciencedirect.com/science/article/pii/S0167278911003393`.

GA Radtke, NG Hadjiconstantinou, W Wagner, Deborah A Levin, Ingrid J Wysong, and Alejandro L Garcia. Low variance particle simulations of the boltzmann transport equation for the variable hard sphere collision model. In *AIP Conference Proceedings-American Institute of Physics*, volume 1333, page 307, 2011.

Gregg A Radtke and Nicolas G Hadjiconstantinou. Variance-reduced particle simulation of the boltzmann transport equation in the relaxation-time approximation. *Physical Review E*, 79(5):056711, 2009.

Gregg A. Radtke, Jean-Philippe M. Péraud, and Nicolas G. Hadjiconstantinou. On efficient simulations of multiscale kinetic transport. *Philosophical Transactions of the Royal Society of London A: Mathematical, Physical and Engineering Sciences*, 371(1982), 2012. ISSN 1364-503X. doi: 10.1098/rsta.2012.0182.

Ethirajan Rathakrishnan. *Gas Dynamics*. PHI Learning Pvt. Ltd., 2013.

Florence Rouyer and Narayanan Menon. Velocity fluctuations in a homogeneous 2D granular gas in steady state. *Physical Review Letters*, 85(17):3676–3679, October 2000. doi: 10.1103/PhysRevLett.85.3676. URL `http://link.aps.org/doi/10.1103/PhysRevLett.85.3676`.

Matthew Rycenga, Claire M Cobley, Jie Zeng, Weiyang Li, Christine H Moran, Qiang Zhang, Dong Qin, and Younan Xia. Controlling the synthesis and assembly of silver nanostructures for plasmonic applications. *Chemical reviews*, 111(6):3669–3712, 2011.

Samuel A Schaaf and Paul L Chambré. *Flow of rarefied gases*. Princenton University Press, 1961.

Anupam Sharma, Lyle N Long, and Ted Krauthammer. Using the direct simulation monte carlo approach for the blast-impact problem. In *The 17th International Symposium on Military Aspects of Blast Simulations*, 2002.

H. Spohn. Kinetics of the bose-einstein condensation. *Physica D*, 239:627–634, 2010.

Natasha K Stout and Sue J Goldie. Keeping the noise down: common random numbers for disease simulation modeling. *Health care management science*, 11(4): 399–406, 2008.

H Struchtrup. Macroscopic transport equations for rarefied gas flows. 2005.

Laura P Swiler and Nicholas J West. Importance sampling: Promises and limitations. In *Proceedings of the 12th AIAA Non-Deterministic Approaches Conference*, volume 96, 2010.

Hideki Takayasu, Misako Takayasu, Astero Provata, and Greg Huber. Statistical properties of aggregation with injection. *Journal of Statistical Physics*, 65(3-4): 725–745, November 1991. ISSN 0022-4715, 1572-9613. doi: 10.1007/BF01053751. URL `http://link.springer.com/article/10.1007/BF01053751`.

Wei-Cheng Tian, Helena KL Chan, Chia-Jung Lu, Stella W Pang, and Edward T Zellers. Multiple-stage microfabricated preconcentrator-focuser for micro gas chromatography system. *Microelectromechanical Systems, Journal of*, 14(3):498–507, 2005.

SA Tison. Experimental data and theoretical modeling of gas flows through metal capillary leaks. *Vacuum*, 44(11):1171–1175, 1993.

E Trizac, A Barrat, and MH Ernst. Boltzmann equation for dissipative gases in homogeneous states with nonlinear friction. *arXiv preprint arXiv:0706.4275*, 2007.

Seiji Ukai et al. On the existence of global solutions of mixed problem for non-linear boltzmann equation. *Proceedings of the Japan Academy*, 50(3):179–184, 1974.

TPC Van Noije and MH Ernst. Velocity distributions in homogeneous granular fluids: the free and the heated case. *Granular Matter*, 1(2):57–64, 1998.

G Venkiteswaran and Michael Junk. A qmc approach for high dimensional fokker–planck equations modelling polymeric liquids. *Mathematics and Computers in Simulation*, 68(1):43–56, 2005a.

Gopalakrishnan Venkiteswaran and Michael Junk. Quasi-monte carlo algorithms for diffusion equations in high dimensions. *Mathematics and Computers in Simulation*, 68(1):23–41, 2005b.

Vishnu Venugopal and Sharath S Girimaji. Unified gas kinetic scheme and direct simulation monte carlo computations of high-speed lid-driven microcavity flows. *Communications in Computational Physics*, 17(05):1127–1150, 2015.

Tamás Vicsek and Anna Zafeiris. Collective motion. *Physics Reports*, 517(3):71–140, 2012.

Cédric Villani. Mathematics of granular materials. *Journal of statistical physics*, 124(2):781–822, 2006.

Wolfgang Wagner. A convergence proof for bird's direct simulation monte carlo method for the boltzmann equation. *Journal of Statistical Physics*, 66(3-4):1011–1044, 1992.

Ian A Waitz, Gautam Gauba, and Yang-Sheng Tzeng. Combustors for micro-gas turbine engines. *Journal of Fluids Engineering*, 120(1):109–117, 1998.

Yu-Hsiang Wang, Chang-Pen Chen, Chih-Ming Chang, Chia-Pin Lin, Che-Hsin Lin, Lung-Ming Fu, and Chia-Yen Lee. Mems-based gas flow sensors. *Microfluidics and nanofluidics*, 6(3):333–346, 2009.

Pierre Welander. On the temperature jump in a rarefied gas. *Arkiv fysik*, 7, 1954.

Craig White, Camilla Colombo, Thomas J Scanlon, Colin R McInnes, and Jason M Reese. Rarefied gas effects on the aerodynamics of high area-to-mass ratio spacecraft in orbit. *Advances in Space Research*, 51(11):2112–2124, 2013.

George M Whitesides and Bartosz Grzybowski. Self-assembly at all scales. *Science*, 295(5564):2418–2421, 2002.

VE Zakharov. Weak turbulence in media with a decay spectrum. *Journal of Applied Mechanics and Technical Physics*, 6(4):22–24, 1965.

VE Zakharov and NN Filonenko. Weak turbulence of capillary waves. *Journal of applied mechanics and technical physics*, 8(5):37–40, 1967.

WD Zhou, B Liu, SK Yu, W Hua, and CH Wong. A generalized heat transfer model for thin film bearings at head-disk interface. *Applied Physics Letters*, 92 (4):043109, 2008.